Comments on Inorganic Chemistry
A Journal of Critical Discussion of the Current Literature

ISSN: (Print) (Online) Journal homepage: https://www.tandfonline.com/loi/gcic20

Optoelectronic Alteration of Metal-Organic Frameworks for Enhanced Photocatalytic Water Splitting Activity Under Solar Radiation

Yahya Absalan, Faezeh Mokari, Behnaz Delaram, Mostafa Gholizadeh & Kambiz Suri

To cite this article: Yahya Absalan, Faezeh Mokari, Behnaz Delaram, Mostafa Gholizadeh & Kambiz Suri (29 Nov 2023): Optoelectronic Alteration of Metal-Organic Frameworks for Enhanced Photocatalytic Water Splitting Activity Under Solar Radiation, Comments on Inorganic Chemistry, DOI: 10.1080/02603594.2023.2285064

To link to this article: https://doi.org/10.1080/02603594.2023.2285064

COMMENTS ON INORGANIC CHEMISTRY
https://doi.org/10.1080/02603594.2023.2285064

Taylor & Francis
Taylor & Francis Group

Optoelectronic Alteration of Metal-Organic Frameworks for Enhanced Photocatalytic Water Splitting Activity Under Solar Radiation

Yahya Absalan[a], Faezeh Mokari[b], Behnaz Delaram[b], Mostafa Gholizadeh[b], and Kambiz Suri[c]

[a]Department of Chemistry, Georgia University, Athens, Georgia, USA; [b]Department of chemistry, Ferdowsi University of Mashhad, Mashhad, Iran; [c]Department of Mechanical and Instrumental Engineering, Academy of Engineering, RUDN University, Moscow, Russia

ABSTRACT

Metal-organic frameworks (MOFs) have been increasingly popular in photocatalytic water-splitting research areas due to their unique, tunable porosity, high stability, large surface activity, and manipulative topology. However, the incapability of MOFs in harvesting broad-solar irradiation and rapid electron-hole pairs recombination has limited their efficiency in practical applications, and their structures allow researchers to manipulate them toward better efficiency. Also, linker modification is achieved by reclaiming the organic linker, which constructs MOFs by functionalizing, changing the ligand's length, and using an aided organic linker. In addition, being a free space in their structure gives this opportunity to modify them easily with other compounds such as inorganic complex compounds and nanoparticles by incorporation, impregnation, and ship-in-a-bottle methods. The objectives of this review article are three-fold. First, to emphasize understanding of the fundamental correlation among promising strategies to improve the optoelectronic properties of MOFs such as light-harvesting capability and photoinduced electron-hole pairs for photocatalytic reactions involving water splitting reaction under broad solar irradiation. Second, to systematically summarize the organic linker modification and incorporation of polyoxometalate, coordination metal complexes, and various nanoparticles. Third, to discuss challenges and future research directions for the development of broad solar band activation of MOFs for photocatalysis purposes.

KEYWORDS

Photocatalyst; water splitting; longer wavelength; metal-organic compound; nanoparticle

CONTACT Yahya Absalan Yahya.absalan@uga.edu Department of Chemistry, Georgia University, Athens, GA 30602, USA

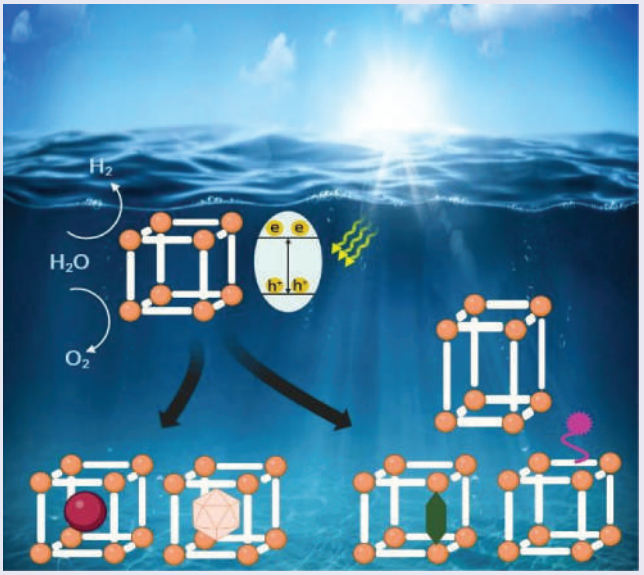

Summary

- Investigation of the different methods for modification of MOFs
- Review of the incorporation of complex compounds into MOFs in detail
- Investigation of all the strategies for incorporation of complex compounds into MOFs

1. Introduction

Fuel and its related fields are of crucial significance as the fuel is the essential driving force of society and almost all the industries. Fossil fuels, including petroleum, coal, and natural gas are the most accessible and useful fuels and the first choice of all the countries due to their ease of storage and transport, cost-effectiveness, and applicability in almost all situations. Some issues such as non-renewability, environmental incompatibility, and hazardous use of these fuels have raised some concerns. Based on the Statistical Review of World Energy, and the U.S. Energy Information Administration[1], oil, natural gas, and coal have been consumed 47 years, 53 years and 133 years ago, leading to the depletion of their resources. Moreover, fossil fuels contribute to the emission of greenhouse gases. Although fossil fuels are not as dangerous as nuclear energy, they can be very menacing if used in con-compliance with the corresponding standards. For instance, as the greenest fossil fuel, natural gas is inflammable with high explosion ability. The mentioned drawbacks have motivated different countries to think about an alternative approach.

Hydrogen gas is one of the promising alternative fuels due to its remarkable advantages, including availability and renewability. Moreover, hydrogen gas is

the most abundant element on the universe, and it is among the ten on the earth.[2] Hydrogen gas is nontoxic without any unexpected impacts such as the production of side products. It can be stated that hydrogen gas has zero greenhouse emission and thus no contribution to the carbon footprint effects. Unlike the fossil fuel, hydrogen gas does not require large-area storage space. Moreover, it generates higher energy compared to the fossil fuels as it can create the highest energy compared to other fuels due to its great gravimetric energy density (120 MJ/kg), which is almost 3 times more than fossil fuels. Hydrogen fuel cells offer higher efficiency as they can generate more than 65% electricity, far higher than the conventional combustion-based power plants (33–35%). However, some challenges in utilizing hydrogen gas as fuel remain. The main one is to produce hydrogen gas in pure form.[3] Another limitation is the technology for storing hydrogen gas. Most of the technologies for storing hydrogen gas lead to different states such as a compressed gaseous state, liquid state or solid-state.[4–7] Moreover, extreme safety measures are required to store the hydrogen gas in the liquid state due to the needs of high pressures around 100 MPa and cryogenic temperature of around −250°C. Unlike storing hydrogen gas in liquid state, storing in solid state does not require high pressure or extremely low cryogenic temperatures.[8,9]

In this regard, different methods have been developed for hydrogen gas production which are mainly based on (i) hydrogen gas production from industrial processes such as steam methane reforming,[10,11] partial oxidation,[12] auto thermal reforming,[13,14] steam iron process[15] and (ii) biological techniques such as dark fermentation,[16] photo-fermentation,[17] hybrid system,[17] and bio-photolysis.[17,18] The economic issues play important roles in choosing the hydrogen gas production method. The overall production costs of hydrogen gas depend on three sources of feedstock, government investment, and energy source[19] (Table 1).

Based on Table 1, the first three methods use fossil fuels, therefore, they are not ideal for hydrogen gas production. Dark fermentation and photo

Table 1. Summary of various H_2 production processes with their feedstock, capital cost, and hydrogen gas cost. Reprinted with permission from Ref.[20] copyright 2021 elsevier publisher

Method	Source of energy	Feedstock	Capital cost (M$)	H_2 cost (US$ per kg)
Steam methane reforming by CCS (CO_2 capture and storage)	Fossil fuels	CH_4	226.3	2.27
Steam methane reforming with no CCS	Fossil fuels	CH_4	18.5	2.08
Auto thermal reforming of CH_4 by CCS	Fossil fuels	CH_4	183.3	1.48
Dark Fermentation	-	Organic Biomass	-	2.57
Photo-Fermentation	Solar light	Organic Biomass	-	2.83
Bio-photolysis by Direct method	Solar light	Water with algae	50 US$ per m2	2.13
Bio-photolysis by Indirect method	Solar light	Water with algae	50 US$ per m2	1.42

fermentation use no source of energy and solar light, respectively. However, the feedstock is organic, which makes them not green methods. Bio-photolysis uses solar light. However, they require algal feedstock. The overall cost of each method lies in the ideal range. According to the United State Department of Energy, the production of hydrogen gas is economically beneficial, thus, it could be a proper alternative to fossil fuels if its final cost reaches 2.00 and 4.00 USD/kg (year 2020).[21]

Recently, production of hydrogen gas through water splitting has become very popular.[22–27] This method uses water and sunlight, i.e., two most abundant natural resources on the earth. The method is absolutely green as all of the components, including the feedstock and sunlight are environmentally benign. Furthermore, this method is circulatable, which prevents energy depletion. This system emits no carbon dioxide, which can be an environmental pollutant if it exceeds normal atmospheric level. Concerning the economic issues, the final cost of this system is affordable due to the use of abundant natural resources. Various methods such as thermochemical water splitting, photobiological water splitting, photoelectrochemical (PEC) water splitting, and photocatalytic water splitting have been developed for water splitting.[20,28–30]

Photocatalytic water splitting generally includes three main steps: i) light absorption, ii) charge separation and transfer, and iii) redox reaction. The photocatalytic process is initiated by light absorption, reflecting the important role of light absorption in the water splitting efficiency. So far, different types of metal organic frameworks (MOFs) have been reported as the catalyst in the photo-induced water splitting chemical process.

This review is based on the design of photo-activated catalysts for water splitting, focusing on light absorption by the incorporation of organic-metal compounds (OMC) and nanoparticles (NPs) into MOFs. OMC and NPs have shown high effectiveness as co-catalysts upon incorporation into the MOFs. Therefore, many researchers have focused on the methods to explore this benefit for different applications. The incorporation of NPs in MOFs leads to the formation of a Schottky junction, which enhances the hoto-induced catalytic properties of the final composite through spatial separation of photo-generated excitons and suppression of their recombination via Schottky barrier diodes. Furthermore, NPs can increase hydrogen gas production due to their catalytic properties.[31–36] Indeed, the modification of MOFs by OMC and NPs is a mutual assistance, leading to a composite with different advantages. MOFs prevent the aggregation of the incorporated compounds during photocatalytic reactions, fortify the number of reactants around the incorporated compound to increase the conversion rate, serve as an electron transporter to the active sites, including OMC or NPs, to enhance their photo-induced catalytic properties since MOFs can have interior substrates of variable sizes and shapes. On the other hand, OMC and NPs benefited MOFs through the light absorption

enhancement by the concentrated local electromagnetic field (CLEF) effect, perfusing hot electrons into MOFs which increments photocatalytic activity.[37]

The present review paper studied the modified MOFs with inorganic complex compounds and nanoparticles, which have been used, as photo-activated catalysts, for water splitting. All kinds of inorganic complex compounds and nanoparticles, their properties, and their effects on different types of MOFs were investigated. Furthermore, different strategies for tuning the optical features of the photocatalysis system were considered. In addition, the methods to modify light absorption are studied for pristine and modified (by OMC and NPs) MOFs.

2. The fundamental aspects of photocatalytic water splitting

2.1. The concept of band gap

Among the reported approaches to hydrogen gas production, photo-induced catalytic water splitting (PWS) is very attractive and thus is the focus of this review. Light absorption is the first step of photocatalytic water splitting, where the light is absorbed and transported to the next step. An improvement in light absorption can accelerate the charge separation of excited electrons and holes in the conduction band (CB) and valance band (VB), respectively. Consequently, it improves the efficiency of hydrogen gas evolution. According to this process, two main factors of light and the light-absorbing compound determine the efficiency of the process.

The energy band gap plays a key role in determining the distance the electrons have to migrate to reach the CB band from the VB band. The energy band gap is changed based on the wavelengths. According to Planck's equation,[38,39] the energy band gap has an opposite relationship with wavelength (1):

$$E_r = h\nu = \frac{hc}{\lambda} \tag{1}$$

Where E is the energy, h is the Planck's constant (6.63×10^{-34} J.s), υ shows the frequency (Hz), c denotes the speed of light (3.0×10^{8} m/s) and λ is the wavelength. As shown by equation 1, a decrease in the energy band gap implies an increase in wavelength. There are two types of energy band gaps: direct and indirect (Figure 1). The difference between direct and indirect band gaps is the location of the momentum of the electron in the CB and VB bands (Figure 1a). In the direct band gap, both CB and VB exhibit equal momenta, which leads to the migration of electrons from the VB to the CB as influenced by the energy that is higher than the energy band gap (hυ > Eg) with small variations in the momenta of the electrons. In the case of indirect band gap, the momentum of an electron is not equal in the VB and CB bands, so the energy needed to excite

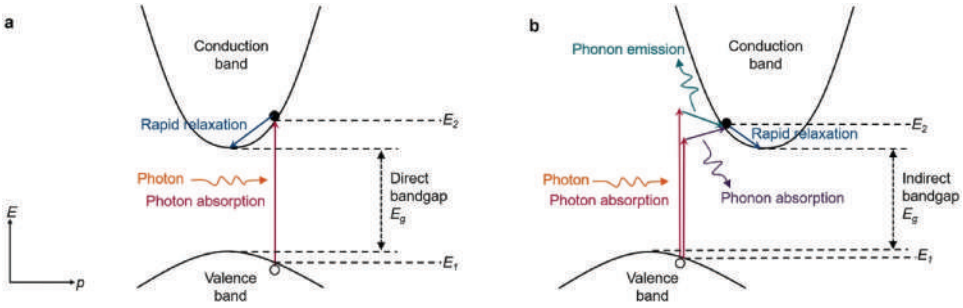

Figure 1. Photon absorption in (a) a direct band gap for an incident photon with energy hv = E_2 – E_1 > eg, and (b) an indirect band gap for a photon with energy hv < E_2 – E_1 and a photon with energy hv > E_2 – E_1. Reprinted with permission from Ref.[21] copyright 2019 ACS publication.

electrons from the VB to CB will be higher than the direct band gap[40,41] (Figure 1b). This difference, in the direct and indirect band gaps, comes from the difference in the electron interactions. In the direct band gap, the electrons interact by a photon (E_2-E_1), while in the case of the indirect band gap, photons and phonons are involved in the electron interactions, which increase or decrease the momentum. The possibility and the rate of the indirect band gap are lower than the direct band gap due to the involvement of three phenomena of electron, photon, and phonon.

A molecule can absorb the light if its energy band gap is the same or lower than the energy of the incident light.

In materials that have a large exciton binding energy, a photon may have just the right amount of energy to form an exciton (bound electron–h), but not enough energy to separate the electron and hole (which are electrically attracted to each other). The distinction between "optical band gap" and "electronic band gap" (or "transport gap") is made in this situation. The threshold for photons to be absorbed is the optical band gap, while the transport gap is the threshold for creating an electron–hole pair that is not bound together. Generally,The optical bandgap is at lower energy than the transport gap.

2.2. Fundamental aspects of photocatalytic water splitting

Concerning suitable material properties for absorption of visible or IR light to promote photocatalytic water splitting, it is worth noting that adjusting the energy band gap to match the visible or IR regions in terms of energy does not lead to splitting water. Water splitting occurs upon the incidence of both reduction and oxidation reactions. The condition for the reduction and oxidation of water involves the VB and CB in 0 V vs normal hydrogen electrode (NHE) (negative side) and 1.23 V vs NHE (positive side), respectively. Moreover, the energies

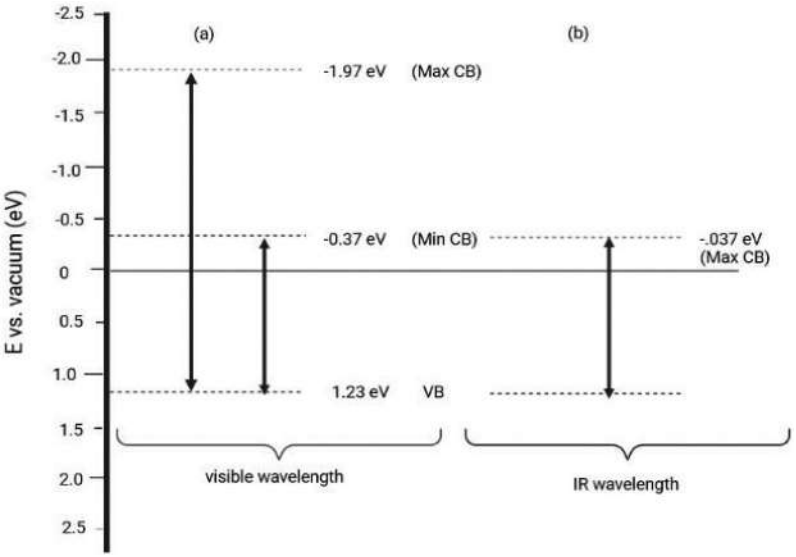

Figure 2. The location of VB and CB for water splitting under (a) visible and (b) IR lights.

of visible and IR spectra are 3.20 > Eg >1.60 eV and Eg <1.60 eV, respectively. As a result, the proper location of the VB for both will be at 1.23 eV. Concerning the CB, it ranges between −0.37 eV (minimum) and −1.97 (maximum) eV in the case of visible wavelength (Figure 2a), and −0.37 (maximum) eV in the case of IR wavelengths (Figure 2b).

In PWS, the hydrogen gas production is achieved by converting solar-to-hydrogen gas (STH).[42] The surface of the catalyst is exposed the sunlight so the catalyst is named photocatalyst. The method has some unique advantages, mainly, its easy operation.

The STH determines the efficiency of the method for converting solar to hydrogen gas. STH can be obtained by the following equation:

$$STH\% = \left(\frac{output\ energy\ of\ hydrogen}{energy\ of\ the\ incident\ solar\ light}\right) AM_{1.5G} \times 100$$

$$= \left(\frac{mmoles\ of\ hydrogen/s \times 237kJ/mol}{P_{total}(mW/cm^2) \times Area(cm^2)}\right) AM_{1.5G} \times 100$$

According to the latest data, the most efficient conversion of water into hydrogen gas with the solar light is around 1.5%. Thus, the method needs to be further explored.[43]

In the case of using photocatalysts, hydrogen and oxygen gases are produced through the following steps:

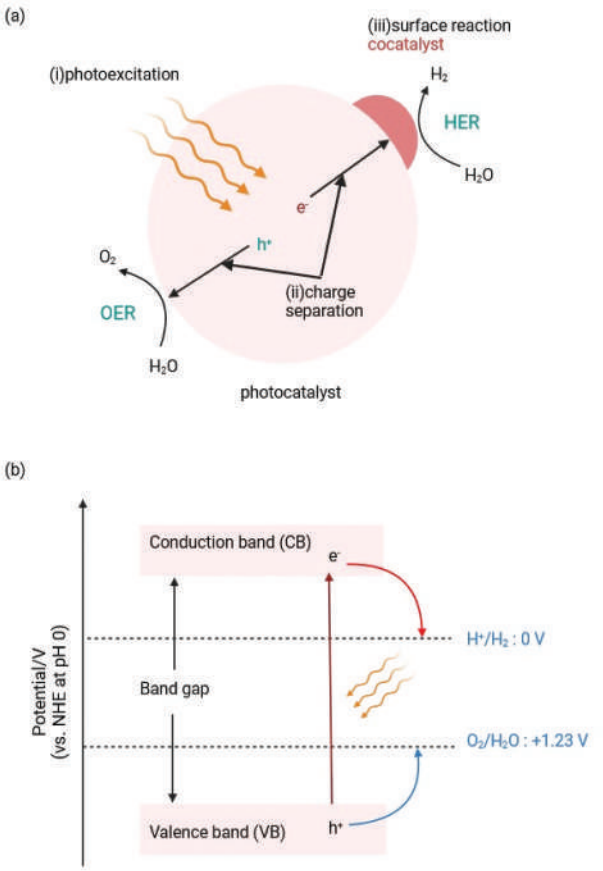

Figure 3. (a) schematic of photocatalytic reactions: (i) photoexcitation, (ii) charge separation, and (iii) surface reactions. (b) relationship between the semiconductor band structure and redox potentials of water splitting.

1$_{st}$ ***Step:*** Excitation of electrons (e-); photocatalyst is exposed to UV, visible, or IR light; leading to the excitation of electrons from the VB to the CB band.

2$_{nd}$ ***Step:*** Formation of holes (h^+); upon the excitation of electrons to the CB, holes are created in the VB.

3$_{rd}$ ***Step:*** Redox reaction; the reduction of water occurs by the excited electrons in the conduction band while its oxidation happens in the valence band by the holes (Fig. 3a)

Thermodynamically, the water splitting is a 4 e^- process, requiring a Gibbs free energy (ΔG) of 237 kJ mol^{-1}. Moreover, as the water splitting reaction applies at least 50% of solar energy, both half reactions are highly energy-demanding.[28] The reduction of water happens when the edge of the conduction band of a photo-induced catalyst locates on the negative part of the reduction potential of the water (0 V vs NHE),

leading to hydrogen gas production. This process is known as hydrogen evolution reaction (HER) (Figure 3b). On the other hand, water oxidation occurs when the top edge of the valence band locates on the positive part of the oxidation potential of water (1.23 eV vs NHE), forming oxygen gas, also known as oxygen evolution reaction (OER)[21,28,44–49] (Figure 3b).

The mentioned mechanism can be summarized as:
Hydrogen evolution reaction:

- in an acidic aqueous solution: $2H^+ + 2e^- \rightarrow H_2$
- in an alkaline aqueous solution: $2H_2O + 2e^- \rightarrow H_2 + 2OH^-$

Oxygen evolution reaction:

- in an acidic aqueous solution: $2H_2O \rightarrow O_2 + 4e^- + 4H^+$
- in an alkaline aqueous solution: $4OH^- \rightarrow O_2 + 4e^- + 2H_2O$

The efficiency of the solar energy can be determined based on photon absorption efficiency ($\eta_{absorption}$), separation efficiency ($\eta_{separation}$), and reaction efficiency ($\eta_{reaction}$). Photon absorption efficiency indicates the fraction of e/h excited by photons. separation efficiency ($\eta_{separation}$) refers to the species exposed to the photon and move toward the surface, while the yield of the surface reaction, which contains the charge species at the border of the solid (surface of the catalyst) and liquid (water) is defined as the reaction efficiency.[21,50,51]

$$\eta_{total} = \eta_{absorption} \times \eta_{separation} \times \eta_{reaction}$$

Noteworthy is that even qualified photocatalysts will not necessarily split water as each reaction requires high activation energy. Moreover, recombination of electrons to the VB does not allow the completion of the water splitting process. It is crucial that the catalyst resist harsh acidic and alkaline environments. Furthermore, the catalyst should be highly recyclable so that it can be re-used efficiently and economically. These issues further highlight the importance of the design of a photo-induced catalyst.[21,42,47]

From kinetic point of view, in photocatalysis, the generation, separation, and transfer of photogenerated carriers usually take a few femto to nanosecond.[52] On the other hand, the electrocatalytic process (i.e., surface redox reaction) takes much longer (micro- to seconds) to achieve and is often the rate-limiting step. Due to different factors OER is often much slower than HER including[53]:

(1) Larger effective mass of a hole than an electron can cause slower hole transfer than electron transfer.
(2) Participation of four holes in OER leads to much larger overpotential and slower reaction kinetics than HER.
(3) An oxygen atom is 16 times as massive as a hydrogen atom so that O_2 diffuse much slower than that of H_2.
(4) Because of high oxygen and low hydrogen affinity of most photocatalyst surfaces, it is difficult for oxygen molecules to desorb from the photocatalyst surface.

Another point which should be considered in PWS is backward reaction and side reaction. Due to the coexisting H_2 and O_2 during PWS, water can be produced through a backward reaction. This can reduce the efficiency of photocatalysts.

On the other hand, H_2O_2 and water can be produced through combination of oxygen gas with electrons. This side reaction has negative effects in H_2 production process.[53]

3. Physicochemical properties of MOFs

Metal–organic frameworks (MOFs) are a special group of coordination polymers (CPs) composed of metal ions, or clusters, and organic linkers. Their unique physical and chemical properties including high surface areas, high porosity, structural tunability, crystalline nature, and high chemical and thermal stability have made them proper candidates for use in different fields[54–56] including the photocatalytic reactions[57–59] [references need to be cited here]. The features mentioned above can improve the photocatalytic reactions by influencing different parts of these reactions.[60]

4. Metal-organic frameworks as photocatalysts

Different compounds have been used as photo-induced catalysts, including semiconductors,[61,62] core-shell[63,64]), and MOFs.[65–67] As indicated above, MOFs are three dimensional structures comprising organic linkers and metal nodes linked by polymeric bonds, which can exhibit optoelectronic properties.[68] The use of MOFs for photocatalytic hydrogen gas production was introduced by Silva and coworkers in 2010[69] (Figure 4). MOFs could be excellent photocatalysts due to their (i) organic linkers which can absorb light from different regions of UV, visible and even IR ranges to excite electrons from highest occupied molecular orbital (HOMO) to lowest unoccupied molecular orbital (LUMO),[60,70,71] (ii) large surface activity with high porosity, which prepares a suitable space for the incorporation of other co-catalyst to increase the photocatalytic behaviors of MOFs,[72–75] (iii) great charge

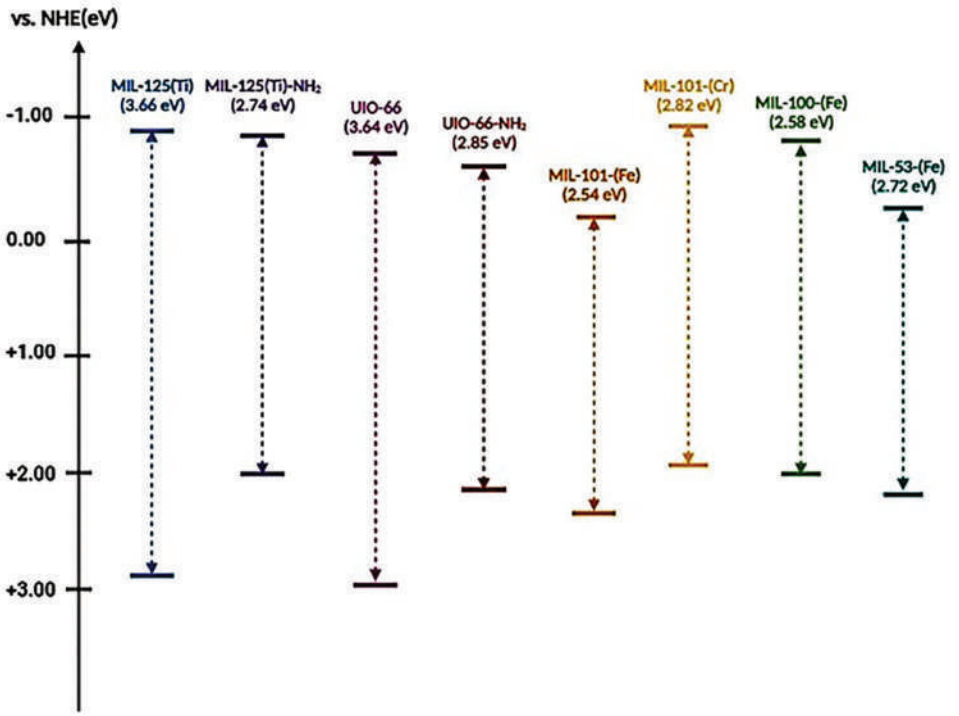

Figure 4. Band gap structures (VB and CB position) of various MOFs used in photocatalysis.

distance to avoid fast recombination,[76,77] (iv) high chemical, and thermal stability which allows long-term use of MOFs,[45,78–80] (v) high flexibility for structural tuning with different properties[81] (vi) high selectivity,[82–84] (vii) cost-effectiveness,[85,86] (viii) the possibility of their functionalization by other groups to modify MOFs depending on their corresponding application[49,87] (ix) high catalytic center due to having metal ions, which accelerate the chemical reactions in the presence of light,[28,88,89] (x) well-ordered crystalline structure of MOFs leads to a clear structure for better engineering,[60,90,91] and (xi) well-constructed heterojunctions and photo-generated electron transfer due to the $\pi - \pi$ interactions in the aromatic ligands of MOFs.[82,92–94] NH_2-UiO-66, NH_2-MIL-125(Ti), and MIL-101 are well-known MOFs for water splitting applications. Most useful MOFs are presented in Table 2.[29,88,166,172–177]

Three main factors determine the efficiency of solar energy in hydrogen gas production: (i) light absorption, (ii) charge separation and transport, and (iii) catalytic center. MOFs are built from the metal clusters (inorganic semiconductor quantum entities), and organic linkers (antenna to activate the semiconductor quantum dots via the linker-to metal cluster charge transfer (LCCT)) (Figure 5a), thus, they can be used as photocatalysts for H_2 production.[60,178,179] Generally, ligands serve as electron donors in MOFs,

Table 2. Mofs used for the photocatalytic water splitting

				Gas evolution rate						Incorporated compounds		
Photocatalyst	Organic linker	Metal cluster	Bandgap	H_2	O_2	TON or TOF	light source	Reaction time	Efficiency	OM	NPs	Ref
Pristine MOFs												
In-MOF	3,3′,5,5′-azoxybenzenetetracarboxylic Acid	In(III)	2.95 eV	777.65 μmol g^{-1} h^{-1}	-	-	visible	4 h	-	-	-	[95]
Ni-MOF	1,4-benzenedicarboxylate	Ni(II)	2.3 eV	200 μmol/h	-	-	visible	3 h	50%			[96]
IEF-13	4,6-tris[4- (phosphonomethyl) phenyl]-1,3,5-triazine	Ni(II)	2.83 eV	2,200 and 1,700 μmolg^{-1}	-	-	visible	22 h	-			[97]
Cu-I-bpy	4,4′-bipyridine	Cu(II)	2.05 eV	7.09 mmolg^{-1} h^{-1}	-	-	visible	-	-			[98]
PCN-415	1,4-benzenedicarboxylate	$[Ti_8Zr_2O_{12}(MeCOO)_{16}]$	3.3eV	44μmol·g^{-1} ·h^{-1}	-	-	visible	24 h	-			[91]
Pt(1.5)/ Ti-MOF-NH_2	2-amino-benzenedicarboxylic acid	Ti(IV)	2.6 eV	516 μmol·g^{-1} ·h^{-1}	-	-	visible	3 h	-			[99]
UiO-66-[FeFe]-$(dcbdt)(CO)_6$	1,4-benzenedicarboxylate	Zr(IV)	-	280 μmol·g^{-1} ·h^{-1}	-	-	visible	-	-			[100]
UiO-66	terephthalate	Zr(IV)	3.05 eV	248 μmol g_{cat}^{-1} h^{-1}	-	-	UV	-	-			[69]
UiO-66(NH_2)	2-aminoterephthalate	Zr(IV)	2.88 eV	372 μmol g_{cat}^{-1} h^{-1}	-	-	UV	-	3.5%			[69]
Ti-MOF-Ru$(tpy)_2$	bis(40-(4-carboxyphenyl)-terpyridine)Ru(II) complex	Ti(IV)	2 eV	181.6 μmol·g^{-1} ·h^{-1}	-	-	visible	9 h	-			[101]
copper(II)-organic framework	4′-(2,4-disulfophenyl)-3,2′:6′,3′′-terpyridine	Cu(II)	2.34 eV	6.99 μmol h^{-1}./ 1.43 μmol h^{-1}	-	-	visible, near infrared	-	0.076%			[102]
(Na/Cu–MOF)	H_2L_1 = 4,4′-(4-(4H–1,2,4-triazol-4-yl)phenylazanediyl)dibenzoic acid; H_4L_2 = citric acid	Cu(II),Na(I)	-	4650 μmol·g^{-1}·h^{-1}	-	-	visible	-	-			[103]
Cu(I)-MOF	anthracene-based bipyridine (BPEA)	Cu(I)	2.13 eV	75.89 mmol/g	-	-	visible	18 h	-			[104]
ZIF-67	2-methylimidazole	Co(II)	4.3 eV	40500 μmol H_2/g	-	TON=8	visible	48 h	-			[105]

(*Continued*)

Table 2. (Continued).

				Gas evolution rate						Incorporated compounds		
Photocatalyst	Organic linker	Metal cluster	Bandgap	H_2	O_2	TON or TOF	light source	Reaction time	Efficiency	OM	NPs	Ref
Pristine MOFs												
UiO-66	1,4-benzenedicarboxylate	Zr(IV)	3.5 eV	4.6 μmol·h^{-1}	-	-	visible	-	0.25%			[106]
Pt/20%-MIL-125-$(SCH_3)_2$	2,5-bis(methylthio)terephthalate	Ti(IV)	2.6 eV	3814.0 μmol$g^{-1}h^{-1}$	-	-	visible	-	8.9%			[107]
USTC-8(In)	tetrakis(4-carboxyphenyl) porphyrin	In(III)	1.79 V	341.3 μmol·g^{-1}·h^{-1}	-	-	visible	-	-			[108]
Pt/TiPF	picolinate	Ti(IV)	-	159.3 μmol h^{-1}/ 0.1 g TiPF catalyst	-	-	visible	24 h	-			[109]
NH_2-MIL-125(Ti)/ B-CTF-1	2-aminoterephthalate	Ti(IV)	-	360 μmol.h^{-1}.g^{-1}	-	-	visible	-	-			[110]
EY/Pd/UiO-66	terephthalate	Zr(IV)	-	235.750μmol h^{-1} g^{-1}	-	-	visible	-	-			[33]
FI/$[Ni_2(PymS)_4]_n$	2-mercapto-pyrimidine	Ni(II)	-	-	-	TOF = 10.6 h^{-1} TON=2.5	visible	-	-			[111]
Pt/Cu-MOF	4′-(2,4-disulfophenyl)-3,20:60,300-terpyridine	Cu(II)	2.39 eV	72.67 μmol h^{-1}	-	-	visible	-	-			[112]
PCN-9-Pt	2,4,6-Tris(4-carboxyphenyl)-1,3,5-triazine	Co(II)	3.00 eV	33.5 μmol g^{-1} h^{-1}	-	-	UV–visible	-	-			[113]
HNTM-Ir/Pt	tetrakis(4-carboxyphenyl) porphyrin	Zr(IV)	-	201.9 μmol h^{-1} g^{-1}	-	-	visible	-	-			[114]
Al-ATA-Ni MOF	2-aminoterephthalate	Al(III)	2.75 eV	36.0 μmol h^{-1}	155 μmol h^{-1}	-	visible	-	-			[115]
Al-TCPP-Pt	4,4′,4″,4‴-(porphyrin-5,10,15,20-tetrayl)tetrabenzoate	Al(III)	-	181 μmol h^{-1} g^{-1}	-	TOF= 35.4 h^{-1}	visible	-	-			[116]
Bi-TBAPy	1,3,6,8-tetrakis(p-benzoic acid) pyrene	Bi(III)	2.67 eV	140 μmol h^{-1} g^{-1}	-	-	visible	-	-			[117]
PNPMOF	2-aminoterephthalate	Al(III)	-	TON = 66	-	TON=66	visible	6 h	-			[118]
MOF-199/Ni	1,3,5-trimesic acid	Cu(II)	2.48 eV	24400 μmol h^{-1} g^{-1}	-	TON= 266 TOF=88.7 h^{-1}	visible	-	7.6%			[119]

(*Continued*)

Table 2. (Continued).

				Gas evolution rate						Incorporated compounds		
Photocatalyst	Organic linker	Metal cluster	Bandgap	H_2	O_2	TON or TOF	light source	Reaction time	Efficiency	OM	NPs	Ref
Pristine MOFs												
$[Cu^{I}_{12}(trz)_8(H_2O)_2][\alpha\text{-}SiW_{12}O_{40}]\cdot 2H_2O$	1-H-1,2,4-triazole	Cu(I)	2.11 eV	192.2 μmol g^{-1} h^{-1}	-	-	visible	240 min	-			[120]
$[Cu^{I}_{12}(trz)_8Cl][\alpha\text{-}PW_{12}O_{40}]$	1-H-1,2,4-triazole	Cu(I)	2.35 eV	-	-	-	visible	240 min	-			[120]
$[Dy_2(abtc)(H_2O)_2(OH)_2]\cdot 2H_2O$	3,3′,5,5′-azobenzene tetracarboxylic acid	Dy^{3+}	2.17 eV	21.53 μmol h^{-1} g^{-1}	-	-	visible	5 h	-			[121]
MIL-101-CH_2@1	benzene-1,4-dicarboxylate	Cr(III)	-	1.5 mmol H2 h^{-1} g^{-1}	-	TON=30	visible	10 h	-			[122]
Pt/MIL-100(Fe)	1,3,5-benzenetricarboxylic acid	Fe(III)	-	109 μmol·g^{-1}·h^{-1}	-	-	visible	-	-			[123]
Ni_x/101/Ey	terephthalate	Cr(III)	3.4 eV	6250 μmol·g^{-1}·h^{-1}	-	-	visible	-	-			[124]
NH_2-MIL-125(Ti)/CN/NiPd	2-aminoterephthalate	Ti(IV)	-	8.7 mmol·g^{-1}·h^{-1}	-	TON=32.4	visible	-	85.7%			[125]
MIL-167	2,5-dihydroxyterephthalic acid	Ti (IV)	-	7.7 μmol h^{-1}	-	-	UV	-	-			[126]
Pt/UiO-66-NH_2	2-aminoterephthalate	Zr(IV)	2.76 eV	50.26 μmol $g^{-1}h^{-1}$	-	-	UV	-	-			[127]
MOF-253-Pt	2,2′-bipyridine-5,5′-dicarboxylic acid	Al	-	100–200 μmol g^{-1} h^{-1}	-	-	visible	-	1.63%			[128]
Pt/NH_2-MIL-101(Cr)	2-aminotere phthalic acid	Cr(III)	-	28.6 μmol	-	TON=110	visible	6 h	-			[129]
Cu-BTC MOF	1,3,5-tricarboxylate	Cu(II)	-	191 μmol·g^{-1}·h^{-1}	-	-	visible	-	-			[130]
MoS_2/UiO-66/CdS	1,4-benzenedicarboxylate	Zr(IV)	-	650 μmol h^{-1}	-	-	visible	-	23.6%			[131]
EY/g-C_3N_4/ZIF-67/MoS_2	2-methylimidazole	Zn(II)	-	309.5 μmol·L^{-1}·g^{-1}·h^{-1}	-	-	visible	-	-			[132]
CdS/UiO-66	1,4-benzendicarboxylate	Zr(IV)	3.5 eV	235 mol h^{-1}	-	-	visible	-	1.2%			[133]
MIL-101(Cr)–Au/TiO_2	tere phthalic acid	Cr(III)	-	903 μmol h^{-1} g^{-1}	-	-	visible	-	-			[134]
Au@CdS/MIL-101	1,4-benzene dicarboxylic acid	Cr(III)	-	250 μmol h^{-1}/10 mg	-	-	visible	-	-			[135]
ErB-sensitized UiO-66	terephthalate	Zr(IV)	-	4.6 μmol·h^{-1}	-	-	visible	-	0.25%			[106]
Ni@NH_2-MIL-125(Ti)	aminoterephthalic acid	Ti(IV)	2.56 eV	6000 μmol g^{-1} h^{-1}	-	TON=472	UV	-	-			[136]

(*Continued*)

Table 2. (Continued).

Photocatalyst	Organic linker	Metal cluster	Bandgap	Gas evolution rate		TON or TOF	light source	Reaction time	Efficiency	Incorporated compounds		Ref
				H_2	O_2					OM	NPs	
Pristine MOFs												
CdS@NU-1000/1% RGO	benzoic acid	Zr(IV)	2.72eV	2.42mmol $gCdS^{-1}$ h^{-1}	-	-	visible	-	0.0137%			[137]
$Cd_{0.5}Zn_{0.5}S$@UCN30	1,4-benzendicarboxylate	Zr(IV)	2.22 eV	1281.1 μmol h^{-1} g^{-1}	-	-	visible	120 min	82%			[138]
OM@MOFs												
Ru-Pt@UIO-67	4,4′-biphenyldicarboxylic acid	Zr(IV)	-	0.5 μmoL	-	-	visible	5 h	-	$Pt(dcbpy)Cl_2$		[139]
Co(II)@MIL-125-NH_2	2-aminobenzene-1,4-dicarboxylate	Ti(IV)	2.6 eV	553 μmol·g^{-1}·h^{-1}	-	TOF=3.36h^{-1}	visible	7.5 h	-	[CoII(TPA)Cl][Cl]		[140]
Co@MOF	2-aminoterephthalic acid	Ti(IV)	2.59 eV	375 μmol(H_2) h^{-1}	-	TOF=0.8 h^{-1}	visible	-	0.5%	cobaloxime		[141]
PTC-19/CdS/MIL-101	terephthalate	Cr(III)	2.14eV	94.9 mmol (gCdS h)$^{-1}$	-	-	visible	-	4.67%	$Ti_6O_4(OiPr)_{10}(O_3P\text{-}Phen)_2(L)_2$ (L =R-1,1′-bi-2-naphthol)		[142]
$[H_6NiSiW_{11}O_{39}]_{0.24}[Fe_3C_{18}H_7O_{14}]\cdot 14H_2O$	trimethyl 1,3,5-benzenetricarboxylate	Fe(III)	-	9.2μmols of H_2	-	TOF=0.00093s^{-1} TON=22.5	visible	12 h	-	$H_6NiSiW_{11}O_{39}$		[143]
$[H_5NiPW_{11}O_{39}]_{0.23}[Fe_3C_{18}H_7O_{14}]\cdot 14H_2O$	trimethyl 1,3,5-benzenetricarboxylate	Fe(III)	-	11μmols	-	TOF=0.0024s^{-1} TON=32	visible	12 h	-	$H_5NiPW_{11}O_{39}$		[143]
$[H_6NiGeW_{11}O_{39}]_{0.26}[Fe_3C_{18}H_7O_{14}]\cdot 14H_2O$	trimethyl 1,3,5-benzenetricarboxylate	Fe(III)	-	45μmols	-	TOF=0.0053s^{-1} TON=110	visible	12 h	-	$H_6NiGeW_{11}O_{39}$		[143]
$[H_6NiSiW_{11}O_{39}]_{0.20}[Zr_6O_4(OH)_{5.4}][C_{14}H_8O_4]_{5.3}.15H_2O$	1,4-benzendicarboxylate	Zr(IV)	-	8.5 μmols of H_2	-	TOF=0.0010s^{-1} TON=20.8	visible	12 h	-	$H_6NiSiW_{11}O_{39}$		[143]
$[H_6NiSiW_{11}O_{39}]_{0.19}[Zr_6O_4(OH)_{5.4}][C_{14}H_8O_4]_{5.3}\cdot 14H_2O$	1,4-benzendicarboxylate	Zr(IV)	-	32μmols	-	TOF=0.0040s^{-1} TON=78.4	visible	12 h	-	$H_6NiSiW_{11}O_{39}$		[143]

(*Continued*)

Table 2. (Continued).

				Gas evolution rate						Incorporated compounds		
Photocatalyst	Organic linker	Metal cluster	Bandgap	H_2	O_2	TON or TOF	light source	Reaction time	Efficiency	OM	NPs	Ref
OM@MOFs												
$[H_6NiSiW_{11}O_{39}]_{0.19}$ $[Zr_6O_4(OH)_{5.4}]$ $[C_{14}H_8O_4]_{5.3}\cdot 13H_2O$	1,4-benzendicarboxylate	Zr(IV)	-	30μmols	-	TOF=0.0035s^{-1} TON=61.2	visible	12 h	-	$H_6NiSiW_{11}O_{39}$		[143]
POM@PSs@MIL-101	terephthalate	Cr(III)	-	25578 $\mu molh^{-1}g^{-1}$	-	TON=236	visible	8 h	-	$Ru(bpy)_3^{2+}$, POM		[144]
SiW_{12}@UiO-67/M/G–CdS	biphenyldicarboxylate	Zr(IV)	2.3 eV	1.27 mmol h^{-1}	-	-	visible	-	-	12-tungstosilicic acid (SiW_{12})		[145]
POM@UiO	$[Ru(bpy)_3]^{2+}$	Zr(IV)	-	699 μmol $h^{-1}g^{-1}$	-	-	visible	14 h	-	$[P_2W_{18}O_{62}]^{6-}$		[146]
Ni_4P_2@MOF-1	$[Ir(ppy)_2(bpy)]^+$	Zr(IV)	-	4.4 *m*mol $h^{-1}g^{-1}$	-	TON=1476	visible	20 h	-	$[Ni_4(H_2O)_2(PW_9O_{34})_2]^{10-}$		[147]
WD-POM@SMOF-1	hexaarmed $[Ru(bpy)_3]^{2+}$	Ru(II)	-	3,553 mmol g^{-1} h^{-1}	-	TON=392	visible	12 h	-	$[P_2W_{18}O_{62}]_6$		[148]
PW_{12}@UiO-NH_2	2-aminoterephthalate	Zr(IV)	2.66 eV	72.7 μmol h^{-1} g^{-1}	-	-	visible	-	-	PW_{12}		[149]
$P_2W_{17}Ni$@MIL-101	terephthalic acid	Cr(III)	-	883 μmol h^{-1} $gPOM^{-1}$	-	TON=33	visible	-	-	$K_8P_2W_{17}(NiOH_2)O_{61}$		[144]
Co-POM	4,4′-(1,4-phenylene)bis-Pyridine	Co(II)	-	2000 *u*mol g^{-1} h^{-1}	-	TON= 700	visible	21h	-	$P_2W_{18}O_{626}$		[150]
Cu–Ni–POM	4,40-(1,4-phenylene)bis-pyridine (PBPY) and oxalate (OX)	Cu(II), Ni(II)	-	833 μmol g^{-1} h^{-1}	-	TON = 550	UV	65 h	-	$P_2W_{18}O_{626}$		[151]
Ni_3PW_{10}@NU-1000	1,3,6,8-tetrakis(p-benzo-ate)pyrene	$Zr_6(\mu_3\text{-}O)_4(\mu_3\text{-}OH)_4(H_2O)_4(OH)_4$	-	3482μmol g^{-1} h^{-1}	-	TON=714	visible	12 h	-	$K_6Na\text{-}Ni_3PW_{10}$		[152]
$Ni_3P_2W_{16}$@NU-1000	1,3,6,8-tetrakis(p-benzo-ate)pyrene	$Zr_6(\mu_3\text{-}O)_4(\mu_3\text{-}OH)_4(H_2O)_4(OH)_4$	-	13051μmol g^{-1} h^{-1}	-	TON=2714	visible	12 h	-	$Na_4Li_5\text{-}Ni_3P_2W_{16}$		[152]
Cu_{24}-Based POM@ZZULI-1	1,3,5-tris(3-(1,3,4-triazol-1-yl) phenyl)-benzene	Cu(II), Cu(I)	1.90 eV	6614 μmol g^{-1} h^{-1}	1032 μmol g^{-1}	-	visible	-	-	$[W_{12}O_40]^{8-}$ and $[W_6O_{19}]^{2-}$		[153]
Pt-PMo/ZIF-67-800	2-methylimidazole	Co(II)	-	TOF= 1.19 s^{-1}	-	TOF= 1.19 s^{-1}	visible	-	-	$H_3PMo_{12}O_{40}$		[154]
SRG2@NMOF-1	oligo-(p-phenylene ethynylene)tetracarboxylate	Zn(II)	2.3 eV	56 μmol g^{-1}	-	-	visible	5 h	52%	sulforhodamine G		[155]

(*Continued*)

Table 2. (Continued).

				Gas evolution rate						Incorporated compounds		
Photocatalyst	Organic linker	Metal cluster	Bandgap	H_2	O_2	TON or TOF	light source	Reaction time	Efficiency	OM	NPs	Ref
NP@MOFs												
Pt@UiO-66(Zr)	terephthalate	Zr(IV)	3.05 eV	116.0 mmol g^{-1} h^{-1}	-	-	visible	-	-		Pt	[156]
CD/CdS@MIL-101(50)	terephthalate	Cr(III)	2.40 eV	14.66 μmol h^{-1}	-	-	visible	-	-		CdS quantum dots, CDs	[157]
MoS_2@ZIF-8	2-methylimidazole	Zn(II)	3.41 eV	29.9 μmol $h^{-1}g^{-1}$	-	-	visible	-	-		MoS_2	[158]
Pt@Pd-PCN-222(Hf)	tetrakis(4-carboxyphenyl) porphyrin	Hf(IV)-oxo cluster	2.14 eV	22674 $\mu mol \cdot g^{-1} \cdot h^{-1}$	-	TON= 4131.2	visible	-	-		Pt	[159]
NH_2-UiO-66 (U6N)	2-aminoterephthalate	Zr(IV)	2.76 eV	36.83 mmol h^{-1} g^{-1}	-	TON=598.67	visible	5 h	-		Pt	[160]
CDs@NH_2-MIL-125(Ti)	2-aminoterephthalate	Ti(IV)		5820.95 μmol g^{-1}	-	-	visible-	-	-		CDs	[161]
Pt@UiO-66-NH_2	2-aminoterephthalate	Zr(IV)	2.76 eV	257.38 μmol $h^{-1}g^{-1}$	-	-	visible	-	-		Pt	[127]
Pt@MIL-125/Au	benzene-1,4-dicarboxylate	Ti(IV)	3.72 eV	1743.0 μmol $h^{-1}g^{-1}$	-	TON=1677	visible	-	-		Pt	[162]
EY-Ni@MOF-5	terephthalate	Zn(II)	-	30.22 mmol h^{-1} g^{-1}	-	-	visible	2 h	16.7%		Ni	[163]
EY/NiMo@MIL-101	terephthalate	Cr(III)	1.56 eV	14.804 μmol $h^{-1}g^{-1}$	-	-	visible-	2h	75.7%		NiMo	[164]
$Cd_{0.2}Zn_{0.8}S$@UiO-66-NH_2	2-aminoterephthalate	Zr(IV)	2.87 eV	5846.5 μmol $h^{-1}g^{-1}$	-	-	visible	-	-		$Cd_{0.2}Zn_{0.8}S$	[165]
$ZnIn_2S_4$@NH_2-MIL-125(Ti)	benzene-1,4-dicarboxylate	Ti(IV)	2.74 eV	2204.2 $\mu mol \cdot h^{-1} \cdot g^{-1}$	-	-	visible	-	4.3%		$ZnIn_2S_4$	[166]
Pt/PCN-777	4,4′,4″-(1,3,5-triazine-2,4,6-triyl)tribenzoic acid	Zr(IV)	3.67 eV	586 $\mu mol \cdot g^{-1} \cdot h^{-1}$	-	-	visible	-	-		Pt	[167]
Pd@MOF-808	1,3,5-trimesic acid	Zr(IV)	3.9 eV	124 μmol g^{-1} h^{-1}	-	-	visible	-	-		Pd	[168]
BiOI@NU-1000	4,4′,4″,4‴-(pyrene-1,3,6,8-tetrayl)tetrabenzoic acid	$Zr_6(\mu_3\text{-}O)_4(\mu_3\text{-}OH)_4(H_2O)_4(OH)_4$	2.78 eV	610 μmol h^{-1} g^{-1}	-	-	visible	-	-		BiOI	[169]
Ni@MOF-5.	1,4-benzodicarboxylate	Zn(II)	-	30.22 mmol h^{-1} g^{-1}[Ni]	-	-	visible	2 h	16.7%		Ni	[163]
Pt(1.5)/MIL-125-NH-CH_2OH	2- aminoterephthalic acid	Ti(IV)	2.76 eV	4,496.4 $\mu mol \cdot g^{-1} \cdot h^{-1}$	-	-	visible	-	-		Pt clusters	[170]
Co_x/MIL-101	Terephthalate	Cr(III)	-	-	6.05 mol/min	TOF=0.012 s^{-1}	visible	70 min	-		cobalt oxide nanoparticles	[171]

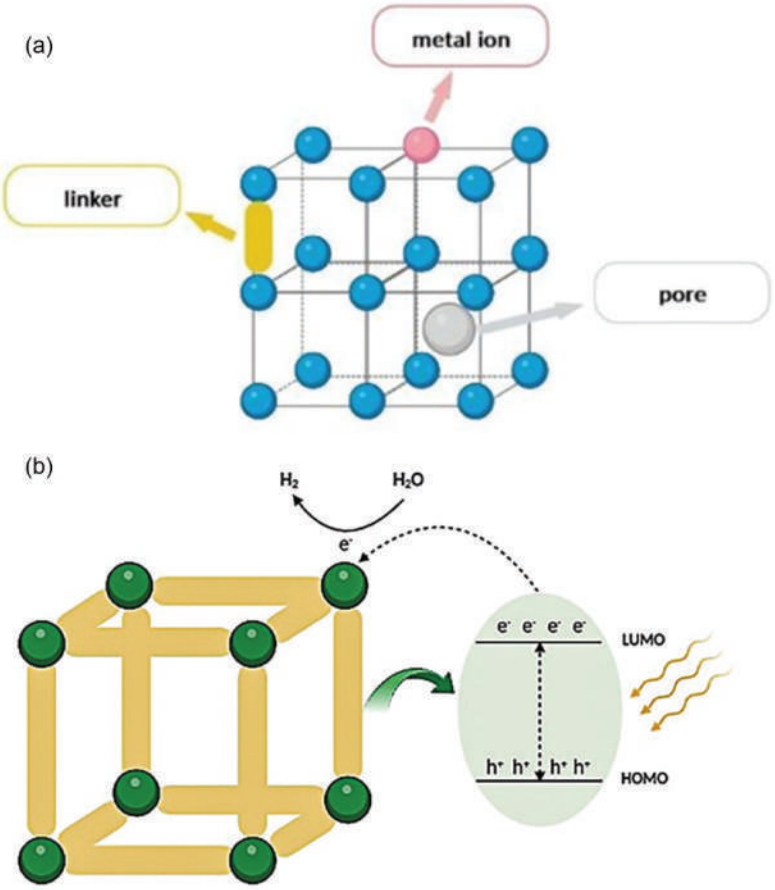

Figure 5. (a) different parts of MOFs. (b) charge migration mechanism of photocatalytic water splitting by MOF.

while metal plays the role of an acceptor. In a pristine MOF, the ligand can absorb light of different wavelengths (UV, visible, and even near IR) and excite the electrons from the HOMO of the ligand to its LUMO. The excited electrons then migrate to the metal center through ligand to metal charge transfer (LMCT) (charge separation and transport). Finally, the redox reaction proceeds in the metal node (catalytic center) as shown in Figure 5b.[160,180,181] Overall, the organic linker used in MOFs are from the aromatic family and $n - \pi^*$ or $\pi^* - \pi^*$ transitions, which occur after light absorption. The conjugated aromatic system of the linker and functional groups used for its modification depend on the wavelength of the absorbed light.[90,182,183] However, this is just a simple vision of a photo-induced catalytic mechanism in pristine MOFs. The above-mentioned three main factors can be modified by different methods to obtain a composite with the maximum hydrogen gas production efficiency.

5. Strategies for enhanced photocatalysis of metal-organic frameworks

The modification of MOFs can involve different parts of pristine MOFs including their organic linker (1st method), or by applying other compounds into the cage of MOFs (2nd method), or both. The first two methods will be explained and the third one is the combination of both methods, which is carried out based on the final use (Figure 6). In the first method, different functional groups are utilized to improve the properties of MOFs such as their porosity, crystallinity, stability, flexibility, and topology. These properties are improved as the functional groups enhance the host-guest chemistry between MOFs (host) and other molecules (guest).[184,185] The functional groups can be categorized based on their role in MOFs or their chemical properties (Figure 6). The role-based functional groups are categorized into coordinating sites and the guest interactive sites as presented by Absalan and coworkers as well as the categorization of functional groups by their chemical properties.[184]

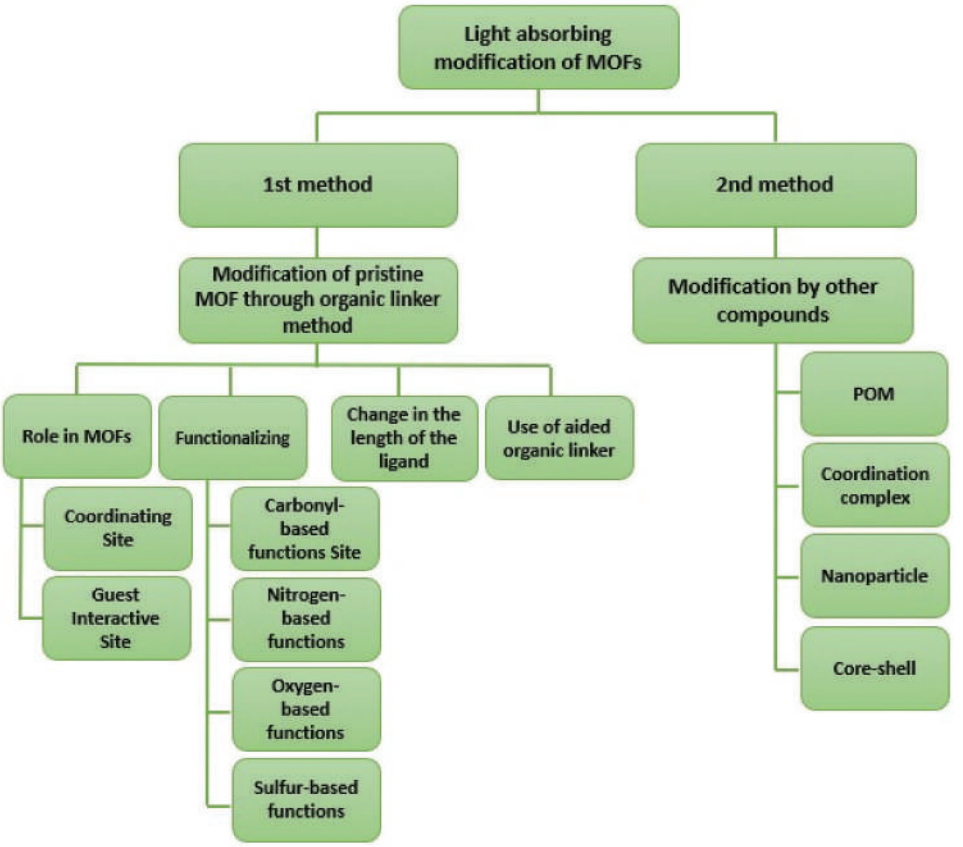

Figure 6. Different methods for modification of MOFs.

The coordinating site functional groups, including sulfonate, phosphonate, carboxylate, and some of the heterocyclic groups (pyridine, azoles, diazines) surround the metal ion in a self-assembling process. On the other hand, guest interactive site functional groups are free to interact with other molecules (guest) and the main functional groups. Urea, amide, oxalamide, imide, triazine, and tetrazine are mostly used as interactive site functional groups (Figure 7). For coordinating site functional groups, the effect of the functional groups must be determined based on reaction solvent, temperature, pH, and metal ions. On the other hand, for guest interactive site functional groups, the effect of the functional groups on the direction of the coordination sites must be researched. In the case of changing the direction of the coordinating site by the functional groups, the chemical structure will be altered, thus, the geometry and the chain must be examined.Additionally, the stability of the chemical structure of MOFs and structure-activity relationship should be considered.[185] Various elements of the periodic table are used in different parts of water splitting photo-induced catalysts[21] (Figure 8a). Based on the hard and soft acid and base (HSAB) theory concerning hard metal – hard base and soft metal – soft base (Figure 8b), the proper metal is chosen based on the ligand.[187–191]

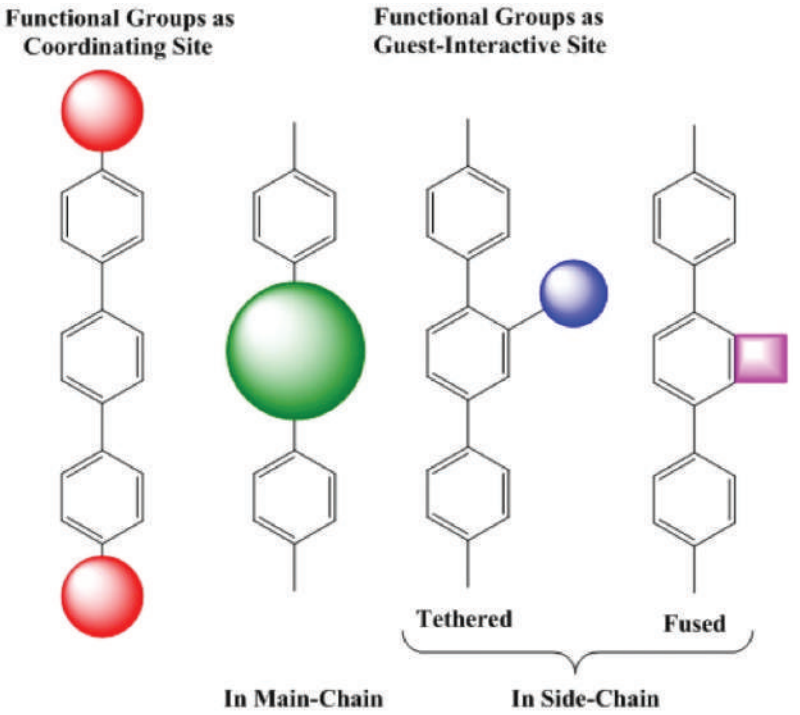

Figure 7. Classification of organic functional groups based on their role and position in the framework. Reprinted with permission from Ref.[184] copyright 2019 elsevier publication.

Figure 8. (a) elements used in different parts of photocatalysts for water splitting. (b) strategies to construct stable MOFs guided by HSAB theory. Reprinted with permission from Ref.[186] copyright 2018 advanced materia.

Other methods of synthesizing MOFs with improved properties utilize nanoparticles,[192–195] metal oxides,[196–199] silica,[200–202] organic polymers,[203–205] quantum dots,[206–210] carbon discs and nanotubes,[211–214] thin films,[73,215] core–shell encapsulation,[216–218] enzymes,[219–224] and organometallic compounds.[225–239] The incorporation of other compounds into the cage of MOFs assists in synthesizing a composite with excellent optical behavior, thermal and chemical stability, and significant catalytic active sites.

5.1. Molecular modification approach

Regarding light absorption, we investigated the main general challenges in the photocatalytic water splitting reaction. In this section, we will go forward more specifically to find what happens if the photocatalyst is a MOF. The most applicable pristine MOFs for water splitting are listed in Table 2.

First of all, we need to know what parts of MOFs are responsible for absorbing light when there is just pristine MOF. Based on the different reports, the organic linker of a pristine MOF is responsible for absorbing light.[240,241] Although, there are some pristine MOFs, in which metal-oxo clusters play an important role in absorbing visible light[242,243] such as Fe-based MOFs, including MIL-53(Fe),[244] MIL-68(Fe)[245] and MIL-100(Fe),[246] organic linkers demonstrate a significant role in tuning the light absorption.

When using pristine MOFs, the main challenge is finding a proper organic linker with the required properties. First, let's see why organic linkers are used in MOFs. Are they used just for absorbing light? To answer this question, first we need to look deeper into the structure of MOFs. The other role of organic linkers is to connect with the existing metal ions in the framework of MOFs. Furthermore, MOFs must maintain their stability in different environments to avoid disintegrating their chemical structures. Moreover, linkers contribute to better electron transport. Porosity, flexibility, and crystallinity are also other properties that can be altered using different organic linkers.[247–250]

Regarding light absorption, the photonic response, can be altered by three methods: ***the change in the length of the ligand***, ***use of an aided organic linker***, and ***replacing or adding functional groups***[251] (Figure 9).

5.1.1. Ligand length extension

The change in the length of the ligands can enhance the light absorption.[252] It also helps in encapsulating extra compounds (such as OMC or NPs) into the cage of MOFs, which can increase the light absorption ability of MOFs. This approach also prepares an opportunity to functionalize MOFs by more functional groups. This strategy has been used by different researchers and resulted in the synthesis of MOF whose properties were eleven times greater than the original MOF. Yaghi and coworkers synthesized a reticular IRMOF-74-I to IRMOF-74-XI by the mentioned strategy.[253] They extended the length of MOF-74 by phenylene ring from one to eleven. The same method was used to synthesize a series of NOTT,[254] UiO,[255] and FCU.[256]

Allendorf and coworkers[252] published theoretical models of organic linkers for light harvesting applications (Figure 10). The organic linkers are capable of donating electrons to the acceptor site of organic photovoltaics under UV-Vis light by tuning the HOMO-LUMO gap (Table 3). Such a difference between the organic linkers can be assigned to their different lengths, achieved by adding up to 11 phenylene rings (DOT I-XI) (Figure 10).

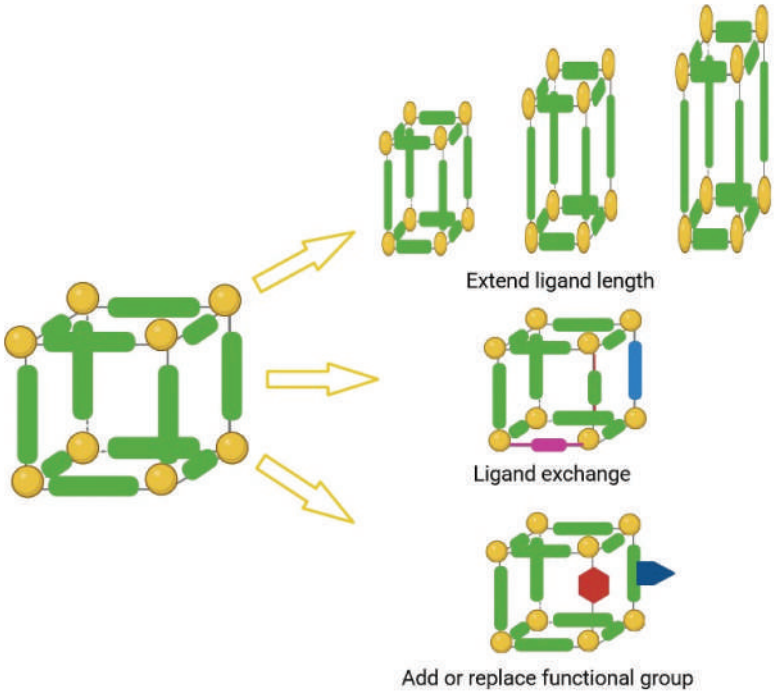

Figure 9. The methods used for functionalization of organic ligands.

The basis for creating these linkers and Secondary building unit (SBU) is to establish a connected π-π network for easy charge transfer. A series of transition metals, including Mg, Mn, Fe, Co, Ni, and Zn has been applied in the structure of MOFs containing the mentioned organic linkers. As an example, the combination of the organic linkers with the Mg ion led to a MOF with an unusual structure (Figure 10). The resulting MOF had no d electrons and Mg^{2+} did not allow MLCT or LMCT, which leads to the formation of HOMO-LUMO on the organic linkers resulting in separation between the linker and the electron acceptor. The mentioned reasons lead to the formation of a MOF whose electronic properties can be ascribed to its organic linkers. The modification of the organic linkers helps the MOF absorb visible light because of the small energy band gap and high oscillations. Furthermore, the obtained MOF will split easier due to its suitable band and acceptor molecules.

5.1.2. Ligand exchange

The strategy of using another linker is helpful when a functional group cannot be directly synthesized. Furthermore, it is a good approach for the synthesis of a thermodynamically unfavorable MOF. Kim and coworkers studied the exchange of carboxylate organic linkers in different MOFs, including MIL-68(In), MIL-53(Al), UiO-66(Zr), and ZIF-71.[257] Their result showed that

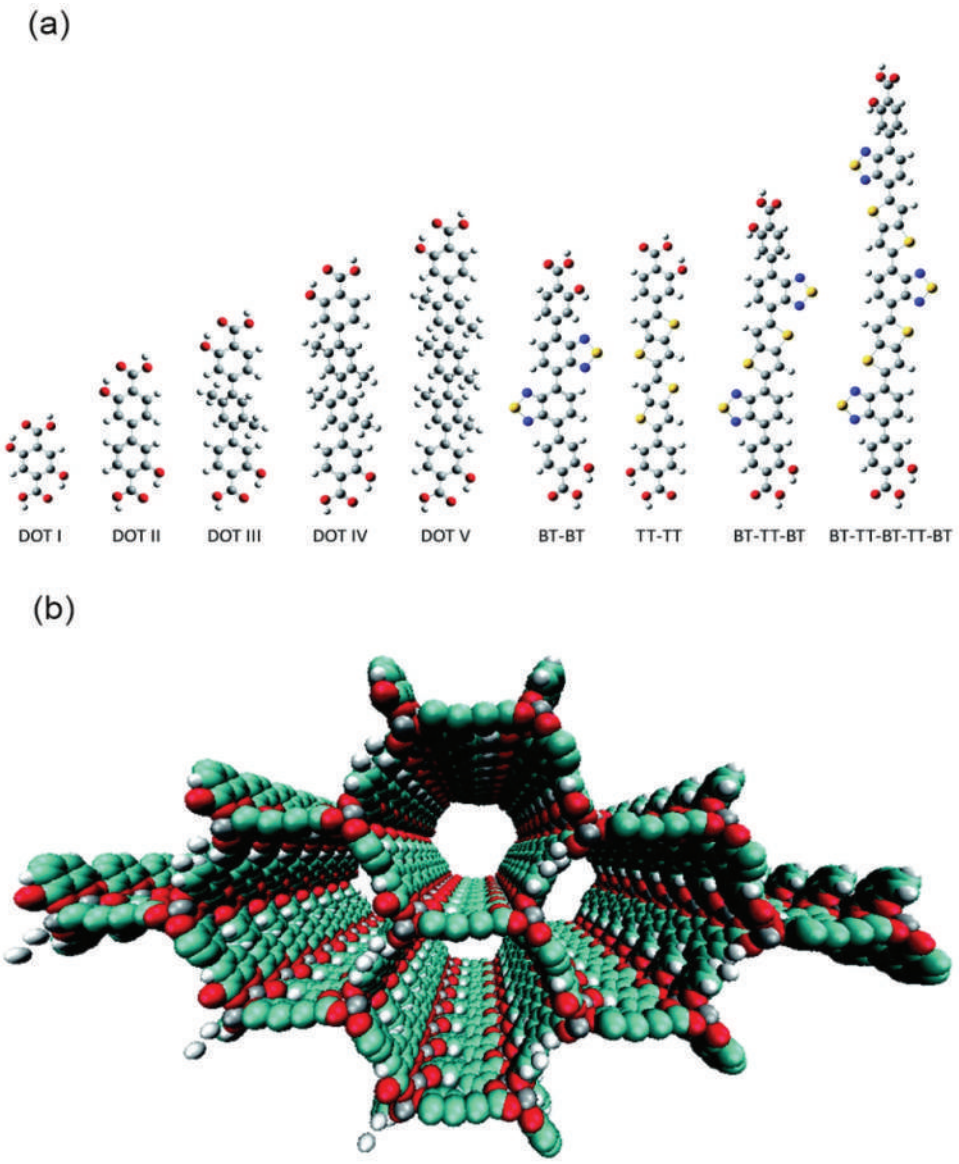

Figure 10. (a)the LC-BLYP/6-311G(d,p) optimized DOT I-VI linkers and proposed BT/TT linker series. (b)A supercell representation of the periodic PBE optimized IRMOF-74-II(Mg) structure. Reprinted with permission from Ref.[252] copyright 2014 RSC chemistry.

MIL-53(Al)-Br/NH_2 is received by the combination of MIL-53(Al)-NH_2 and MIL-53(Al)-Br MOFs. The same experiment was also carried out by other researchers.[258] The pore dimensions in the MOF materials can be increased by replacing the shorter linkers with longer ones with no loss of crystallinity. This technique is beneficial because it 1) increases the porosity of MOF; 2) avoids the possibility of interpenetration, provided that a non-interpenetrated MOF is used as the starting material; and 3) produces thermodynamically

Table 3. Optimal values, HOMO/LUMO energies, fundamental gaps (HOMO-LUMO), optical gaps (S0 →S1 transition) and oscillator strengths of DOT IV and the BT/TT series predicted at the LC-BLYP/6-311 G(d,p) level of theory. All values are in eV; oscillator strengths are unitless. Reprinted with permission from Ref.[252] copyright 2014 RSC chemistry

Linker	Optimal μ	HOMO	LUMO	Fundamental gap	Optical gap	Oscillator strength
DOT I	.2715	−7.9	−0.6	7.3	3.3	0.115
DOT II	.2507	−8.4	−0.5	7.9	4.1	0.304
DOT III	.2089	−7.9	−0.4	7.5	4.1	0.407
DOT IV	.2021	−7.8	−0.3	7.6	4.1	0.367
DOT V	.1811	−7.7	−0.4	7.3	4.0	0.350
TT–TT	.1829	−6.9	−1.0	5.8	3.1	2.161
BT–BT	.1825	−7.4	−1.8	5.6	2.8	0.813
BT–TT–BT	.1655	−6.7	−1.9	4.8	2.4	1.384
BT–TT–BT–TT–BT	.1420	−6.2	−2.2	4.1	1.9	2.066
PCBM	.1958	−7.4	−2.1	5.3	2.3	0.002
PC71 BM	.1724	−7.1	−2.2	4.9	2.2	0.006
P3HT	.1419	−5.9	−1.0	4.9	2.6	2.434

unfavorable structures. As an example, bio-MOF-101 was converted to bio-MOF-100 via exchanging 2,6 -naphthalenedicarboxylate (NDC) with 4,4'-biphenyldicarboxylate (BPDC).[258]

Another ligand exchange approach involves bridging-ligand replacement in extended 2D and 3D MOFs. For instance, crystals of PPF-18 were transformed to crystals of PPF-27 by exchanging the bridging linker of *N,N*'-di-pyridyl-naphthalenetetracarboxydiimide (DPNI) with 4,4' -bipyridine (BPY).[259]

5.1.3. Surface functionalization

Functionalization of organic linkers by other groups such as carbonyl-based, nitrogen-based, oxygen-based, and sulfur-based groups is an attractive strategy[260,261] (Table 4).[184] Carbonyl-based functional groups have mutual host-guest chemistry due to the presence of the carbonyl group while the differences in the host-guest chemistry are mainly because of the groups such as amine and hydroxyl attaching to the carbonyl group. The nitrogen-based groups have N and they are mainly used in the structure of MOFs. Oxygen-based functions are polar and rich in electrons due to the high electronegativity of the oxygen atoms. Sulfur-based functional groups also offer several advantages including electron-rich sulfur atoms which can be exploited in the design of polar and electron-rich MOFs. The use of different functional groups can provide several advantages, including flexibility and easy tuning through in-situ syntheses, post-synthesis, or linker exchange.

The effect of different functional groups on the organic linker of NU-1000 MOF was investigated.[181] The study showed that the functional groups affect highest occupied crystal orbital (HOCO) and lowest unoccupied crystal orbital (LUCO).[262] Researchers functionalized NU-1000 with carboxylates,[263]

Table 4. Common functional groups commonly used in the synthesis of MOFs

(I) Carbonyl-based functions: *urea*, *amide*, *oxalamide*, *squaramide*, *ketone*, *imide* and *carboxyl*.

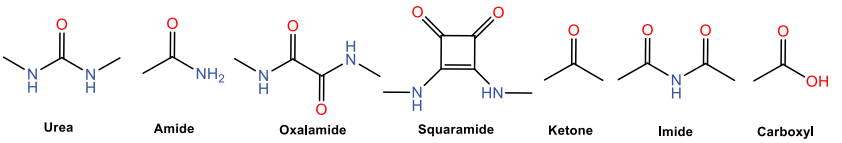

(II) Nitrogen-based functions: (a) *heterocyclic azine N-based functions*, (b) *heterocyclic-azole Based functions*, (c) *noncyclic N-based functions*, and (d) *ionic N-based functions*.

(a) Heterocyclic azine-based functions: In this group, the (–CH) motifs in the benzene ring are replaced by nitrogen atoms.

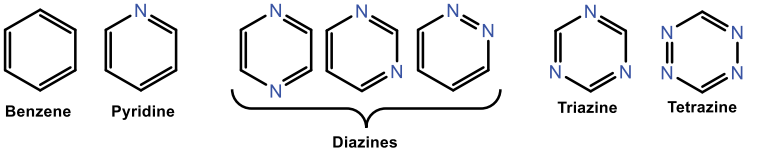

(b) Heterocyclic azole-based functions: They have Lewis basic nitrogen atoms with sp^2 hybrid acting as coordinating and guest interactive sites in supramolecular chemistry and construction of coordination complexes and polymers especially MOFs.

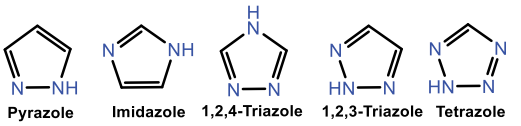

(c) Acyclic N-based functions: They include sp^2 and sp^3 hybrid nitrogen atoms.

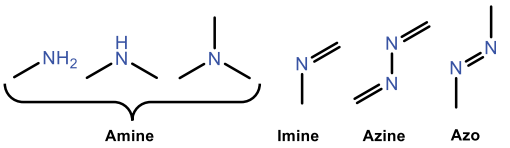

(d) Cationic N-based functions: They interact with anionic, polar, and quadrupolar species through electrostatic interaction, dipole-dipole and dipole-quadrupole interactions. The obtained MOF offers a new method for synthesizing ionic MOFs.

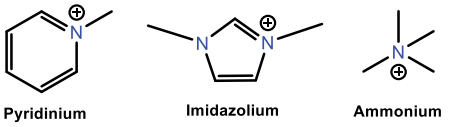

(III) Oxygen-based functions: *hydroxy*, *ether*, *N-oxide*, *azoxy*, *oxodiazole*, and *oxopyridine*.

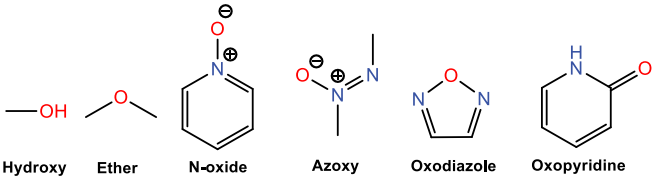

(*Continued*)

Table 4. (Continued).

(IV) Sulfur-based functions: *thiol*, *sulfide*, *sulfonate*, *thiourea*, *thiadiazole*, and *thiocatechol*.

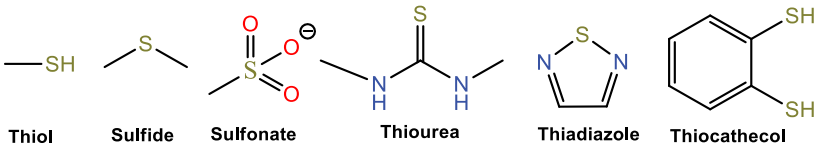

(V) Other functional groups: halogen-based functions fluoro, nitro, and phosphonate.

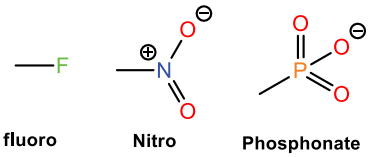

phosphonates,[264] perfluoroalkanes,[265] and fluorine.[266] The results illustrate varied behaviors of MOFs as a result of different functionalization methods. However, it is possible to prepare two main categories: donor (F, Cl, I, CN, CHO, and NO_2) and acceptor (OH, $OCOCH_3$, NH_2, and $N(CH_3)_2$) (Figure 11)

The popular MOF PCN-415 exhibits energy band gap at 3.3 eV, which does not permit the use of MOF in visible light. The same limitation is also observed in other MOFs systems including UiO-66 and MIL-125. Modification with amino groups showed a redshift toward the absorption of visible light[267]

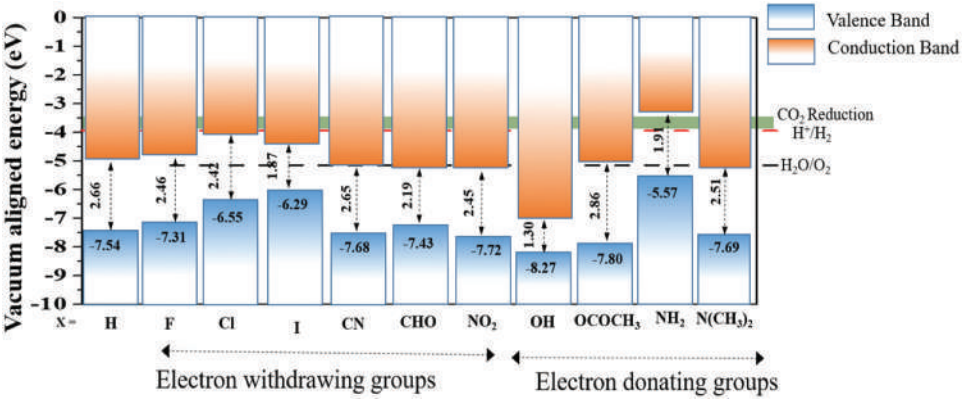

Figure 11. Band edge alignment of Cd_6Se_6@NU-1000 and linker-functionalized Cd_6Se_6@NU-1000. HOCO and LUCO are from the linker and the CdSe for all of the cases. The horizontal black and red dashed lines correspond to the standard electrode potentials (ε°, in V vs SHE) of the OER and HER, respectively, at pH = 7 and T = 298.15 K. The green band corresponds to the standard electrode potentials (ε°, in V vs SHE) of CO_2 reduction in aqueous solutions at pH = 7 and T = 298.15 K. The valence band is the blue lower bar, while the conduction band is the orange upper bar. The HOCO is the top of the blue bar, and the LUCO is the bottom of the orange bar. The band gap (in eV) is written between the bars. Reprinted with permission from Ref.[181] copyright 2020 ACS publication.

Eddaoudi and coworkers replaced 1,4- naphthalenedicarboxylate functional group in the face-centered cubic (FCU) MOF with different groups, including 2-aminoterephthalate (BDC-NH_2), 2-fluoro terephthalate (BDC-F), or 2-nitroterephthalate (BDC-NO_2).[268] Zhang and coworkers used a post synthesis strategy for the modification of organic linkers by functional groups.[269] They applied a methyl group on the pyridyl site of MOF-867. The diazotization method was also employed for replacing amino groups by the azide group in MOFs. The method is reversible by the usage of H_2S.[270] Organic functional groups have also been used to alter the photonic response of the organic linker of MOFs. Forgan and coworkers functionalized Zr-MOFs with naphthyl and benzothiadiazole.

One of the most challenging issues in the light absorption and use of functional groups is the interpretation of the chemical structure-light absorptivity relationship, which is structure- and solvent-dependent. For example, Moggach and coworkers designed ZIF-90 and ZIF-65 with polar functional groups.[261] Their results showed different effects of the same functional groups when comparing ZIF-90 and ZIF-65. Higher light absorption is another advantage of the proper functional group. Silva and coworkers used UiO-66 for hydrogen gas production from water. They reported an increase in hydrogen gas evolution from 2.4 to 2.8 ml just by adding NH_2 to the structure of UiO-66 MOF.[69]

Wan and coworkers employed methylthio via terephthalic acid ligand to obtain MIL-125 by the post synthesis strategy[107](Figure 12a). The modification led to the formation of a composite capable of absorbing visible light due to the presence of the methylthio group donating 3p electrons of S to the aromatic rings (Figure 12b). This functional group illustrates absorption even better than the amino group, showing a 9% rise in the hydrogen gas production efficiency from water.

It should be noticed that, although organic linkers play as electron donors (VB; HOMO) in MOFs, in some cases metal ions also illustrate the same behavior and help in enhancing the light absorption. For example, Shi and coworkers synthesized three types of MOFs based on Cu-X-bpy, where X=Cl, Br, I) for the photocatalytic water splitting.[271] The halogen atoms changed the energy band gap to 1.85 eV (Cl), 1.90 eV (Br), and 2.00 eV (I) (Figure 12c). The DFT calculations illustrates that the CB and VB are related to the organic linker (2p orbitals) and copper ions (3p orbitals). The electrons migrate from the metal ions (Cu_2X_2) (VB) to the N and C atoms of the organic linker and the reduction of water proceeds.

Lu and coworkers synthesized MOF based on the indium (III) to be used as a photocatalyst for H_2 production.[95] In (III) was employed as it is a P-block metal which can alter its valence to produce various forms with different chemical behaviors. In (III) also exhibits high photoluminescence properties

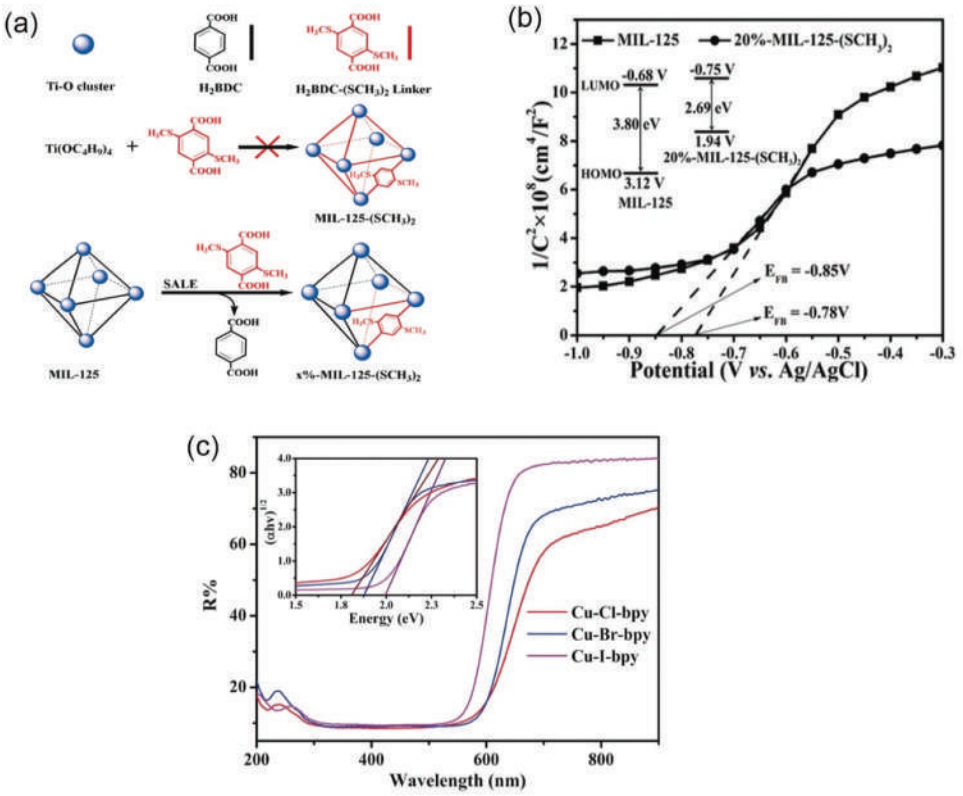

Figure 12. (a) synthesis diagram of x%-MIL-125-$(SCH_3)_2$. Reprinted with permission from Ref.[107] copyright 2017 German Chemical Society (b) mott-schottky plots of MIL-125 and 20%- MIL-125-$(SCH_3)_2$. Reprinted with permission from Ref.[107] copyright 2017 German Chemical Society (c) the UV–vis DRS of cu-X-bpy. Inset: tauc plots. Reprinted with permission from Ref.[271] copyright 2017 German Chemical Society.

because it is a d^{10} metal. Due to its low splitting energy, this element can enhance the light absorption.[272–277]

In addition to the mentioned discussions, the photosensitization of the organic linker should be close to the metal center. Lan and coworkers synthesized two new MOFs based on Ruthenium (Ru) and porphyrin derivatives to be used as water splitting photocatalysts.[278] In addition to the self-properties of porphyrin in absorbing light, the photosensitizing properties of porphyrin are also close to Ru which can increase the number of excited electrons from VB to CB, enhancing HER activity around 30 times more than that of homogeneous catalysts. Besides the close photosensitization, porphyrin is also an effective parameter. Porphyrin is a strong organic heterocyclic compound capable of absorbing visible light, and so is suitable starting material for the synthesis of different MOFs.

Zhao and coworkers synthesized two-dimensional MOFs using transition metals and tetrazole annulene for water splitting.[279] Tri-functional MOFs catalysts such as Ir-TAAA and Rh-TAA demonstrated proper features comparable with other well-known visible-light water splitting photocatalysts. Ir-TAA is a highly active photocatalyst for the reduction of water with ΔG of 0.17 eV. Moreover, Rh-TAA also showed excellent photocatalytic behavior with the OER of 0.4 V and ΔG <0.33 eV, compared with Pt/RuO_2 (an oxide photocatalyst).[280] Further, Fe-based MOFs showed high activity toward absorbing visible light because of their Fe-oxo-cluster. Iron-based MOFs are becoming increasingly popular in use for water oxidation reactions. These MOFs are efficiently used in the catalysis of water splitting to produce hydrogen gas.[281,282] In addition, absorption of visible light by highly active trinuclear clusters of Iron-based MOFs such as MIL-188, MIL-101, and MIL-126 can be increased by adding an amino group on the organic linker.[283] Moreover, Lionet and coworkers[284] reported on the Iron-based MOFs (MIL-88B) with the organic linker terephthalic acid and different functional groups (Figure 13).

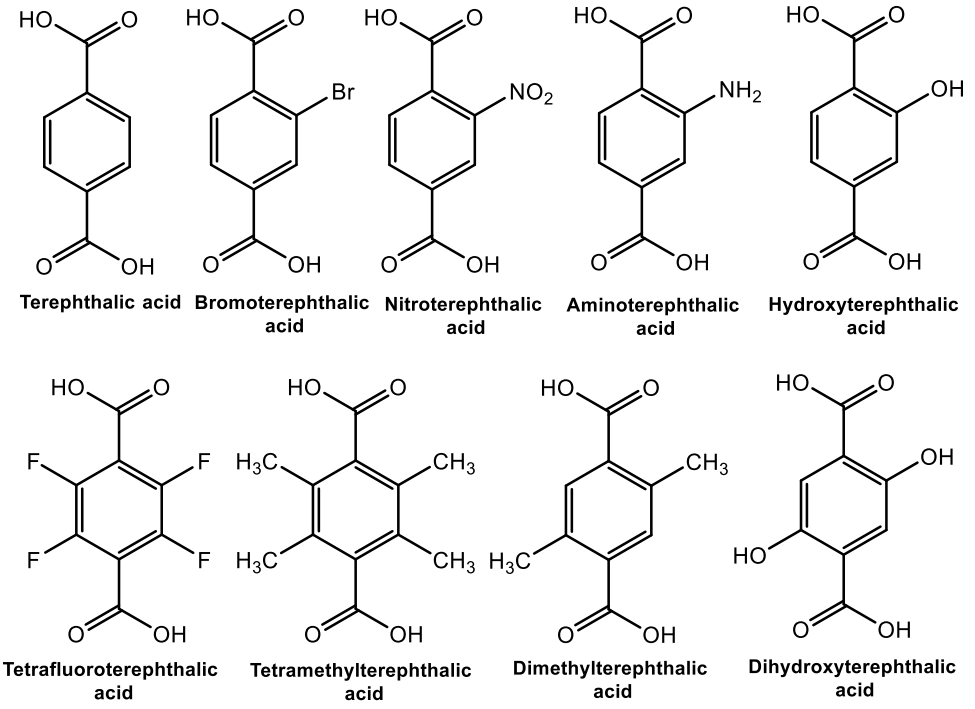

Figure 13. List of linkers employed for MIL-88B synthesis. Reprinted with permission from Ref.[284] copyright 2019 ACS publication.

The developed MOFs were tested for the water oxidation reactions. The results showed the electron-donating and electron-accepting properties of the organic linker and the metal ions, respectively. The use of tetrafluoroterephthalic acid, as the organic linker, led to a five-fold increment in the activity of the MIL-88B MOF compared to its pure form. It should be noticed that functionalization is not always effective. For example, Horiuchi and coworkers explored all functionalized organic linkers (except tetrafluoroterephthalic acid) and showed lower photocatalytic activity compared to the pristine MOF. The reason for this disadvantage could be the diversity in hydroxylation rates of the organic linkers. However, it is possible to use some active or reactive groups for adjusting the hydroxylation rates.

Besides the surface activity and the energy band gap, electronic structure is another effective parameter. As some systems did not show proper photocatalytic behavior even with the best surface activity and the energy band gap. According to Shen and coworkers, electronic structure is a key parameter which needs to be accurately investigated.[285] They did experiments using a series of UiO-66-MOFs that were functionalized with NH_2, NO_2, and Br in reference to a control UiO-66-MOF that had H in place of NH_2, NO_2, and Br. They employed three functionalized-UiO-66 as photocatalysts for the oxidation of aqueous As(III) reaction. The liquid-solid reactions largely depend on the surface activity of the photocatalysts.[286] Theoretically, a photocatalyst with larger surface activity can better catalyze a liquid-solid reaction due to the improved transition of charge carriers. The experiment showed that the order of the surface activity is as follow: UiO-66-H > UiO-66-NH_2 > UiO-66-NO_2 > UiO-66-Br, but the rate of the reaction was decreased as follow: UiO-66-NH_2 > UiO-66 > UiO-66-Br > UiO-66-NO_2 (Figure 14).

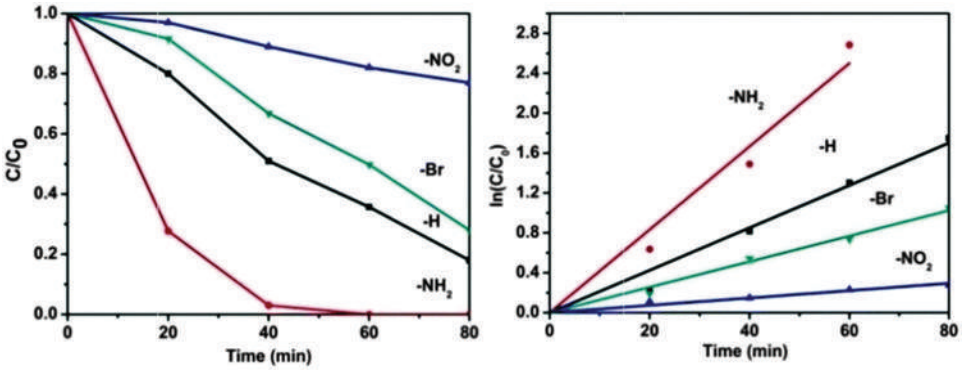

Figure 14. Photocatalytic oxidation of aqueous As(III) over UiO-66-X (X = H, NH_2, NO_2 and br) under simulated sunlight (320–780 nm). Reaction solution: 40 mg photocatalyst, 40 ml2mg L^{-1} As(III) aqueous solution. Reprinted with permission from Ref.[285] copyright 2014 RSC chemistry.

Further study confirmed the critical role of electronic structure in the photocatalytic behavior of the catalyst as supported by Hammett's σ_m values. The mentioned value demonstrates how various substituents affect the electronic behavior of a given aromatic structure.[287] The positive and negative values of σ show the electron-withdrawing and electron-donating groups, respectively. The correlation can be found by the plot obtained from log Kx versus σ_m (Table 5).

The plot illustrates the reason for the best activity of NH_2 despite its smaller surface activity (Figure 15)

MOFs can be modified in terms of organic linker and metal ions. However, organic linkers play a more important role in light harvesting and it is possible to absorb even visible light by a proper design and modification. However, the maximum absorbed wavelength is reported to be 500 nm for an electron donor such as triethanolamine.[289] Hydrogen gas is not evolved even in the presence of methanol or ethylenediaminetetraacetic acid (EDTA) as a sacrificial electron donor. The limitation is associated with the low visible light responsivity and low oxidation ability of the organic linker in MOFs, necessitating the modification with extra organic linkers with high photo-response and low frontier orbitals (HOMO-LUMO) in the visible range with proper location of HOMO (1.23 eV), which can be obtained by incorporation of other compounds such as OM and NPs.

5.2. Molecular association approach

Light harvesting is one of the most important parts of photocatalytic water splitting. Two main methods can be used to enhance the light absorption ability of MOFs. In the first method, pristine MOFs is modified through functionalization which changes the length of the ligands using different organic linkers. The second method involves the incorporation of other compounds including organometallic compounds and nanoparticles in the cage of MOFs.

Modification of MOFs by applying OMC is one of the most effective approaches, not just in absorbing a corresponding type of light, but also in providing an opportunity to properly adjust the valence and conduction bands.

Table 5. Apparent first-order rate constants K_X, relative initial rates with respect to the unfunctionalized material. Reprinted with permission from Ref.[285] copyright 2014 RSC chemistry

UiO-66-X	$K_x[h^{-1}]$	Log K_x/K_H	σ
H	0.0266	0	0
NH_2	0.0417	0.3443	−0.161
NO_2	0.00369	−0.6747	0.71
Br	0.0128	−0.3040	0.393

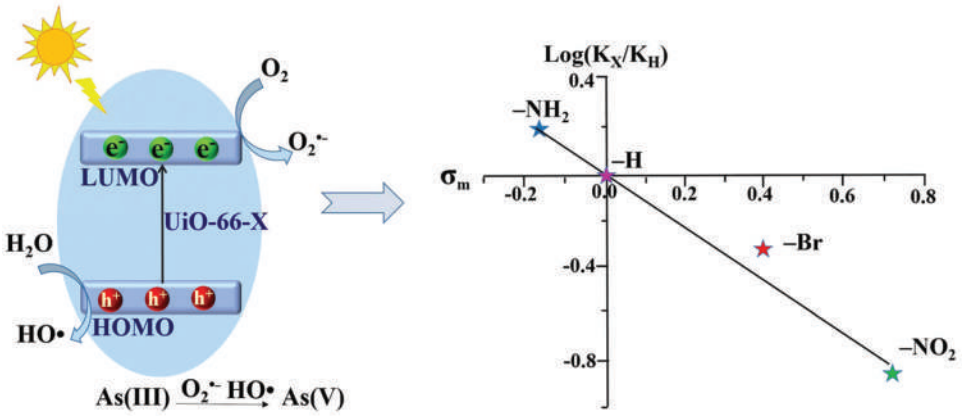

Figure 15. Proposed mechanism (left) and Hammett plot (right) for photocatalytic oxidation of As(III) by UiO-66–X (X = H, NH_2, NO_2 or br). Reprinted with permission from Ref.[288] copyright 2019 RSC chemistry.

Numerous OMCs with different structures have been loaded into the sites of MOFs among which, POMs, free noble coordination complex of Ni, Co, and noble metal coordination complexes such as Pt, and Rh can be mentioned.[45,141]

The pores of MOFs offer proper sites to load OMC. Loading OMC into MOFs with different organic linkers and metal ions can enhance its photocatalytic ability. HER is most affected by the application of OMCs. OMCs behave as co-catalysts, assisting in migration of electrons by reducing their recombination with holes. The most effective role of OMCs is tuning the band gap of the final composite. In some cases, they extend the absorption of final composite to longer wavelengths such as visible or near IR.

Regarding light absorption, chromophore properties are the most required characteristics of the organic ligands in OMCs. The chromophores are involved in some important functions, including (i) proper reactivity and sufficiently prolonged excited state for light absorption (ii) The capability to be incorporated in the directional transfer of electrons by a quenching mechanism, and (iii) generating the ground state through further extra redox reactions. Some popular chromophores have been used for the photocatalytic water splitting such as acridine dyes, metalloporphyrins, transition metal phthalocyanines, and noble metal complexes.[290]

The energy of the organic linker can be transferred from different functions to porphyrin, including naphthyl moiety or pyrene through different bonds including molecules or hydrogen bonds.[291] Among different porphyrin derivatives, triphenylamine-based multibranched porphyrin molecules can serve

as sensitizers in a composite, further contributing to the photocatalytic water splitting.[292]

The attractive properties of nanoparticles (NPs) due to their small size make them a promising additive for MOFs. The small size of nanoparticles leads their high surface to their volume ratio, enhancing their catalytic activity. Two types of NPs have been encapsulated in MOFs: (i) plasmonic NPs (Au,[293,294] Ag,[295,296] and Al[297]) which are used to perfuse hot electrons and (ii) NPs with high catalytic activity (Pt[298,299] and Au@PtAg[300]) which are used to trap electrons.

According to the synergistic effect and the ability of MOFs for immobilizing NPs, the electron transport from MOF to NPs will be facilitated, incrementing visible and even NIR lights absorption.

5.2.1. Incorporation of coordination metal complexes

Noble metal complexes showed excellent ability in absorbing light; thus, their application into the pores of MOFs could be a versatile method to extend light absorption to the visible range. Yang and coworkers synthesized Ru-complex-sensitized MIL-125-NH_2(Ti) through encapsulation of RuII-polypyridyl complexes into the MOF.[301] It should be noted that encapsulation of complex compounds into MOFs can mutually assist in enhancing the ability of the final composite. For example, $[Ru(bpy)_3]Cl_2$ used in the previous experiment is a homogeneous catalyst with difficult recycling in an aqueous reaction. Using MOFs, it can be converted to a heterogeneous catalyst. Yang and coworkers showed a reduction in the energy band gap of MOFs from 3.7 eV to 1.72 eV upon using the Ru-complex, which makes the final composite absorb visible range. Horiuchi and coworkers incorporated Ru(II) complex (bis(40-(4-carboxyphenyl)-terpyridine); $Ru(tpy)_2$) into Ti-MOF (MIL-125-NH_2(Ti)) to be used as a hydrogen gas production photocatalyst.

As an incorporated coordination complex, $Ru(tpy)_2$ can absorb visible light (620 nm) due to its lower HOMO level compared to the organic linker of the MOF (BDC-NH_2), making it a proper coordination to be encapsulated in MOFs. In addition to the mentioned advantages, the final composite can work with different sacrificial electron donors such as triethanolamine (TEOA) and EDTA, offering wider flexibility in the operation.

Platinum is a noble metal used a lot for photocatalytic water splitting under visible light. Pt is usually used in the colloidal form or diffused on the surface of the support through covalent interactions between platinum and porphyrin.[302,303] Iridium and complexes are two other noble complexes which can be used for harvesting visible light. Ir(III) complexes have the ability of the direct electron transferrin for reducing, long excited-state lifetimes, and high photosensitizing ability, which develop the MLCT transferring.[304] However, Ir complexes cannot withstand high temperatures

in addition to difficult separation.[305] The economic issues are one of the main drawbacks of the noble metals, which further limit their applicability.

There are some OMCs free of noble metals which have been encapsulated into MOFs. Li and coworkers loaded Co(II) complex into MIL-125-NH_2 (Ti) cavities with different concentrations through the ship-in-bottle method for hydrogen gas production through water splitting.[140] The result showed that the UV-Vis range can be strongly absorbed by loading C(II) complex which increased by raising the concentration of Co(II) complex. Similar work was also carried out by Reek and coworkers.[141]

Natural phenomena have always been the best guide for the development of science in different areas. Photosynthesis is also one of these phenomena, which can be the best guide for the photocatalytic reactions. Various researchers use it for mimicking the photocatalytic water splitting.[306,307] Photosynthesis uses sunlight for hydrogen gas production. This phenomenon occurs in three steps: light-absorption (chlorophyll), electron transfer, and water splitting into hydrogen and oxygen gases. All these steps are conducted by a hydrogenase enzyme (H_2ases). The best-known enzymes are [Fe]–H_2ases, [NiFe]–H_2ases and [FeFe]–H_2ases as they can reduce protons to hydrogen gas between 6000 and 9000 H_2/s.[308] Organometals have been widely used for the synthesis of H_2ases. Diverse $[Fe_2S_2]$ complexes were synthesized to mimic the photosynthesis process for hydrogen gas production. Porphyrin derivatives are the most useful organic linker in photocatalytic application, especially water splitting, due to their strong visible light absorption. Feng and coworkers synthesized a new composite from organometallic $[Fe_2S_2]$ complex $[(1\text{-}SCH_2)_2NC(O)C_5H_4N]$–$[Fe_2(CO)_6]$ coupled with a zirconium-porphyrin MOF. The final composite showed high ability in harvesting visible light, due to the presence of porphyrin (organic linker), Zn (metal ion of MOF), and $[Fe_2S_2]$ complex. The structure of the composite is constructed by the porphyrin, which coordinates the Zn metal ion in the center, coupled with $[Fe_2S_2]$ complex through different bonds.

The same experiment was also carried out using different compounds ($[Co^{III}(dmgH)_2(py)Cl]$ complex (dmgH = dimethylglyoximate and py = pyridine) and Zn(II)-porphyrin) under visible light by other researchers.[309]

The uniformity of the final composite also plays an important role in absorbing light. The incorporated OMCs on the surface of MOFs do not allow the final composite to absorb higher wavelength light.[310] The same method has been also carried out with the noble metals using porphyrin, where two noble metals are connected together (Figure 16). The system exhibited excellent photocatalytic water splitting.[311,312]

The higher activity is because of the electron density due to the π donating iodo ligands.[313,314]

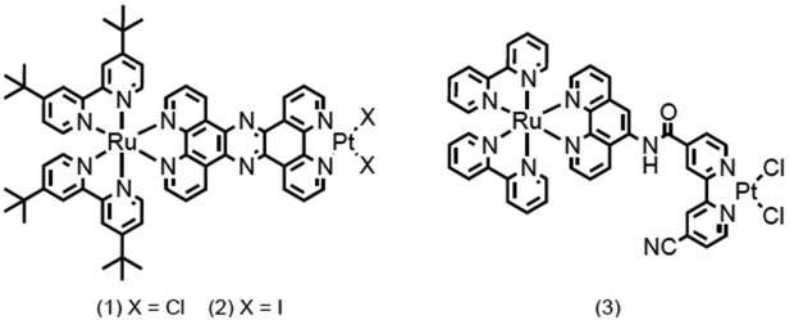

Figure 16. Molecular structure of selected heterodinuclear ru-pt hydrogen evolving complexes. Reprinted with permission from Ref.[290] copyright 2017 ChemPubSocEurope.

5.2.2. Incorporation of polyoxometalates (POMs)

POMs have been used in different MOFs for water splitting and hydrogen gas production due to their fascinating properties.[149,151–153,315–317]

They are categorized as anionic metal oxide clusters, which are mostly formed through the first-row transition metals, including Mo, V, W, Nb, and Ta with the highest state (+4, +5, and + 6).[318] Some properties such as using d^0 transition metals, oxide ions, and the same electronic behavior (well-constructed HOMO-LUMO orbitals) make them similar to semiconductors.[319,320] POMs offer fast photoresponsivity at redox reactions due to their ability to store electrons and protons in just one molecule.[321] However, they suffer from some disadvantages, including poor visible absorption (high UV absorption), small surface area (<10 $m^2 g^{-1}$), and easy self-aggregation. As noticed, the incorporation of other compounds into MOFs has mutual assistance. MOFs can be used to overcome the drawbacks of POMs and use their advantages (high UV response, high thermal stability, and tuneable redox behavior). On the other hand, MOFs can enhance the functionality of POMs and form a composite with several advantages besides their high light absorption.[322–324] Moreover, the use of complex compounds such as $[Ru(bpy)_3]^{2+}$ and $[Ir(ppy)_2(bpy)]^+$ in the structure of POMs could be an ideal strategy to overcome the low visible light absorption.[325,326] Zhang and coworkers synthesized a composite using POM$[P_2W_{18}O_{62}]_6$, Zr-MOF (MIL-101) and a complex compound of Ru ($[Ru(bpy)_x]^{2+}$) for hydrogen gas production under visible light. The use of the Ru complex leads to the absorption of visible light.[144,327]

Kong and coworkers applied the complex compounds of $Ir(ppy)_2(bpy)]^+$ and $[Ru(bpy)_3]^{2+}$ to construct MOFs and encapsulated Ni-POM (Ni_4P_2-POMs). They applied the final composite for the photocatalytic water splitting under visible light.[147]

Both complexes, as the linkers of the MOFs, can absorb visible light and lead to the migration of electrons from HOMO to LUMO followed by their transfer to the POM. Due to the presence of $[Ru(bpy)_3]^{2+}$, the final composite absorbs visible light in the range of 598–633 nm which are related to the energy gaps between the excited and ground states of the photosensitizer (1.96 and 2.08 eV, respectively).

The synergistic effect can also help in absorbing light of longer wavelengths. Shi and coworkers synthesized a composite of MOF with POM to be used as a photocatalyst for water splitting and producing hydrogen and oxygen gases.[153] The result showed that although POM and MOF are not able to absorb visible light alone, their synergistic effects make the final composite absorb visible light.[149] In another experiment, Jiao and coworkers addressed the incorporation of POM(P_2W_{18}) into the MOF of Nu-1000 with the use of Pt NPs for photocatalysis applications.[325] The results showed that this combination of POM and MOFs can successfully enhance the photocatalytic hydrogen gas production due to the presence of POM as a separator, for the photogenerated charge carriers in MOF host (Figure 17).

The excellent photocatalytic activity of the composite can be assigned to its high photo response and efficient electron transfer due to the presence of MOF (host molecule) and POM (guest molecule), enabling the final composite to absorb visible light. Kong and coworkers encapsulated POM into UiO-MOFs for hydrogen gas production under visible light.[147] They loaded POM $[Ni_4(H_2O)_2(PW_9O_{34})_2]_{10}$-$(Ni_4P_2)$ into $[Ru(bpy)_2(-dbbpy)]^{2+}$, and $[Ir(ppy)_2(dbbpy)]^+$ (dbbpy = 2,20-bipyridine-5,50-dibenzoate) for the synthesis of Ni_4P_2@- MOF-1 and Ni_4P_2@MOF-2, from UiO-MOF-1 and UiO-MOF-2, respectively. It should be noticed that the incorporation of a noble metal cannot always enhance the absorption of longer wavelengths. Hill and coworkers synthesized a composite of POM@MOF with the usage of Keggin POMs ($H_3PW_{12}O_{40}$), MOF (NH_2-MIL-53) and Pt for the hydrogen gas evolution.[119] The pristine NH_2-MIL-53 could absorb visible light at 450 nm due to the presence of NH_2 and lone pair n-π^* transition of the amino groups. However, after adding Pt, the harvesting of visible light was reduced due to the combination of Pt and POM, which interfere with the light harvesting of 2-aminoterephthalate groups (organic linker of the MOF).

Synthesis of noble-free POMs was also studied by different researchers.[90] Kogerler and coworkers encapsulated Co-POM and Fe-POM into Fe-based MOF (MIL-100(Fe) and used them as water splitting photocatalysts.[328]

Shi and coworkers synthesized the first noble-free POM@MOFs for the evolution of hydrogen and oxygen gases under visible light.[153] They synthesized $\{CuI_{24}$ $(\mu_3$ -Cl)$_8$ $(\mu_4$ -Cl)$_6\}$-based polyoxometalate (POM)@metal–organic framework (MOF) (ZZULI-1), as a robust dual functionalized photocatalyst. The existence of multi-active units in the final composite and the

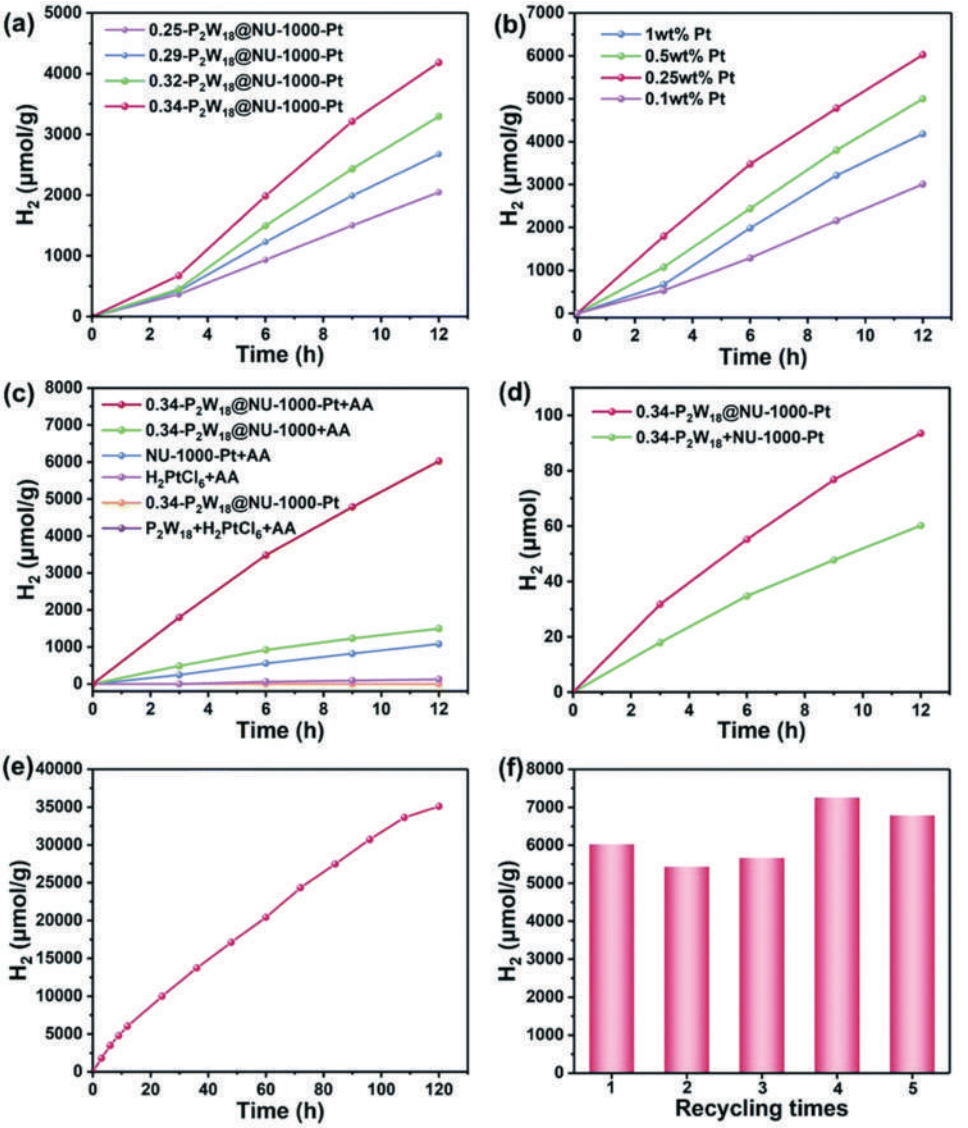

Figure 17. Photocatalytic hydrogen gas evolution of P_2W_{18}@NU-1000 with different molar ratios of P_2W_{18}/NU-1000. Conditions: 10 mg catalysts, pH 4.5, 1 wt% pt. (b) photocatalytic hydrogen gas evolution tests using various feedstocks of pt. Conditions: 10 mg 0.34-P_2W_{18}@NU-1000 photocatalyst, pH. 5.5. (c) comparison profiles of photocatalytic hydrogen gas production with different catalysts and reaction conditions (the specific content of pt contained in the reaction systems is 0.25 wt%). The common conditions: pH=5.5, 300WXe-lamp. (d) the comparison profiles of the photocatalytic hydrogen gas production for 0.34-P_2W_{18}@NU-1000 and P_2W_{18} + NU-1000. Conditions: pH=5.5, 0.25 wt.% pt. The contents of P_2W_{18} and NU-1000 are equal to that of 0.34-P_2W_{18}@NU-1000. (e) long-term photocatalytic hydrogen gas production test using the 0.34-P_2W_{18}@NU-1000 composite with 0.25 wt.% pt at pH=5.5. (f) the photocatalytic recycle tests of the 0.34-P_2W_{18}@NU-1000 photocatalyst. Conditions: 10 mg 0.34-P_2W_{18}@NU-1000 photocatalyst, 0.25 wt% pt, 300 W xe-lamp, and 20 mL of 1 M AA aqueous at pH=5.5. Reprinted with permission from Ref.[325] copyright 2021 RSC chemistry.

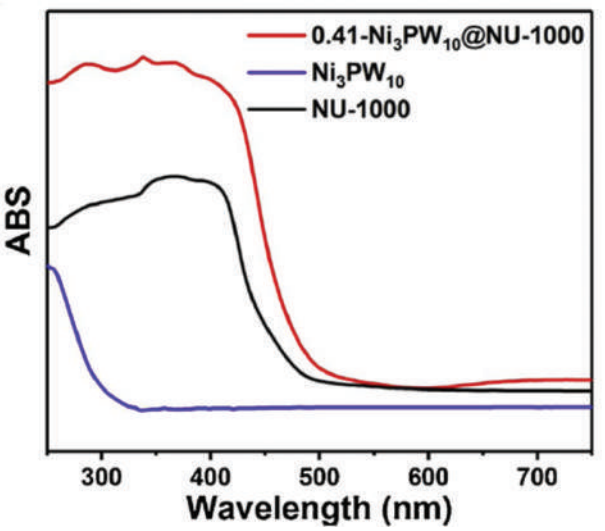

Figure 18. UV–vis diffuse reflectance spectra of Ni_3PW_{10}, NU-1000 and 0.41- Ni_3PW_{10}@NU-1000. Reprinted with permission from Ref.[152] copyright 2021 elsevier publication.

redox behavior of the POM and MOF resulted in the absorption of visible light, for the first time, by the POM@MOF composite.

Besides the adjustment of POM or complex compounds, proper tuning of the MOF is also effective in avoiding the use of noble metals. NU-1000 is one of the useful MOFs, especially for water splitting, which is highly photo-responsive. It is composed of $Zr_6(\mu_3\text{-}O)_4(\mu_3\text{-}OH)_4(H_2O)_4(OH)_4$ nodes and 1,3,6,8-tetrakis(p-benzoate)pyrene (TBAPy).[137,329] The combination of NU-1000 with proper POMs offers a composite responsive to visible light. Jiao and coworkers synthesized two types of POM@MOFs through the use of NU-1000 (Zr), different Keggin POMs of ($K_6N_a[Ni_3(H_2O)_3PW_{10}O_{39}H_2O]$, and a Wells-Dawson-type ($Na_4Li_5[Ni_3(OH)_3(H_2O)_3P_2W_{16}O_{59}]$ to be used as photocatalyst for hydrogen gas production under natural sunlight.[152] Results illustrated that the combination of the POM into the MOF could increase the ability of the composite in absorbing longer wavelengths up to 556 nm (Figure 18). However, the first linker for the absorption of visible light is the linker of NU-1000 (1,3,6,8-tetrakis (p-benzoate) pyrene).

Despite the ability of POMs to widely absorb UV light, the absorption of visible light in the composite of POM@MOFs has been rarely reported. On the other hand, the application of noble metal complexes or ions has been reported.[139,159] The visible light absorption can be attributed to the charge transfer between the noble metals and ligand (MLCT) as well as intersystem crossing to the MLCT state. Further electron transition from the complex compound to POM further facilitates the catalytic reduction.

5.2.3. Incorporation of metal-based nanoparticles

Nanoparticles (NPs) are regularly used for the modification of MOFs. Similar to the case of OMCs, NPs have mutual assistance, which can enhance stability, recyclability, and light absorptions of the final composite.

The attractive properties of NPs are attributable to their individual small size which drastically increases their catalytic activity because of their high surface to their volume ratio, a large ratio of atoms, and a large density of the unsaturated sites. Regarding light absorption, loading metal rarely improves the absorption of visible light. However, some reports showed that the synergistic effect of some metals (such as noble metals) improved visible light absorption.[330] For instance, in the case of ZIF-8 MOF, the MOF is not photocatalytically active; but the final composite is able to absorb visible light due to the localized surface plasmon resonance (LSPR) effect of NPs.[331,332]

Among NPs, the small and noble nanoparticles are the most useful nanoparticles with different structures and abilities. The most effective way of using MOFs, as a host for NPs, is increasing the stability of the NPs.[333,334] NPs are mainly electron acceptors and mediators due to their low Fermi energy level.[288] Song and coworkers did an experiment to find if MOFs and their organic linkers are effective in absorbing light when NPs are incorporated or if NPs are the main players in light harvesting.[334] Four pristine photoactive MOFs (MIL-101(Al)–NH_2, MIL-53(Al)–NH_2, MIL-101(Cr)–NH_2, and MIL-53(Cr)–NH_2) and three non-photoactive MOFs (MIL-101(Cr), MIL-53 (Cr), and MIL-53(Al)) were selected and were incorporated into Ni and Co NPs. The result illustrated that the photoactive MOFs are significantly more active than non-photoactive MOFs, confirming the role of the organic linker in harvesting visible light for hydrogen gas evolution. In the next step, the photoactive MOFs and non-photoactive MOFs were encapsulated by NPs and compared. The results were similar to the case of the pristine MOFs. They were more active than the previous studies done by the bimetallic NPs such as PdCo NPs[335] and Pd/SiO_2-$CoFe_2O_4$.[336] However, NPs can affect the light absorption properties of the final composite and extend their absorption range to visible and even NIR ranges due to the synergistic effect and the ability of MOFs for immobilizing NPs with the light-active functional groups of the organic linker (e.g., NH_2), which increases the electron transport from MOFs to NPs, as the catalytic center. Due to their LSPR effects, the incorporation of noble NPs can help the final composite in absorbing visible light.[337,338] Two types of NPs are used in MOFs for enhancing light absorption: (i) plasmonic NPs (Au[293,294] Ag,[295,296] and Al NPs[297] which are used for enhancement of the light absorption and perfuse of hot electrons and (ii) NPs with high catalytic activity (Pt,[298,299] and Au@PtAg[300]) which are employed as an efficiency electrons trapper. There are different examples of incorporating NPs in MOFs to enhance the photocatalytic ability. Although

they are not used for the water splitting applications, their effect on the light absorption is an advantage, which can be expanded for different applications. Shen and co-workers incorporated palladium nanoparticles into the UiO-66 (NH_2) MOF.[339] Regarding the light absorption, the result showed that the doping Pd nanoparticle incremented the intensity of the visible light absorption (Figure 19a). The size effect of NPs has been also investigated.[342–345] Chang and co-workers studied the size selectivity of the bimetallic NP of PtCo encapsulated in UiO-66 MOF.[345] They showed that the synergistic effect of Pt NPs led to olefins hydrogenation and the size selectivity effects endowed via the MOFs shell. Xiao and co-workers encapsulated Pt NPs into the cage of UiO-66-NH_2 to be used as a photocatalyst for hydrogen gas production.[127] The result indicated the significance of the site of NPs. They synthesized two composites with the same MOF and NP but with different Pt NP sites: on the surface of MOF (Pt/UiO-66-NH_2) and embedded into the cage of MOF (Pt@UiO-66-NH_2). Both samples showed almost the same behavior in

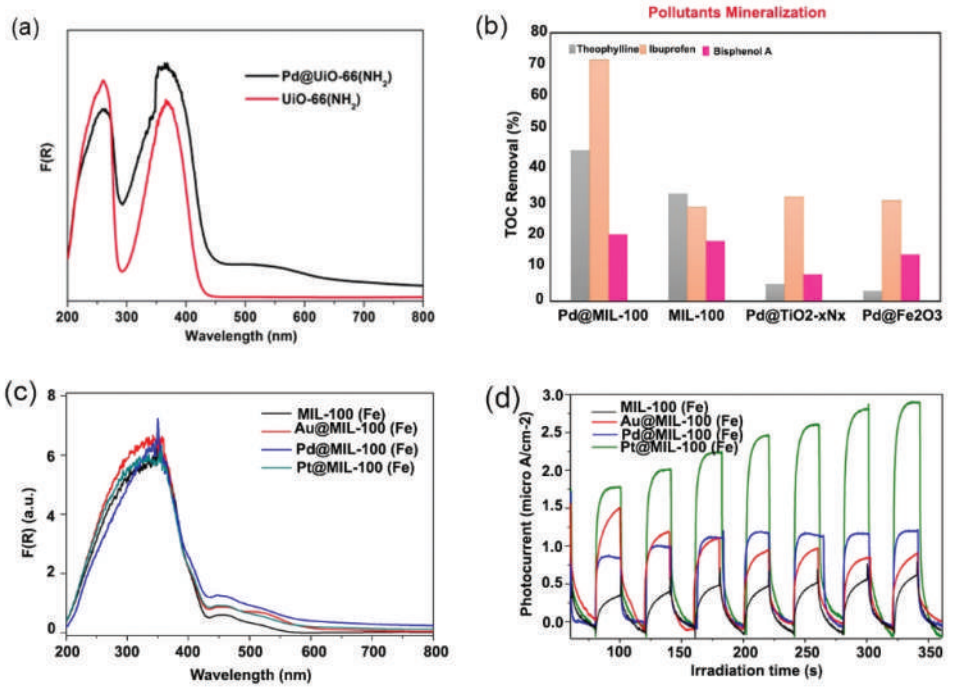

Figure 19. (a)uv-vis diffuse reflectance spectra of UiO-66(NH_2) and Pd@UiO-66(NH_2). Reprinted with permission from Ref.[339] copyright 2013 RSC chemistry. (b) TOC removal efficiency of theophylline, ibuprofen and bisphenol a by different photocatalysts. Reaction conditions: 5 mg photocatalyst, 40 ml PPCPs (20 mg L^{-1}), 40 µl H_2O_2, pH 4. Reprinted with permission from Ref.[340] copyright 2013 RSC chemistry. (c) UV-vis DRS spectra and (d) photocurrent response of MIL-100(Fe) and M@MIL-100(Fe). Reprinted with permission from Ref.[341] copyright 2015 Springer publication.

absorbing light in the range of 300 and 450 nm. However, the intensity of the absorption is far higher in Pt@UiO-66-NH_2 compared to Pt/UiO-66-NH_2 due to the lower distance between Pt NP and the host MOF, leading to significant scattering at long wavelengths (Figure 22a).

Further studies have been carried out on the incorporation of Pd NPs.[330,339,347] In addition, Liang and coworkers[340] synthesized the Pd@MIL-100(Fe) composite with loading 1 wt.% of H_2PdCl_4, as a precursor of the Pd nanoparticle, which resulted in higher surface activity than the pristine MIL-100(Fe). The final composite could absorb higher visible light due to the incorporation of Pt NPs and the photocatalytic ability of Pd@MIL-100(Fe) was remarkably enhanced toward degradation of some pharmaceutical products (Figure 19b).

Liang and coworkers incorporated different NPs (such as Au, Pd, and Pt, with respective size of 15, 12, and 2 nm) into the Fe-based MOF and compared their photocatalytic ability under visible light.[341] The result revealed the electron acceptor role of NPs as they accept electron from the LUMO of the MOF (MIL-100(Fe)), reducing the NPs. The synthesized composites were used for removing MO and Cr(VI) under visible light. Among the obtained composites, Pt@MOF showed higher photocatalytic ability followed by the MOF combined with Pd, Au, and pristine, respectively. These observations can be assigned to their ability in absorbing visible light (Figure 19c)

Pt NPs are active and showed high promises as a co-catalyst for MOFs in water splitting applications.[160] Regarding light absorption, they can affect the energy band gap of the final composite and hence its absorption range. The energy band gap of U6N- MOF is 2.88 eV which declined to 2.76 eV after modification by Pt NPs (Figure 19d).[272,348]

Thus, the incorporation of noble NPs into the cage of MOFs remarkably increases the visible light absorption of the final composite and its lifetime.

On the other hand, silver NPs illustrate a remarkable electron sink because of the construction of Schottky junctions at the junction of Ag-MOFs.[288] This property hinders the recombination of electrons and holes and increases the photocatalytic ability of the composite. For instance, after incorporation of Ag NPs into MIL-125(Ti), Ag@MIL-125(Ti) was able to degrade 93% of RhB after 8 min under visible light, while this rate was just 8% for the pristine MOF.[349]

The noble-free NPs were also studied as co-catalyst of MOFs for hydrogen gas production, due to their economic advantages and abundance.[350] Zhen and coworkers constructed the composite of Ni@MOF-5 by the impregnation method[163] and applied it as a photocatalyst for producing hydrogen gas. Their result showed the production of 302.2 mol of hydrogen gas after 2 h in the presence of Eosin (EY), which was around six times higher than the case with Ni Np as cocatalyst (Figure 20)

EY plays a decisive role in absorbing visible light. Upon exposure to visible light, the electrons are excited from the HOMO to the LUMO state, leading to

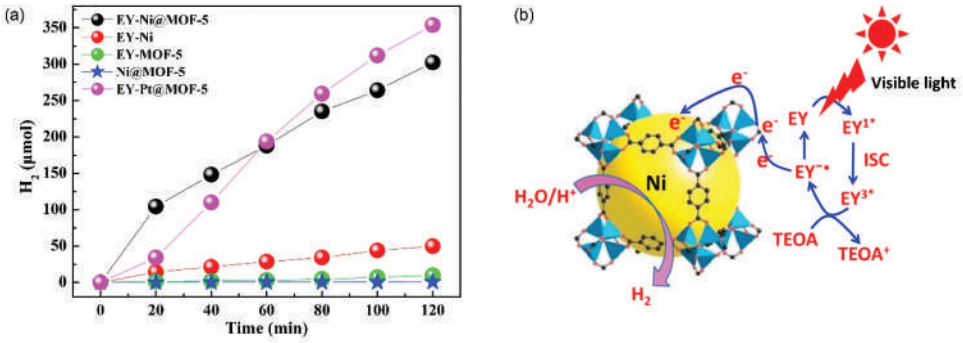

Figure 20. (a) H_2 production in different systems. Reprinted with permission from Ref.[163] copyright 2015 Springer publication. (b) the mechanism for H_2 evolution (TEOA as a sacrificial donor) over the EY sensitized Ni@MOF-5. Reprinted with permission from Ref.[163] copyright 2015 Springer publication.

the formation of EY^{1*} followed by the formation of a lowest-lying EY^{3*} (the triplet excited state). Based on the results, it is believed that the electrons migrate from EY to MOF-5 and then are captured by Ni NPs to carry out the photocatalytic hydrogen gas evolution (Figure 20).[351] The Ni NPs serve as the electron acceptor in the catalytic reaction.

As has been already mentioned (OMCs@MOFs), NU-1000 MOF is a proper MOF for water splitting, whose photocatalytic water splitting properties are increased by the encapsulation of different compounds. Different studies have addressed the use of these properties to modify them by applying NPs such as nickel sulfide,[352] molybdenum oxide, and Cu-oxo cluster.[353,354] CdS nanocluster was encapsulated into NU-1000 MOF to form a binary compound, leading to 10-fold enhancement in the photocatalytic activities.[137] After modification, the light absorption of the final composite was extended toward visible range. Choudhuri and coworkers encapsulated CdSe nanoclusters in NU-1000 MOF to improve photocatalytic application of the composite (Figure 21).[181]

Based on the DFT method, the HOCO and LUMO states are located in the organic linker, functionalized by NH_2) of the MOF and Cd_6Se_6 cluster, respectively. In addition, the HOMO and LUMO of the composite are categorized in two pure and mixed orbitals at 1.99–2.47 eV and 2.63–3.19 eV, respectively, providing an opportunity to absorb visible light. The transitions, including linker to the linker ($\pi \rightarrow \pi^*$ and $n \rightarrow \pi^*$ transitions) and linker to cluster, are related to the conjugated π orbitals in the organic linker. In the case of the presence of NH_2 in the linker, the NB orbital on the N atom participates in the visible light transitions.

In addition to single NPs, bimetallic alloy NPs are also encapsulated into the cage of different MOFs for photocatalytic purposes. For instance, the

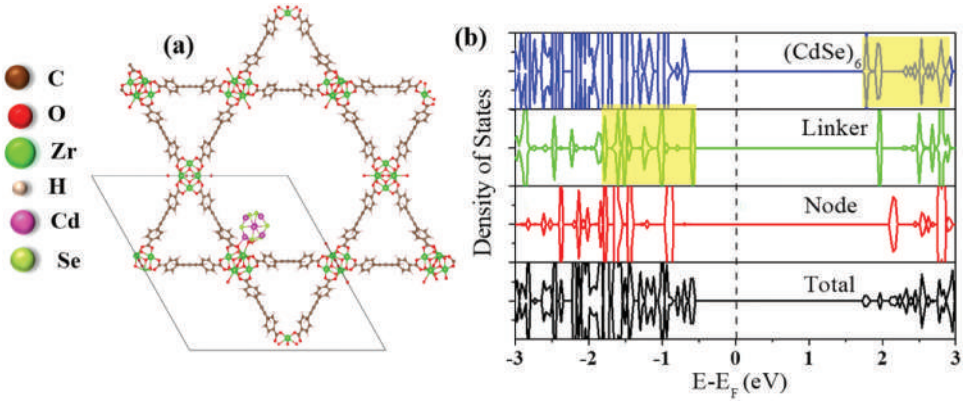

Figure 21. (a) structure of the Cd_6Se_6 cluster encapsulated in NU-1000 at a node site (Cd_6Se_6@NU-1000). The unit cell of the system is denoted by a solid line. (b) total and partial density of states of Cd_6Se_6@NU-1000. The fermi level is set to zero as marked by a black dashed line. The HOCO is on the linker, while the LUCO is on the cluster. The highest-energy occupied orbitals on the linker and the lowest-energy unoccupied orbitals on the cluster are highlighted in yellow. Reprinted with permission from Ref.[181] copyright 2020 ACS publication.

bimetallic NPs of PtPd alloy were incorporated into the cage of ZIF-8.[355] ZIF-8 was also used as the host for other bimetallic NPs such as CuPd to be used for Cr(VI) reduction.[356] The result illustrated that the modified MOF is highly activated under visible light (89% Cr reduction) compared to the pristine MOF (22% Cr reduction), as a result of the LSPR effect. Other compounds were also tested for further control. The result for the Cr reduction showed that CuPd bimetallic NP can reduce Cr more than Cu@ZIF-8, Pd@ZIF-8, ZIF-8, CuPd, Pd, and Cu when incorporated into ZIF-8. The synergistic effect is also another parameter, which improves the performance of the final composite, as well as OMCs.

Wang and coworkers also used the same nanoparticle, but accompanied with $[Ir(PPY)_2(-BPY)]^+$ in order to encapsulating UiO-67(Zr) and UiO-69 (Zr) and applied them for producing hydrogen gas.[128] The composites absorbed visible light longer than 420 nm to produce H_2 after 48 h. The results showed that the synergistic behavior of the complex and NP from the MLCT state led to the remarkable photocatalytic activity of the final composite under the visible light. The complex is decomposed by increasing the volume of the reduced hydrogen gas.

The metal-organic nanoparticles were also incorporated into MOFs for enhancing the photocatalytic features. Kampouri and coworkers studied the effect of Ni-phosphide nanoparticle (Ni_2P) on the MOF (MIL-125-NH_2) photocatalyst for water splitting applications.[357] The final composite showed the ability to generate hydrogen gas around 895 $mmol^{-1}g^{-1}$ under visible light. By 2017, it was the most powerful MOF in hydrogen gas production, even 3 times more than the Pt@MIL-125-NH_2 composite. The composite performed the highest quantum efficiency of 27 and 6.6% at 400–450 nm.

5.2.4. Incorporation of carbon-based nanoparticles

Carbon nanodots (CDs) are a class of zero-dimensional nanomaterials which have attracted huge research interest in catalysis, energy conversion, and drug delivery due to their unique physical and chemical properties, such as low toxicity, up-conversion photoluminescence property, and fast electron transfer capability.[346,358] CDs are characterized by their highly visible light harvesting. Although CDs were used as photocatalysts, they were rarely encapsulated in MOFs till 2018.[359,360] MOFs have been used as templates for the synthesis of CDs with different sizes by the pore space of MOFs. Zhang used the light properties of CDs and encapsulated them into NH_2-UiO-66 and used the heterojunction effects of g-C_3N_4 to apply as a photocatalyst for water splitting.[361] The result showed a 32.4, 38.6- and 17.5-times enhancement in hydrogen gas evolution of bulk g-C_3N_4, NH_2-UiO-66 and NH_2-UiO-66/g-C_3N_4, respectively. The DRS analysis also showed a remarkable enhancement in absorbing longer wavelengths of UV-Vis range (440 nm; Pure g-C_3N_4) to 800 nm for the CD@NH_2-UiO-66/g-C_3N_4 composite. The energy band gap of g-C_3N_4, NH_2-UiO-66, NH_2-UiO-66/g-C_3N_4, CD@NH_2-UiO-66/g-C_3N_4 was also reduced from 2.93 eV, to 2.92 eV, 2.86 eV, and 2.79 eV, respectively, further confirming longer visible light absorption (Figure 22b).

In another example, carbon nanodots (CDs) were in-situ formed in the pores of NH_2-MIL-125(Ti) and uniformly dispersed in MOF with better contact with the central metal cluster, which improves the photogenerated charge carriers transfer to the central metal cluster. This structure was used as a bifunctional photocatalyst for simultaneous NO removal and H_2 evolution under visible light.[161]

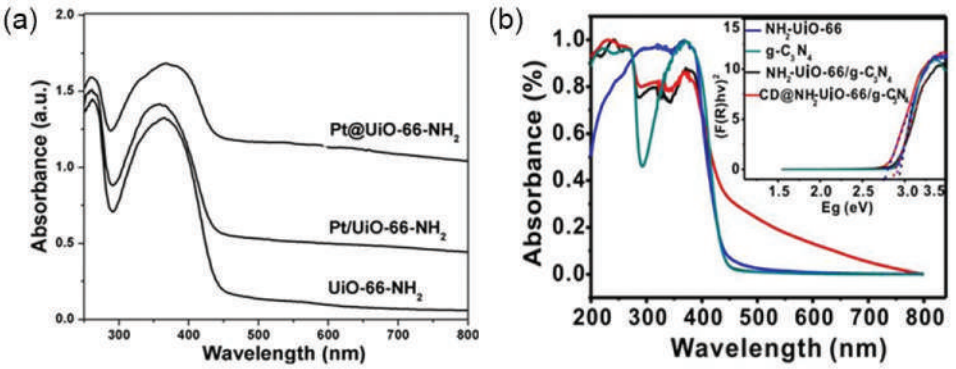

Figure 22. (a)uv/vis diffuse reflectance spectra. Reprinted with permission from Ref.[127] copyright 2016 German chemical society. (b) DRS spectra and tauc plots of g-C_3N_4, NH_2-UiO-66, NH_2-UiO-66/g-C_3N_4 and CD@NH_2-UiO-66/g-C_3N_4 (inset). Reprinted with permission from Ref.[346] copyright 2015 ACS publication.

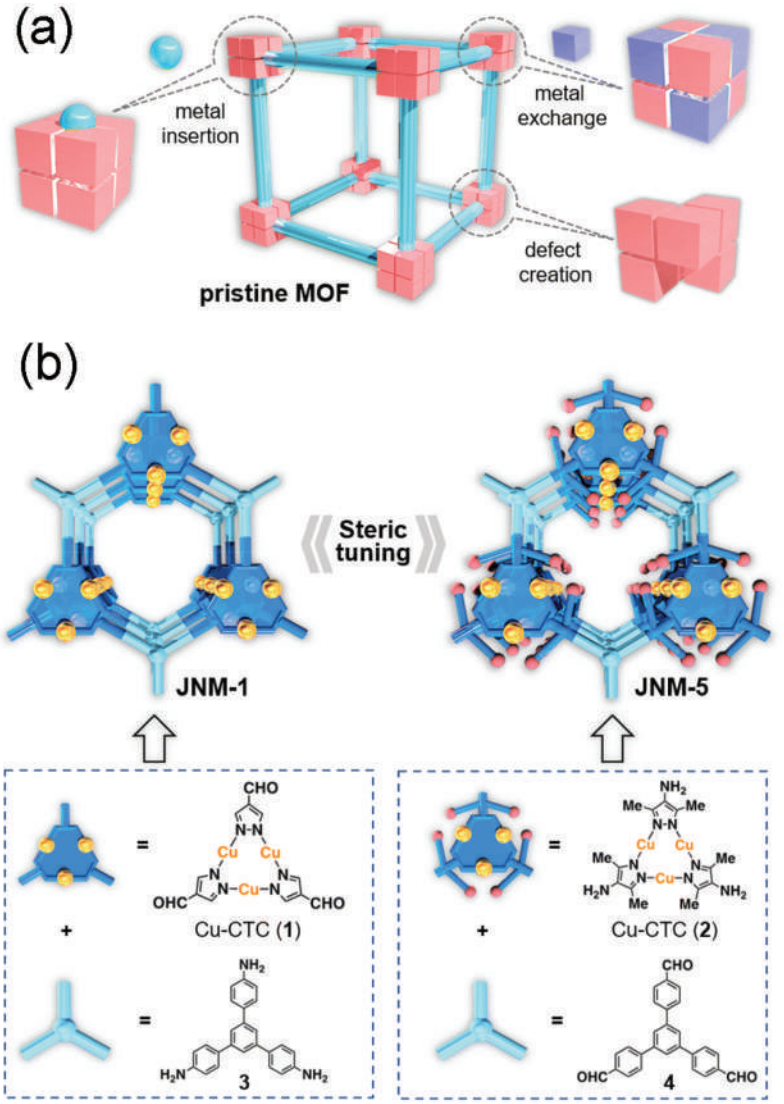

Figure 23. (a) the conventional way for tuning the catalytic performance via modification of metal nodes including metal insertion, metal exchange and defect creation. (b) steric tuning of metal nodes.[371] copyright 2023 RSC Chemistry.

5.2.5. Incorporation of quantum dots

Quantum dots (QDs) are zero-dimensional (0D) semiconductor nanocrystal materials from II–VI, III–V, or IV elements with a diameter of 2–10 nm with extensive applications in the fields of sensing, catalysis, nano-medicine, and bio-imaging due to their excellent size-dependent tunable electronic properties and stability in aqueous systems. Due to their surface area and quantum detention upshot, quantum dot materials have some advantages juxtaposed

with traditional chromophores, such as extensive absorption bands, low photobleaching, thin and even emission bands, extended lifetimes, and high quantum yields.

Owing to their unique properties, MOFs can provide a platform for loading QDs and prevent them from aggregation. Encapsulation of QDs in MOFs leads to a stable hybrid and enhances the physicochemical properties of MOFs. As an example, Mao and coworkers reported the synthesis of a series of thiol-laced UiO-66-type framework linked to Cd^{2+} ions to form UiOS-CdS composite materials for photocatalytic H_2 evolution. This structure provides sufficient surficial active sites and facilitates the migration and separation of charge carriers and the diffusion of reactant and product molecules. Furthermore, the thio-Cd bridge promotes the photocatalytic H_2 production performance by affecting the charge separation.[362]

5.2.6. Development of MOF nodes

As it is mentioned above, different strategies can affect catalytic performance of MOFs including the modification of metal nodes, the introduction of organic linkers with functional groups, and the encapsulation of other active species. Metal nodes can be modified by metal exchange,[363] defect creation, metal insertion and steric tuning of MOF nodes via ligand modification.[364]

Metal exchange on the nodes of a MOF contains some difficulties such as saturated coordination environments, challenging kinetic barriers, and diffusion limitations.[365] Some efforts have been made to overcome these difficulties. For example, PCN-426-Cr(III) was synthesized by exchanging Mg(II) with Cr(III) through clever metalation of Mg(II) with Fe(II) in the framework, followed by air oxidation to form Fe(III), formed PCN-426-Fe(III) that readily exchanges Fe(III) for Cr(III).This approach is used to overcome the disability of direct exchanging of Mg(II) with Cr(III).[366] In another example, four materials with UiO-66 structure were studied differing on the composition of the metal node (Zr or Ce or bimetallic Zr- Ce) and the substituent on the linker (terephthalate or aminoterephthalate). The results indicated that intrinsic sites in UiO-66 were able to activate molecular H_2 and promote selective hydrogenation reactions of polar X=Y multiple bonds of organic substrates in the absence of any guest.[367]

Another effective way to improve catalytic performance of MOFs is to create rich open metal sites (defect) on nodes of MOFs. To prepare defective MOFs, two strategies including de novo synthesis and post-synthetic methods are utilized.[368] For instance, Ye and coworkers synthesized MOF-808(Zr) with plentiful open metal sites and hierarchical porosity and used in oxidative desulfurization (ODS) and acetalization reaction. The results experimental and theoretical calculation proved that the formation of Zr-OH/OH_2 on the Zr–O cluster affects its reaction with oxidants to form peroxo-zirconium species for oxidizing sulfur compounds.[369]

Metal insertion is introduction of other metal ion in the structure of MOFs which can improve the electrical conductivity, stability and capacitance of the MOFs in comparison with single metal MOFs. As an example, in 2017 Zn/Ni-MOF was prepared by partially substituting Ni^{2+} with Zn^{2+}, which ion diffusion and transfer time (13.3 s) is much smaller than that of single metal Ni-MOF (33 s).[370]

The steric tuning of MOF nodes via ligand modification is rarely discussed as a way of improvement of catalytic performance of MOFs. The modification of organic linkers can cause the structural transformation of metal nodes and produce completely different MOF structures. Duan and coworkers synthesized two (Cu-CTU)-based MOFs called JNM-5 and JNM-1. In JNM-5 bulky groups were inserted in organic linker enhancing steric hindrance and partial coverage on copper open sites in (Cu-CTU)-based MOF in comparison with JNM-1 (Figure 23). The results demonstrated that introduction of steric hindrance (methyl groups) on the organic linkers, chemical stability and catalytic performance of MOFs improved.[371]

5.2.7. MOF-based S-scheme heterojunction photocatalysts

Photocatalytic hydrogen gas production as a green, safe, and low-cost strategy is a proper process to produce hydrogen gas which is one of the promising alternative fuels due to its remarkable advantages. Two important limitations of this technology, decreasing efficiency of this method, are recombination of photogenerated carriers and wide band gap. To solve these problems, a variety of methods have been employed, including particle size regulation,[372] carbon material modification,[373] metal deposition,[374] element doping,[375] and heterojunction construction.[376]

Traditional heterojunctions such as type II and z-scheme heterojunctions suffer from different disadvantages. For example, type-II heterojunction cannot retain the strong redox ability of single catalysts. In addition, side reactions in Z-scheme heterojunction may cause unexpected charge transfer path.[377] S-scheme heterojunction overcomes these shortcomings by its unique mechanism. S-scheme is composed of a RP (reduction-photocatalyst) and a cross-banded OP (oxidation-photocatalyst) in which the Fermi energy level and CB position of the reduction photocatalyst (RP) are both above oxidation photocatalyst (OP) (Figure 24).[379]

Constructing S-scheme heterojunction by composition of MOFs with other photocatalysts can improve the light absorption capacity and the carrier separation efficiency. For instance, Shao and coworkers synthesized a double S-scheme ZIF-67@GDY/CuI heterojunction with graphdiyne (g-C_nH_{2n-2}) nanosheets coated ZIF-67. This double S-scheme heterojunction makes the contact between the catalysts closer, accelerates the interfacial charge transfer process, and effectively improves the redox ability of the catalyst.[380]

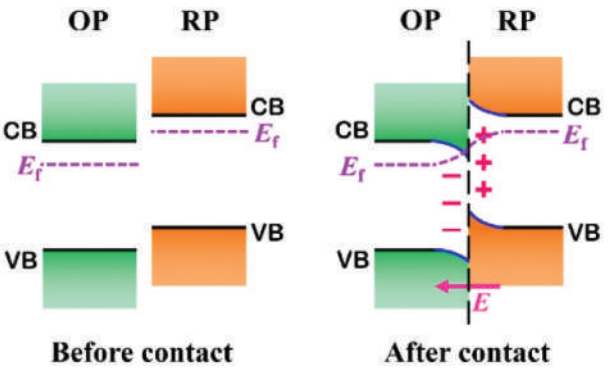

Figure 24. The formation process of S-scheme heterojunctions.[378] copyright 2022 elsevier publication.

6. Conclusion and future outlook

This review addressed different strategies to tune the light absorption of MOFs for water splitting applications.

Light absorption is one of the main steps in photocatalytic water splitting regardless of the type of photocatalysts. The photocatalytic process is initiated by light absorption; thus, light absorption plays a very important role in the water-splitting efficiency. UV and visible light are the most well-known types of light in the photocatalytic areas. Most researchers are trying to find a way for absorbing visible light, to use the sunlight (visible wavelength: 42–43%). In this context, development of a strategy for tuning MOFs to absorb longer-wavelength light (visible light) is highly desirable.

Most of the well-known MOFs cannot absorb visible light. However, due to their high flexibility in tuning the structure, it is possible to modify MOFs through different strategies to extend their absorption range to longer wavelengths, even toward the near IR light.

Two main steps are generally adopted to tune the light absorption ability of MOFs. (i) Modification of pristine MOFs through the organic linker, which is the most effective part of a MOF in absorbing light and (ii) modification of MOFs by immobilizing other compounds. Regarding the modification of pristine MOFs, the organic linker can be modified by (i) a change in its length, (ii) using different organic linkers in a MOF, and (iii) functionalizing. The incorporation of OMCs and NPs could be also effective. OMCs can mostly affect the LUMO in the hydrogen gas evolution reactions. They can tune the energy band gap of the composite. OMCs are constructed by the chromophore ligands, promoting the ability of final composites in absorbing visible and even near IR wavelengths. Therefore, it is an impressive strategy to tune the energy band gap to absorb light with longer wavelengths. OMCs-based noble metals are the

most effective OMCs due to their different advantages including stability, and absorbing visible light, making them the most promising OMCs for enhancing the photocatalytic applications of MOFs. However, their high cost has limited their applications. Alternative metal ions such as cobalt, nickel and iron were used to combine with organic chromophore ligands to form proper noble-free OMCs, which can be incorporated into MOFs.

On the other hand, NPs can increment light absorption ability of the system due to their small size. The LSPR effect of NPs promotes the visible light absorption of the final composite. In addition, the synergistic effect is one of the main parameters in the usefulness of the combination of NPs and MOFs.

Although numerous papers are daily reported on the light absorption ability of MOFs by different strategies, some challenges have remained:

(i) MOFs are synthesized mostly at the lab scale and the synthesis of photoactivated MOFs is limited. The biggest barrier is the complexity of the synthesis methods.
(ii) Although many MOFs-based OMCs and NPs have been synthesized, still OMCs and NPs-based noble metals are the most useful compounds. It has been shown that mainly late transition metals (on the right side of the d-block, from group 8 to 11 (and 12 if it is counted as transition metals) and their oxides are effective, either as bulk materials, in colloidal form, or deposited on electrodes. Moreover, ligands with S-donor, as well as N-atoms (such as thiosemicarbazone and Salen), can increase the stability, electrochemical properties, and appropriate energy levels (such as porphyrins and other tetrapyrrolic derivatives).
(iii) Most of the synthesized MOFs are not able to be activated even under UV light and multifunctional linkers should be used to help in absorbing light with longer wavelength.
(iv) In order to improve the ability of light absorption and better interaction with the substrate, synthesized MOFs can be reduced to nano-size.
(v) Not only experimental studies but also theoretical studies on MOFs-based photocatalysts can use to anticipate the influence of different parts such as pore shape/size, energy bandgap, active sites, etc. in photocatalytic water splitting.

Briefly, although photocatalytic water splitting is a very challenging method, for the past two decades, many studies have been devoted to developing different methods for synthesizing MOFs capable of catalyzing the reactions and promising results are anticipated with the accurate design of a MOF.

Abbreviation used

PWS	Photocatalytic Water Splitting
STH	solar-to-hydrogen
MOFs	Metal Organic Frameworks
VB	Valence band
CB	Conduction band
HER	hydrogen evolution reaction
NHE	Normal hydrogen electrode
OER	oxygen evolution reaction
LMCT	ligand to metal charge transfer
LCCT	the linker-to metal cluster charge transfer
POM	polyoxometalate
OMC	Organic-Metal Compounds
NPs	nanoparticles
E_g	Energy band gap
OMC@MOFs	Incorporation of organic-metal compounds with metal organic frameworks
NPs@MOFs	Incorporation of nanoparticles with metal organic frameworks
ORR	oxygen reduction reaction
MLCT	Metal ligand charge transfer
LSPR	localized surface plasmon resonance
HOCO	highest occupied crystal orbital
LUCO	lowest unoccupied crystal orbital
NB	None bond
PCLEF	plasmonic concentrated local electromagnetic field
CDs	Carbon nanodots
LLES	the low-lying excited states
MLCT	metal-to-ligand charge-transfer
LC	ligand-centered
MC	metal-centered
PL	photo-luminescent
PEC	photoelectrochemical
CPs	Coordination polymers
HOMO	Highest occupied molecular orbital
LUMO	Lowest unoccupied molecular orbital
HSAB	Hard and Soft Acids and Bases
QDs	Quantum dots
ODS	Oxidative desulfurization
RP	Reduction photocatalyst
OP	Oxidation photocatalyst
SBU	Secondary building unit
EDTA	Ethylenediaminetetraacetic acid
SHE	Standard hydrogen electrode
CLEF	concentrated local electromagnetic field

Acknowledgments

This paper was supported by the Ferdowsi University of Mashhad Research Council and the RUDN University Strategic Academic Leadership Program.

Disclosure statement

No potential conflict of interest was reported by the author(s).

Funding

The work was supported by the Ferdowsi University of Mashhad [3/56852]; RUDN University [AAAA-A19-119092390076-7].

References

[1] World Energy Statistics - Worldometer, (n.d.). https://www.worldometers.info/energy/ (accessed May 29, 2022).
[2] Jena, P. Materials for hydrogen storage: Past, present, and future. *J. Phys. Chem. Lett.* 2011, 2(3), 206–211. DOI: https://doi.org/10.1021/jz1015372.
[3] Pareek, A.; Dom, R.; Gupta, J.; Chandran, J.; Adepu, V.; Borse, P. H. Insights into Renewable Hydrogen Energy: Recent Advances and Prospects. *Mater. Sci. Energy Technol.* 2020, 3, 319–327. DOI: 10.1016/J.MSET.2019.12.002.
[4] García-Holley, P.; Schweitzer, B.; Islamoglu, T.; Liu, Y.; Lin, L.; Rodriguez, S.; Weston, M. H.; Hupp, J. T.; Gómez-Gualdrón, D. A.; Yildirim, T., et al. Benchmark Study of Hydrogen Storage in Metal–Organic Frameworks Under Temperature and Pressure Swing Conditions. *Acs. Energy. Lett.* 2018, 3(3), 748–754. DOI: https://doi.org/10.1021/acsenergylett.8b00154.
[5] Modisha, P. M.; Ouma, C. N. M.; Garidzirai, R.; Wasserscheid, P.; Bessarabov, D. The Prospect of Hydrogen Storage Using Liquid Organic Hydrogen Carriers. *Energy. Fuels.* 2019, 33(4), 2778–2796. DOI: 10.1021/ACS.ENERGYFUELS.9B00296.
[6] Rusman, N. A. A.; Dahari, M. A Review on the Current Progress of Metal Hydrides Material for Solid-State Hydrogen Storage Applications. *Int. J. Hydrogen. Energy.* 2016, 41(28), 12108–12126. DOI: 10.1016/J.IJHYDENE.2016.05.244.
[7] Barthelemy, H.; Weber, M.; Barbier, F. Hydrogen Storage: Recent Improvements and Industrial Perspectives. *Int. J. Hydrogen Energy.* 2017, 42, 7254–7262. DOI: 10.1016/J.IJHYDENE.2016.03.178.
[8] Okolie, J. A.; Patra, B. R.; Mukherjee, A.; Nanda, S.; Dalai, A. K.; Kozinski, J. A. Futuristic Applications of Hydrogen in Energy, Biorefining, Aerospace, Pharmaceuticals and Metallurgy. *Int. J. Hydrogen Energy.* 2021, 46, 8885–8905. DOI: 10.1016/J.IJHYDENE.2021.01.014.
[9] Krasae-In, S.; Stang, J. H.; Neksa, P. Development of large-scale hydrogen liquefaction processes from 1898 to 2009. *Int. J. Hydrogen Energy.* 2010, 35, 4524–4533. DOI: 10.1016/J.IJHYDENE.2010.02.109.
[10] Levalley, T. L.; Richard, A. R.; Fan, M. The Progress in Water Gas Shift and Steam Reforming Hydrogen Production Technologies - a Review. *Int. J. Hydrogen. Energy.* 2014, 39, 16983–17000. DOI: 10.1016/j.ijhydene.2014.08.041.
[11] Westermann, P.; Jørgensen, B.; Lange, L.; Ahring, B. K.; Christensen, C. H. Maximizing Renewable Hydrogen Production from Biomass in a Bio/Catalytic Refinery. *Int. J. Hydrogen Energy.* 2007, 32, 4135–4141. DOI: 10.1016/j.ijhydene.2007.06.018.
[12] Koh, A. C. W.; Chen, L.; Kee Leong, W.; Johnson, B. F. G.; Khimyak, T.; Lin, J. Hydrogen or Synthesis Gas Production via the Partial Oxidation of Methane Over Supported Nickel-Cobalt Catalysts. *Int. J. Hydrogen. Energy.* 2007, 32, 725–730. DOI: 10.1016/j.ijhydene.2006.08.002.

[13] Baruah, R.; Dixit, M.; Basarkar, P.; Parikh, D.; Bhargav, A. Advances in Ethanol Autothermal Reforming. *Renewable Sustainable Energy Rev*. 2015, 51, 1345–1353. DOI: 10.1016/j.rser.2015.07.060.

[14] De Castro, J.; Rivera-Tinoco, R.; Bouallou, C. Hydrogen production from natural gas: Auto-Thermal Reforming and CO_2 capture. *Chem. Eng. Trans*. 2010, 21, 163–168. DOI: 10.3303/CET1021028.

[15] Rydén, M.; Arjmand, M. Continuous Hydrogen Production via the Steam-Iron Reaction by Chemical Looping in a Circulating Fluidized-Bed Reactor. *Int. J. Hydrogen. Energy*. 2012, 37, 4843–4854. DOI: 10.1016/j.ijhydene.2011.12.037.

[16] Hawkes, F. R.; Dinsdale, R.; Hawkes, D. L.; Hussy, I. Sustainable fermentative hydrogen production: Challenges for process optimisation, in. *Int J. Hydrogen Energy, Pergamon*. 2002, 27, 1339–1347. DOI: 10.1016/S0360-3199(02)00090-3.

[17] Nikolaidis, P.; Poullikkas, A. A Comparative Overview of Hydrogen Production Processes. *Renewable Sustainable Energy Rev*. 2017, 67, 597–611. DOI: 10.1016/j.rser.2016.09.044.

[18] Ghosh, S.; Chowdhury, R.; Bhattacharya, P. A Review on Single Stage Integrated Dark-Photo Fermentative Biohydrogen Production: Insight into Salient Strategies and Scopes. *Int. J. Hydrogen. Energy*. 2018, 43, 2091–2107. DOI: 10.1016/j.ijhydene.2017.12.018.

[19] Abdalla, A. M.; Hossain, S.; Nisfindy, O. B.; Azad, A. T.; Dawood, M.; Azad, A. K. Hydrogen production, storage, transportation and key challenges with applications: A review. *Energy Convers. Manag*. 2018, 165, 602–627. DOI: 10.1016/j.enconman.2018.03.088.

[20] Kumar, R.; Kumar, A.; Pal, A. An Overview of Conventional and Non-Conventional Hydrogen Production Methods. *Mater. Today Proc*. 2020, 5353–5359. doi: 10.1016/j.matpr.2020.08.793.

[21] Wang, Q.; Domen, K. Particulate Photocatalysts for Light-Driven Water Splitting: Mechanisms, Challenges, and Design Strategies. *Chem. Rev*. 2020, 120, 919–985. DOI: 10.1021/acs.chemrev.9b00201.

[22] Fujishima, A.; Honda, K. Electrochemical Photolysis of Water at a Semiconductor Electrode. *Nature*. 1972, 238, 37–38. DOI: 10.1038/238037a0.

[23] Sumner, L.; Sakthivel, N. A.; Schrock, H.; Artyushkova, K.; Dass, A.; Chakraborty, S. Electrocatalytic Oxygen Reduction Activities of Thiol-Protected Nanomolecules Ranging in Size from Au28(SR)20 to Au279(SR)84. *J. Phys. Chem. C*. 2018, 122(43), 24809–24817. DOI: https://doi.org/10.1021/acs.jpcc.8b07962.

[24] Jones, T. C.; Sumner, L.; Ramakrishna, G.; Bin Hatshan, M.; Abuhagr, A.; Chakraborty, S.; Dass, A. Bulky T-Butyl Thiolated Gold Nanomolecular Series: Synthesis, Characterization, Optical Properties, and Electrocatalysis. *J. Phys. Chem. C*. 2018, 122(31), 17726–17737. DOI: https://doi.org/10.1021/acs.jpcc.8b01106.

[25] Kumar, B.; Kawawaki, T.; Shimizu, N.; Imai, Y.; Suzuki, D.; Hossain, S.; Nair, L. V.; Negishi, Y. Gold Nanoclusters as Electrocatalysts: Size, Ligands, Heteroatom Doping, and Charge Dependences. *Nanoscale*. 2020, 12, 9969–9979. DOI: 10.1039/d0nr00702a.

[26] Kawawaki, T.; Negishi, Y.; Kawasaki, H. Photo/Electrocatalysis and Photosensitization Using Metal Nanoclusters for Green Energy and Medical Applications. *Nanoscale Adv*. 2020, 2, 17–36. DOI: 10.1039/c9na00583h.

[27] Liu, M.; Zhao, Z.; Duan, X.; Huang, Y. Nanoscale Structure Design for High-Performance Pt-Based ORR Catalysts. *Adv.Mate*. 2019, 31, 1802234. DOI: 10.1002/adma.201802234.

[28] Sonowal, K.; Saikia, L. Metal–Organic Frameworks and Their Composites for Fuel and Chemical Production *Via* CO $_2$ Conversion and Water Splitting. *R.S.C. Adv*. 2022, 12, 11686–11707. DOI: 10.1039/D1RA09063A.

[29] Kim, H.; Kim, N.; Ryu, J. Porous Framework-Based Hybrid Materials for Solar-To-Chemical Energy Conversion: From Powder Photocatalysts to Photoelectrodes. *Inorg. Chem. Front*. 2021, 8, 4107–4148. DOI: 10.1039/d1qi00543j.

[30] Zaman, N.; Noor, T.; Iqbal, N. Recent Advances in the Metal-Organic Framework-Based Electrocatalysts for the Hydrogen Evolution Reaction in Water Splitting: A Review. *R.S. C. Adv*. 2021, 11, 21904–21925. DOI: 10.1039/d1ra02240g.

[31] Mao, S.; Shi, J. W.; Sun, G.; Ma, D.; He, C.; Pu, Z.; Song, K.; Cheng, Y. Au nanodots@thiol-UiO66@$ZnIn_2S_4$ Nanosheets with Significantly Enhanced Visible-Light Photocatalytic H_2 Evolution: The Effect of Different Au Positions on the Transfer of Electron-Hole Pairs. *Appl. Catal. B*. 2021, 282, 119550. DOI: 10.1016/j.apcatb.2020.119550.

[32] Cure, J.; Mattson, E.; Cocq, K.; Assi, H.; Jensen, S.; Tan, K.; Catalano, M.; Yuan, S.; Wang, H.; Feng, L., et al. High Stability of Ultra-Small and Isolated Gold Nanoparticles in Metal-Organic Framework Materials. *J. Mater. Chem. A Mater*. 2019, 7, 17536–17546. DOI: 10.1039/c8ta12334a.

[33] Jin, Z.; Yang, H. Exploration of Zr–Metal–Organic Framework as Efficient Photocatalyst for Hydrogen Production. *Nanoscale Res. Lett*. 2017, 12, 1–10. DOI: 10.1186/s11671-017-2311-6.

[34] Chen, Y.; Ji, S.; Sun, W.; Lei, Y.; Wang, Q.; Li, A.; Chen, W.; Zhou, G.; Zhang, Z.; Wang, Y., et al. Engineering the Atomic Interface with Single Platinum Atoms for Enhanced Photocatalytic Hydrogen Production. *Angewandte Chemie*. 2020, 132, 1311–1317. DOI: 10.1002/ange.201912439.

[35] Zhang, H.; Li, Q.; Weng, B.; Xiao, L.; Tian, Z.; Yang, J.; Liu, T.; Lai, F. Edge Engineering of Platinum Nanoparticles via Porphyrin-Based Ultrathin 2D Metal–Organic Frameworks for Enhanced Photocatalytic Hydrogen Generation. *Chem. Eng. J.*, 442 (2022), 136144. DOI: 10.1016/j.cej.2022.136144.

[36] Fateeva, A.; Chater, P. A.; Ireland, C. P.; Tahir, A. A.; Khimyak, Y. Z.; Wiper, P. V.; Darwent, J. R.; Rosseinsky, M. J. A Water-Stable Porphyrin-Based Metal–Organic Framework Active for Visible-Light Photocatalysis. *Angew. Chem. Int. Ed*. 2012, 51, 7440–7444. DOI: 10.1002/anie.201202471.

[37] Guo, J.; Wan, Y.; Zhu, Y.; Zhao, M.; Tang, Z. Advanced Photocatalysts Based on Metal Nanoparticle/metal-Organic Framework Composites. *Nano Res*. 2021, 14, 2037–2052. DOI: 10.1007/s12274-020-3182-1.

[38] Absalan, Y.; Alabada, R.; Ryabov, M.; Tolstoy, V.; Butusov, L.; Nikolskiy, V.; Kopylov, V.; Gholizadeh, M.; Kovalchukova, O. Removing Organic Harmful Compounds from the Polluted Water by a Novel Synthesized Cobalt(ii) and Titanium(iv) Containing Photocatalyst Under Visible Light. *Environ. Nanotechnol. Monit. Manag*. 2020, 14, 100304. DOI: 10.1016/j.enmm.2020.100304.

[39] Razavi, M. R.; Absalan, Y.; Gholizadeh, M.; Strashnov, S.; Kovalchukova, O. Removing bromophenol blue from the aqueous environment by $Ti_xNi_yLa_mO_z$ photocatalyst under different conditions. *Environ. Technol. Innovations*. 2022, 26, 102385. DOI: 10.1016/J.ETI.2022.102385.

[40] Mishra, U. K.; Singh, J. *Semiconductor Device Physics and Design*; Springer Netherlands: 2008. doi: 10.1007/978-1-4020-6481-4.

[41] Kasap, S. *Optoelectronics & Photonics: Principles & Practices*; Pearson Education, 2013; p 544.

[42] Wang, Z.; Li, C.; Domen, K. Recent Developments in Heterogeneous Photocatalysts for Solar-Driven Overall Water Splitting. *Chem. Soc. Rev*. 2019, 48, 2109–2125. DOI: 10.1039/c8cs00542g.

[43] Wang, Q.; Hisatomi, T.; Jia, Q.; Tokudome, H.; Zhong, M.; Wang, C.; Pan, Z.; Takata, T.; Nakabayashi, M.; Shibata, N., et al. Scalable Water Splitting on Particulate Photocatalyst Sheets with a Solar-To-Hydrogen Energy Conversion Efficiency Exceeding 1%. *Nat. Mater*. 2016, 15, 611–615. DOI: 10.1038/nmat4589.

[44] Kawawaki, T.; Kataoka, Y.; Ozaki, S.; Kawachi, M.; Hirata, M.; Negishi, Y. Creation of Active Water-Splitting Photocatalysts by Controlling Cocatalysts Using Atomically Precise Metal Nanoclusters. *Chem. Commun*. 2021, 57(4), 417–440. DOI: https://doi.org/10.1039/d0cc06809h.

[45] Jaryal, R.; Kumar, R.; Khullar, S. Mixed Metal-Metal Organic Frameworks (MM-MOFs) and Their Use as Efficient Photocatalysts for Hydrogen Evolution from Water Splitting Reactions. *Coord. Chem. Rev*. 2022, 464, 214542. DOI: 10.1016/j.ccr.2022.214542.

[46] Luo, H.; Zeng, Z.; Zeng, G.; Zhang, C.; Xiao, R.; Huang, D.; Lai, C.; Cheng, M.; Wang, W.; Xiong, W., et al. Recent Progress on Metal-Organic Frameworks Based- and Derived-Photocatalysts for Water Splitting. *Chem. Eng. J*. 2020, 383, 123196. DOI: 10.1016/j.cej.2019.123196.

[47] Qi, M. Y.; Conte, M.; Anpo, M.; Tang, Z. R.; Xu, Y. J. Cooperative Coupling of Oxidative Organic Synthesis and Hydrogen Production Over Semiconductor-Based Photocatalysts. *Chem. Rev*. 2021, 121, 13051–13085. DOI: 10.1021/acs.chemrev.1c00197.

[48] Liu, Y.; Tang, C.; Cheng, M.; Chen, M.; Chen, S.; Lei, L.; Chen, Y.; Yi, H.; Fu, Y.; Li, L. Polyoxometalate@metal-Organic Framework Composites as Effective Photocatalysts. *ACS Catal*. 2021, 11, 13374–13396. DOI: 10.1021/acscatal.1c03866.

[49] Xiao, Y.; Guo, X.; Yang, N.; Zhang, F. Heterostructured MOFs Photocatalysts for Water Splitting to Produce Hydrogen. *J. Energy Chem*. 2021, 58, 508–522. DOI: 10.1016/j.jechem.2020.10.008.

[50] Chen, Z.; Dinh, H. N.; Miller, E. Photoelectrochemical Water Splitting: Standards, Experimental Methods, and Protocols. 2013. DOI: 10.1007/978-1-4614-8298-7.

[51] Li, R.; Li, C. Photocatalytic Water Splitting on Semiconductor-Based Photocatalysts. In *Advances in Catalysis*; Academic Press Inc: 2017; pp. 1–57. doi:10.1016/bs.acat.2017.09.001

[52] Kranz, C.; Wachtler, M. Characterizing Photocatalysts for Water Splitting: From Atoms to Bulk and from Slow to Ultrafast Processes. *Chem. Soc. Rev*. 2021, 50, 1407–1437. DOI: 10.1039/D0CS00526F.

[53] Bie, C.; Wang, L.; Yu, J. Challenges for Photocatalytic Overall Water Splitting. *Chem*. 2022, 8, 1567–1574. DOI: 10.1016/j.chempr.2022.04.013.

[54] Li, H.; Wang, K.; Sun, Y.; Lollar, C. T.; Li, J.; Zhou, H. C. Recent Advances in Gas Storage and Separation Using Metal–Organic Frameworks. *Mater. Today*. 2018, 21, 108–121. DOI: 10.1016/J.MATTOD.2017.07.006.

[55] Zhu, L.; Liu, X. Q.; Jiang, H. L.; Sun, L. B. Metal–Organic Frameworks for Heterogeneous Basic Catalysis. *Chem. Rev*. 2017, 117, 8129–8176. DOI: 10.1021/acs.chemrev.7b00091.

[56] Lustig, W. P.; Mukherjee, S.; Rudd, N. D.; Desai, A. V.; Li, J.; Ghosh, S. K. Metal–Organic Frameworks: Functional Luminescent and Photonic Materials for Sensing Applications. *Chem. Soc. Rev*. 2017, 46, 3242–3285. DOI: 10.1039/C6CS00930A.

[57] Xie, M. H.; Yang, X. L.; Zou, C.; De Wu, C. A Sn IV –Porphyrin-based Metal–Organic Framework for the Selective Photo-Oxygenation of Phenol and Sulfides. *Inorg. Chem*. 2011, 50, 5318–5320. DOI: 10.1021/ic200295h.

[58] Wu, P.; He, C.; Wang, J.; Peng, X.; Li, X.; An, Y.; Duan, C. Photoactive Chiral Metal–Organic Frameworks for Light-Driven Asymmetric α-Alkylation of Aldehydes. *J. Am. Chem. Soc.* 2012, 134, 14991–14999. DOI: 10.1021/ja305367j.

[59] Fu, Y.; Sun, D.; Chen, Y.; Huang, R.; Ding, Z.; Fu, X.; Li, Z. An Amine-Functionalized Titanium Metal–Organic Framework Photocatalyst with Visible-Light-Induced Activity for CO_2 Reduction. *Angew. Chem. Int. Ed.* 2012, 51(14), 3364–3367. DOI: https://doi.org/10.1002/ANIE.201108357.

[60] Xiao, J. D.; Jiang, H. L. Metal–Organic Frameworks for Photocatalysis and Photothermal Catalysis. *Acc. Chem. Res.* 2018, 52, 356–366. DOI: 10.1021/acs.accounts.8b00521.

[61] Nguyen, V. Q.; Mady, A. H.; Mahadadalkar, M. A.; Baynosa, M. L.; Kumar, D. R.; Rabie, A. M.; Lee, J.; Kim, W. K.; Shim, J. J. Highly Active Z-Scheme Heterojunction Photocatalyst of Anatase TiO_2 Octahedra Covered with C-MoS_2 Nanosheets for Efficient Degradation of Organic Pollutants Under Solar Light. *J. Colloid. Interface. Sci.* 2022, 606, 337–352. DOI: 10.1016/j.jcis.2021.07.128.

[62] Soares, L.; Alves, A. Photocatalytic Properties of TiO_2 and TiO_2/WO_3 Films Applied as Semiconductors in Heterogeneous Photocatalysis. *Mater. Lett.* 2018, 211, 339–342. DOI: 10.1016/j.matlet.2017.10.023.

[63] Hong, Y.; Li, C.; Yin, B.; Li, D.; Zhang, Z.; Mao, B.; Fan, W.; Gu, W.; Shi, W. Promoting Visible-Light-Induced Photocatalytic Degradation of Tetracycline by an Efficient and Stable beta-Bi_2O_3@g-C_3N_4 Core/Shell Nanocomposite. *Chem. Eng. J.* 2018, 338, 137–146. DOI: 10.1016/j.cej.2017.12.108.

[64] Liu, Q.; Li, Z.; Liu, Q.; Cheng, C.; Song, M.; Huang, C. Photocatalysis Under Shell: Co@bn Core–Shell Composites for Efficient EY-Sensitized Photocatalytic Hydrogen Evolution. *Appl. Surf. Sci.* 2020, 514, 146096. DOI: 10.1016/j.apsusc.2020.146096.

[65] Wang, Z.; Liu, Z.; Huang, J.; Chen, Y.; Su, R.; He, J.; Lv, G.; Gao, B.; Zhou, W.; Wang, Y., et al. Zr_6O_8-porphyrinic MOFs as Promising Catalysts for the Boosting Photocatalytic Degradation of Contaminants in High Salinity Wastewater. *Chem. Eng. J.* 2022, 440, 135883. DOI: 10.1016/j.cej.2022.135883.

[66] Chen, S.; Yang, F.; Gao, H.; Wang, J.; Chen, X.; Zhang, X.; Li, J.; Li, A. Construction of Dual Ligand Ti-Based MOFs with Enhanced Photocatalytic CO_2reduction Performance. *Journal Of CO2 Utilization*. 2021, 48, 101528. DOI: 10.1016/j.jcou.2021.101528.

[67] Li, G.; Li, F.; Liu, J.; Fan, C. Fe-Based MOFs for Photocatalytic N_2 Reduction: Key Role of Transition Metal Iron in Nitrogen Activation. *J. Solid State Chem.* 2020, 285, 121245. DOI: 10.1016/j.jssc.2020.121245.

[68] Zeng, L.; Guo, X.; He, C.; Duan, C. Metal–Organic Frameworks: Versatile Materials for Heterogeneous Photocatalysis. *ACS Catal.* 2016, 6, 7935–7947. DOI: 10.1021/acscatal.6b02228.

[69] Gomes silva, C.; Luz, I.; Llabrés i xamena, F. X.; Corma, A.; García, H. Water Stable Zr-Benzenedicarboxylate Metal-Organic Frameworks as Photocatalysts for Hydrogen Generation, Chemistry. *A European Journal*. 2010, 16, 11133–11138. DOI: 10.1002/chem.200903526.

[70] Wang, W.; Xu, X.; Zhou, W.; Shao, Z. Recent Progress in Metal-Organic Frameworks for Applications in Electrocatalytic and Photocatalytic Water Splitting. *Adv Sci.* 2017, 4, 1600371. DOI: 10.1002/advs.201600371.

[71] Pratik, S. M.; Cramer, C. J. Predicted Efficient Visible-Light Driven Water Splitting and Carbon Dioxide Reduction Using Photoredox-Active UiO-NDI Metal Organic Framework. *J. Phys. Chem. C.* 2019, 123(32), 19778–19785. DOI: https://doi.org/10.1021/acs.jpcc.9b05693.

[72] Peng, X.; Ye, L.; Ding, Y.; Yi, L.; Zhang, C.; Wen, Z. Nanohybrid Photocatalysts with $ZnIn_2S_4$ Nanosheets Encapsulated UiO-66 Octahedral Nanoparticles for Visible-Light-

Driven Hydrogen Generation. *Appl. Catal. B*. 2020, 260, 118152. DOI: 10.1016/j.apcatb.2019.118152.

[73] Gu, Z. G.; Zhang, J. Epitaxial Growth and Applications of Oriented Metal–Organic Framework Thin Films. *Coord. Chem. Rev*. 2019, 378, 513–532. DOI: 10.1016/J.CCR.2017.09.028.

[74] Jiao, L.; Jiang, H. L. Metal-Organic-Framework-Based Single-Atom Catalysts for Energy Applications. *Chem*. 2019, 5, 786–804. DOI: 10.1016/j.chempr.2018.12.011.

[75] Xu, H.; Ci, S.; Ding, Y.; Wang, G.; Wen, Z. Recent Advances in Precious Metal-Free Bifunctional Catalysts for Electrochemical Conversion Systems. *J. Mater. Chem. A Mater*. 2019, 7, 8006–8029. DOI: 10.1039/c9ta00833k.

[76] Zhang, T.; Lin, W. Metal-Organic Frameworks for Artificial Photosynthesis and Photocatalysis. *Chem. Soc. Rev*. 2014, 43, 5982–5993. DOI: 10.1039/c4cs00103f.

[77] Zhang, F.; Jiang, D.; Zhang, X. Porous NiO Materials Prepared by Solid-State Thermolysis of a Ni-MOF Crystal for Lithium-Ion Battery Anode. *Nano-Struct. Nano-Object*. 2016, 5, 1–6. DOI: 10.1016/j.nanoso.2015.12.002.

[78] Bagheri, M.; Masoomi, M. Y.; Morsali, A. High Organic Sulfur Removal Performance of a Cobalt Based Metal-Organic Framework. *J. Hazard. Mater*. 2017, 331, 142–149. DOI: 10.1016/j.jhazmat.2017.02.037.

[79] Liu, X. L.; Yin, Q.; Huang, G.; Liu, T. F. Stable pyrazolate-based metal-organic frameworks for drug delivery. *Inorg. Chem. Commun*. 2018, 94, 21–26. DOI: 10.1016/j.inoche.2018.06.001.

[80] Lee, G. J.; Chien, Y. W.; Anandan, S.; Lv, C.; Dong, J.; Wu, J. J. Fabrication of Metal-Doped BiOi/MOF Composite Photocatalysts with Enhanced Photocatalytic Performance. *Int. J. Hydrogen. Energy*. 2021, 46, 5949–5962. DOI: 10.1016/j.ijhydene.2020.03.254.

[81] Kataoka, Y.; Sato, K.; Miyazaki, Y.; Masuda, K.; Tanaka, H.; Naito, S.; Mori, W. Photocatalytic Hydrogen Production from Water Using Porous Material $[Ru_2(p\text{-}BDC)_2]_n$. *Energy Environ. Sci*. 2009, 2, 397–400. DOI: 10.1039/b814539c.

[82] Liu, Y.; Liu, Z.; Huang, D.; Cheng, M.; Zeng, G.; Lai, C.; Zhang, C.; Zhou, C.; Wang, W.; Jiang, D., et al. Metal or Metal-Containing Nanoparticle@mof Nanocomposites as a Promising Type of Photocatalyst. *Coord. Chem. Rev*. 2019, 388, 63–78. DOI: 10.1016/j.ccr.2019.02.031.

[83] Huang, G.; Yang, Q.; Xu, Q.; Yu, S.-H.; Jiang, H.-L. Polydimethylsiloxane Coating for a Palladium/MOF Composite: Highly Improved Catalytic Performance by Surface Hydrophobization. *Angewandte Chemie*. 2016, 128, 7505–7509. DOI: 10.1002/ange.201600497.

[84] Shi, Y.; Yang, A. F.; Cao, C. S.; Zhao, B. Applications of MOFs: Recent Advances in Photocatalytic Hydrogen Production from Water. *Coord. Chem. Rev*. 2019, 390, 50–75. DOI: 10.1016/j.ccr.2019.03.012.

[85] Kong, X.; Pan, Q.; Song, S.; He, Z.; Zeng, T.; Yu, Y. Dual Metal UiO-Type Metal–Organic Frameworks for Solar-Driven Photocatalytic Hydrogen Evolution. *J. Phys. Chem. C*. 2021, 125, 20320–20330. DOI: 10.1021/acs.jpcc.1c05866.

[86] Nguyen, P. T. K.; Nguyen, H. T. D.; Nguyen, H. N.; Trickett, C. A.; Ton, Q. T.; Gutiérrez-Puebla, E.; Monge, M. A.; Cordova, K. E.; Gándara, F. New Metal-Organic Frameworks for Chemical Fixation of CO_2. *ACS Appl. Mater. Interfaces*. 2018, 10, 733–744. DOI: 10.1021/acsami.7b16163.

[87] Xiao, J.-D.; Jiang, H.-L. Thermally Stable Metal-Organic Framework-Templated Synthesis of Hierarchically Porous Metal Sulfides: Enhanced Photocatalytic Hydrogen Production. *Small*. 2017, 13, 1700632. DOI: 10.1002/smll.201700632.

[88] Wang, Z.; Huang, J.; Mao, J.; Guo, Q.; Chen, Z.; Lai, Y. Metal–Organic Frameworks and Their Derivatives with Graphene Composites: Preparation and Applications in Electrocatalysis and Photocatalysis. *J. Mater. Chem. A*. 2020, 8, 2934–2961. DOI: 10.1039/c9ta12776c.

[89] Wang, J. L.; Wang, C.; Lin, W. Metal–Organic Frameworks for Light Harvesting and Photocatalysis. *ACS Catal*. 2012, 2, 2630–2640. DOI: 10.1021/cs3005874.

[90] Whelan, É.; Steuber, F. W.; Gunnlaugsson, T.; Schmitt, W. Tuning Photoactive Metal–Organic Frameworks for Luminescence and Photocatalytic Applications. *Coord. Chem. Rev*. 2021, 437, 213757. DOI: 10.1016/J.CCR.2020.213757.

[91] Yuan, S.; Qin, J. S.; Xu, H. Q.; Su, J.; Rossi, D.; Chen, Y.; Zhang, L.; Lollar, C.; Wang, Q.; Jiang, H. L., et al. Cluster: An Ideal Inorganic Building Unit for Photoactive Metal-Organic Frameworks. *ACS Cent. Sci*. 2018, 4, 105–111. DOI: 10.1021/acscentsci.7b00497.

[92] Reddy, D. A.; Kim, Y.; Gopannagari, M.; Kumar, D. P.; Kim, T. K. Recent Advances in Metal-Organic Framework-Based Photocatalysts for Hydrogen Production. *Sustain. Energy Fuels*. 2021, 5, 1597–1618. DOI: 10.1039/c9se00749k.

[93] Tu, T. N.; Nguyen, M. V.; Nguyen, H. L.; Yuliarto, B.; Cordova, K. E.; Demir, S. Designing Bipyridine-Functionalized Zirconium Metal–Organic Frameworks as a Platform for Clean Energy and Other Emerging Applications. *Coord. Chem. Rev*. 2018, 364, 33–50. DOI: 10.1016/j.ccr.2018.03.014.

[94] Zhu, J.; Li, P. Z.; Guo, W.; Zhao, Y.; Zou, R. Titanium-Based Metal–Organic Frameworks for Photocatalytic Applications. *Coord. Chem. Rev*. 2018, 359, 80–101. DOI: 10.1016/J.CCR.2017.12.013.

[95] Lu, C.; Xiong, D.; Chen, C.; Wang, J.; Kong, Y.; Liu, T.; Ying, S.; Yi, F. Y. Indium-Based Metal-Organic Framework for Efficient Photocatalytic Hydrogen Evolution. *Inorg. Chem*. 2022, 61, 2587–2594. DOI: 10.1021/acs.inorgchem.1c03628.

[96] Morshedy, A. S.; Abd El Salam, H. M.; El Naggar, A. M. A.; Zaki, T. Hydrogen Production and in situ Storage Through Process of Water Splitting Using Mono/Binary Metal–Organic Framework (MOF) Structures as New Chief Photocatalysts. *Energy. Fuels*. 2020, 34, 11660–11669. DOI: 10.1021/acs.energyfuels.0c01559.

[97] Salcedo-Abraira, P.; Vilela, S. M. F.; Babaryk, A. A.; Cabrero-Antonino, M.; Gregorio, P.; Salles, F.; Navalón, S.; García, H.; Horcajada, P. Nickel Phosphonate MOF as Efficient Water Splitting Photocatalyst. *Nano Res*. 2020, 14, 450–457. DOI: 10.1007/S12274-020-3056-6.

[98] Shi, D.; Zheng, R.; Sun, M.-J.; Cao, X.; Sun, C.-X.; Cui, C.-J.; Liu, C.-S.; Zhao, J.; Du, M. Semiconductive Copper(i)–Organic Frameworks for Efficient Light-Driven Hydrogen Generation without Additional Photosensitizers and Cocatalysts. *Angewandte Chemie*. 2017, 129, 14829–14833. DOI: 10.1002/ANGE.201709869.

[99] Toyao, T.; Saito, M.; Horiuchi, Y.; Mochizuki, K.; Iwata, M.; Higashimura, H.; Matsuoka, M. Efficient Hydrogen Production and Photocatalytic Reduction of Nitrobenzene Over a Visible-Light-Responsive Metal–Organic Framework Photocatalyst. *Catal. Sci. Technol*. 2013, 3, 2092–2097. DOI: 10.1039/C3CY00211J.

[100] Pullen, S.; Fei, H.; Orthaber, A.; Cohen, S. M.; Ott, S. Enhanced Photochemical Hydrogen Production by a Molecular Diiron Catalyst Incorporated into a Metal–Organic Framework. *J. Am. Chem. Soc*. 2013, 135, 16997–17003. DOI: 10.1021/ja407176p.

[101] Toyao, T.; Saito, M.; Dohshi, S.; Mochizuki, K.; Iwata, M.; Higashimura, H.; Horiuchi, Y.; Matsuoka, M. Development of a Ru Complex-Incorporated MOF Photocatalyst for Hydrogen Production Under Visible-Light Irradiation. *Chem. Commun*. 2014, 50, 6779–6781. DOI: 10.1039/c4cc02397h.

[102] Song, T.; Zhang, L.; Zhang, P.; Zeng, J.; Wang, T.; Ali, A.; Zeng, H. Stable and Improved Visible-Light Photocatalytic Hydrogen Evolution Using Copper(ii)–Organic Frameworks: Engineering the Crystal Structures. *J. Mater. Chem. A*. 2017, 5, 6013–6018. DOI: 10.1039/C7TA00095B.

[103] Shi, D.; Cui, C. J.; Hu, M.; Ren, A. H.; Bin Song, L.; Sen Liu, C.; Du, M. A Microporous Mixed-Metal (Na/Cu) Mixed-Ligand (Flexible/Rigid) Metal–Organic Framework for Photocatalytic H_2 Generation. *J. Mater. Chem. C*. 2019, 7, 10211–10217. DOI: 10.1039/C9TC03342D.

[104] Chen, D. M.; Sun, C. X.; Sen Liu, C.; Du, M. Stable Layered Semiconductive Cu(i)–Organic Framework for Efficient Visible-Light-Driven Cr(vi) Reduction and H_2 Evolution. *Inorg. Chem*. 2018, 57, 7975–7981. DOI: 10.1021/acs.inorgchem.8b01137.

[105] Pattengale, B.; Yang, S.; Lee, S.; Huang, J. Mechanistic Probes of Zeolitic Imidazolate Framework for Photocatalytic Application. *ACS Catal*. 2017, 7(12), 8446–8453. DOI: https://doi.org/10.1021/acscatal.7b02467.

[106] Yuan, Y. P.; Yin, L. S.; Cao, S. W.; Xu, G. S.; Li, C. H.; Xue, C. Improving Photocatalytic Hydrogen Production of Metal–Organic Framework UiO-66 Octahedrons by Dye-Sensitization. *Appl. Catal. B*. 2015, 168-169, 572–576. 168–169. DOI: 10.1016/J.APCATB.2014.11.007.

[107] Han, S. Y.; Pan, D. L.; Chen, H.; Bu, X. B.; Gao, Y. X.; Gao, H.; Tian, Y.; Li, G. S.; Wang, G.; Cao, S. L., et al. A Methylthio-Functionalized-MOF Photocatalyst with High Performance for Visible-Light-Driven H_2 Evolution. *Angew. Chem. Int. Ed*. 2018, 57(31), 9864–9869. DOI: 10.1002/ANIE.201806077.

[108] Leng, F.; Liu, H.; Ding, M.; Lin, Q. P.; Jiang, H. L. Boosting Photocatalytic Hydrogen Production of Porphyrinic MOFs: The Metal Location in Metalloporphyrin Matters. *ACS Catal*. 2018, 8(5), 4583–4590. DOI: https://doi.org/10.1021/acscatal.8b00764.

[109] Truong, Q. D.; Hoa, H. T.; Le, T. S. Pt Nanoparticles Loaded Titanium Picolinate Framework for Photocatalytic Hydrogen Generation. *Catal. Commun*. 2015, 59, 55–60. DOI: 10.1016/J.CATCOM.2014.09.045.

[110] Li, F.; Wang, D.; Xing, Q. J.; Zhou, G.; Liu, S. S.; Li, Y.; Zheng, L. L.; Ye, P.; Zou, J. P. Design and Syntheses of MOF/COF Hybrid Materials via Postsynthetic Covalent Modification: An Efficient Strategy to Boost the Visible-Light-Driven Photocatalytic Performance. *Appl. Catal. B*. 2019, 243, 621–628. DOI: 10.1016/J.APCATB.2018.10.043.

[111] Feng, Y.; Chen, C.; Liu, Z.; Fei, B.; Lin, P.; Li, Q.; Sun, S.; Du, S. Application of a Ni Mercaptopyrimidine MOF as Highly Efficient Catalyst for Sunlight-Driven Hydrogen Generation. *J. Mater. Chem. A*. 2015, 3, 7163–7169. DOI: 10.1039/C5TA00136F.

[112] Song, T.; Zhang, P.; Zeng, J.; Wang, T.; Ali, A.; Zeng, H. Tunable Conduction Band Energy and Metal-To-Ligand Charge Transfer for Wide-Spectrum Photocatalytic H_2 Evolution and Stability from Isostructural Metal-Organic Frameworks. *Int. J. Hydrogen. Energy*. 2017, 42, 26605–26616. DOI: 10.1016/J.IJHYDENE.2017.09.081.

[113] Zhang, R.; Liu, Y.; Wang, J.; Wang, Z.; Wang, P.; Zheng, Z.; Qin, X.; Zhang, X.; Dai, Y.; Huang, B. Post-Synthetic Platinum Complex Modification of a Triazine Based Metal Organic Frameworks for Enhanced Photocatalytic H_2 Evolution. *J. Solid State Chem*. 2019, 271, 260–265. DOI: 10.1016/J.JSSC.2019.01.006.

[114] He, T.; Chen, S.; Ni, B.; Gong, Y.; Wu, Z.; Song, L.; Gu, L.; Hu, W.; Wang, X. Zirconium–Porphyrin-based Metal–Organic Framework Hollow Nanotubes for Immobilization of Noble-Metal Single Atoms. *Angewandte Chemie*. 2018, 130, 3551–3556. DOI: 10.1002/ANGE.201800817.

[115] An, Y.; Liu, Y.; An, P.; Dong, J.; Xu, B.; Dai, Y.; Qin, X.; Zhang, X.; Whangbo, M.-H.; Huang, B. NiIi Coordination to an Al-Based Metal–Organic Framework Made from

2-Aminoterephthalate for Photocatalytic Overall Water Splitting. *Angewandte Chemie*. 2017, 129, 3082–3086. DOI: 10.1002/ANGE.201612423.

[116] Fang, X.; Shang, Q.; Wang, Y.; Jiao, L.; Yao, T.; Li, Y.; Zhang, Q.; Luo, Y.; Jiang, H. L. Single Pt Atoms Confined into a Metal–Organic Framework for Efficient Photocatalysis. *Adv.Mate*. 2018, 30, 1705112. DOI: 10.1002/ADMA.201705112.

[117] Xiao, Y.; Guo, X.; Liu, J.; Liu, L.; Zhang, F.; Li, C. Development of a Bismuth-Based Metal-Organic Framework for Photocatalytic Hydrogen Production. *Chin. J. Catal*. 2019, 40, 1339–1344. DOI: 10.1016/S1872-2067(19)63329-2.

[118] Guo, W.; Lv, H.; Chen, Z.; Sullivan, K. P.; Lauinger, S. M.; Chi, Y.; Sumliner, J. M.; Lian, T.; Hill, C. L. Self-Assembly of Polyoxometalates, Pt Nanoparticles and Metal–Organic Frameworks into a Hybrid Material for Synergistic Hydrogen Evolution. *J. Mater. Chem. A Mater*. 2016, 4, 5952–5957. DOI: 10.1039/C6TA00011H.

[119] Zhao, J.; Wang, Y.; Zhou, J.; Qi, P.; Li, S.; Zhang, K.; Feng, X.; Wang, B.; Hu, C. A Copper(ii)-Based MOF Film for Highly Efficient Visible-Light-Driven Hydrogen Production. *J. Mater. Chem. A Mater*. 2016, 4, 7174–7177. DOI: 10.1039/C6TA00431H.

[120] Zhao, X.; Zhang, S.; Yan, J.; Li, L.; Wu, G.; Shi, W.; Yang, G.; Guan, N.; Cheng, P. Polyoxometalate-Based Metal–Organic Frameworks as Visible-Light-Induced Photocatalysts. *Inorg. Chem*. 2018, 57, 5030–5037. DOI: 10.1021/acs.inorgchem.8b00098.

[121] Yu, Q.; Dong, H.; Zhang, X.; Zhu, Y. X.; Wang, J. H.; Zhang, F. M.; Sun, X. J. Novel Stable Metal–Organic Framework Photocatalyst for Light-Driven Hydrogen Production. *CrystEngcomm*. 2018, 20, 3228–3233. DOI: 10.1039/C8CE00386F.

[122] Roy, S.; Bhunia, A.; Schuth, N.; Haumann, M.; Ott, S. Light-Driven Hydrogen Evolution Catalyzed by a Cobaloxime Catalyst Incorporated in a MIL-101(cr) Metal–Organic Framework, Sustain Energy Fuels. *Sustain Energy Fuels*. 2018, 2(6), 1148–1152. DOI: https://doi.org/10.1039/C8SE00072G.

[123] Wang, D.; Song, Y.; Cai, J.; Wu, L.; Li, Z. Effective Photo-Reduction to Deposit Pt Nanoparticles on MIL-100(fe) for Visible-Light-Induced Hydrogen Evolution. *New. J. Chem*. 2016, 40(11), 9170–9175. DOI: https://doi.org/10.1039/C6NJ01989G.

[124] Liu, X. L.; Wang, R.; Zhang, M. Y.; Yuan, Y. P.; Xue, C. Dye-Sensitized MIL-101 Metal Organic Frameworks Loaded with Ni/NiO $_x$ Nanoparticles for Efficient Visible-Light-Driven Hydrogen Generation. *APL Mater*. 2015, 3, 104403. DOI: 10.1063/1.4922151.

[125] Xu, J.; Gao, J.; Wang, C.; Yang, Y.; Wang, L. NH_2-MIL-125(Ti)/graphitic Carbon Nitride Heterostructure Decorated with NiPd Co-Catalysts for Efficient Photocatalytic Hydrogen Production. *Appl. Catal. B*. 2017, 219, 101–108. DOI: 10.1016/J.APCATB.2017.07.046.

[126] Assi, H.; Pardo Pérez, L. C.; Mouchaham, G.; Ragon, F.; Nasalevich, M.; Guillou, N.; Martineau, C.; Chevreau, H.; Kapteijn, F.; Gascon, J., et al. Investigating the Case of Titanium(iv) Carboxyphenolate Photoactive Coordination Polymers. *Inorg. Chem*. 2016, 55(15), 7192–7199. DOI: https://doi.org/10.1021/acs.inorgchem.6b01060.

[127] Xiao, J. D.; Shang, Q.; Xiong, Y.; Zhang, Q.; Luo, Y.; Yu, S. H.; Jiang, H. L. Boosting Photocatalytic Hydrogen Production of a Metal–Organic Framework Decorated with Platinum Nanoparticles: The Platinum Location Matters. *Angew. Chem. Int. Ed*. 2016, 55, 9389–9393. DOI: 10.1002/ANIE.201603990.

[128] Zhou, T.; Du, Y.; Borgna, A.; Hong, J.; Wang, Y.; Han, J.; Zhang, W.; Xu, R. Post-Synthesis Modification of a Metal–Organic Framework to Construct a Bifunctional Photocatalyst for Hydrogen Production. *Energy Environ. Sci*. 2013, 6, 3229–3234. DOI: 10.1039/C3EE41548A.

[129] Wen, M.; Mori, K.; Kamegawa, T.; Yamashita, H. Amine-Functionalized MIL-101(cr) with Imbedded Platinum Nanoparticles as a Durable Photocatalyst for Hydrogen

Production from Water. *Chem. Commun*. 2014, 50, 11645–11648. DOI: 10.1039/c4cc02994a.

[130] Shi, X.; Zhang, J.; Cui, G.; Deng, N.; Wang, W.; Wang, Q.; Tang, B. Photocatalytic H_2 Evolution Improvement for H Free-Radical Stabilization by Electrostatic Interaction of a Cu-BTC MOF with ZnO/GO. *Nano Res*. 2018, 11(2), 979–987. 2017). DOI: https://doi.org/10.1007/S12274-017-1710-4.

[131] Shen, L.; Luo, M.; Liu, Y.; Liang, R.; Jing, F.; Wu, L. Noble-Metal-Free MoS_2 Co-Catalyst Decorated UiO-66/CdS Hybrids for Efficient Photocatalytic H_2 Production. *Appl. Catal. B*. 2015, 166-167, 445–453. 166–167. DOI: 10.1016/J.APCATB.2014.11.056.

[132] Tian, L.; Yang, X.; Liu, Q.; Qu, F.; Tang, H. Anchoring Metal-Organic Framework Nanoparticles on Graphitic Carbon Nitrides for Solar-Driven Photocatalytic Hydrogen Evolution. *Appl. Surf. Sci*. 2018, 455, 403–409. DOI: 10.1016/J.APSUSC.2018.06.014.

[133] Zhou, J. J.; Wang, R.; Liu, X. L.; Peng, F. M.; Li, C. H.; Teng, F.; Yuan, Y. P. In situ Growth of CdS Nanoparticles on UiO-66 Metal-Organic Framework Octahedrons for Enhanced Photocatalytic Hydrogen Production Under Visible Light Irradiation. *Appl. Surf. Sci*. 2015, 346, 278–283. DOI: 10.1016/J.APSUSC.2015.03.210.

[134] Tilgner, D.; Kempe, R. A Plasmonic Colloidal Photocatalyst Composed of a Metal–Organic Framework Core and a Gold/Anatase Shell for Visible-Light-Driven Wastewater Purification from Antibiotics and Hydrogen Evolution. *Chem. Eur. J*. 2017, 23, 3184–3190. DOI: 10.1002/CHEM.201605473.

[135] Wang, Y.; Zhang, Y.; Jiang, Z.; Jiang, G.; Zhao, Z.; Wu, Q.; Liu, Y.; Xu, Q.; Duan, A.; Xu, C. Controlled Fabrication and Enhanced Visible-Light Photocatalytic Hydrogen Production of Au@cds/MIL-101 Heterostructure. *Appl. Catal. B*. 2016, 185, 307–314. DOI: 10.1016/J.APCATB.2015.12.020.

[136] Meyer, K.; Bashir, S.; Llorca, J.; Idriss, H.; Ranocchiari, M.; van Bokhoven, J. A. Photocatalyzed Hydrogen Evolution from Water by a Composite Catalyst of NH_2-MIL-125(Ti) and Surface Nickel(ii) Species. *Chem. Eur. J*. 2016, 22, 13894–13899. DOI: 10.1002/CHEM.201601988.

[137] Bag, P. P.; Wang, X. S.; Sahoo, P.; Xiong, J.; Cao, R. Efficient Photocatalytic Hydrogen Evolution Under Visible Light by Ternary Composite CdS@NU-1000/RGO. *Catal. Sci. Technol*. 2017, 7, 5113–5119. DOI: 10.1039/C7CY01254C.

[138] Liang, Q.; Jin, J.; Liu, C.; Xu, S.; Yao, C.; Li, Z. Fabrication of the Ternary Heterojunction $Cd_{0.5}Zn_{0.5}S$@UIO-66@g-C_3N_4 for Enhanced Visible-Light Photocatalytic Hydrogen Evolution and Degradation of Organic Pollutants. *Inorg. Chem. Front*. 2018, 5, 335–343. DOI: 10.1039/C7QI00638A.

[139] Hou, C. C.; Li, T. T.; Cao, S.; Chen, Y.; Fu, W. F. Incorporation of a $[Ru(dcbpy)(bpy)_2]^{2+}$ Photosensitizer and a $Pt(dcbpy)Cl_2$ Catalyst into Metal–Organic Frameworks for Photocatalytic Hydrogen Evolution from Aqueous Solution. *J. Mater. Chem. A*. 2015, 3, 10386–10394. DOI: 10.1039/C5TA01135C.

[140] Li, Z.; Xiao, J. D.; Jiang, H. L. Encapsulating a Co(ii) Molecular Photocatalyst in Metal–Organic Framework for Visible-Light-Driven H $_2$ Production: Boosting Catalytic Efficiency via Spatial Charge Separation. *ACS Catal*. 2016, 6, 5359–5365. DOI: 10.1021/acscatal.6b01293.

[141] Nasalevich, M. A.; Becker, R.; Ramos-Fernandez, E. V.; Castellanos, S.; Veber, S. L.; Fedin, M. V.; Kapteijn, F.; Reek, J. N. H.; Van Der Vlugt, J. I.; Gascon, J. Co@NH_2-MIL-125(Ti): Cobaloxime-Derived Metal-Organic Framework-Based Composite for Light-Driven H_2 Production. *Energy Environ. Sci*. 2015, 8, 364–375. DOI: 10.1039/c4ee02853h.

[142] Jiang, Z.; Liu, J.; Gao, M.; Fan, X.; Zhang, L.; Zhang, J. Assembling Polyoxo-Titanium Clusters and CdS Nanoparticles to a Porous Matrix for Efficient and Tunable

H_2-Evolution Activities with Visible Light. *Adv.Mate*. 2017, 29, 1603369. DOI: 10.1002/ADMA.201603369.

[143] Shah, W. A.; Ibrahim, S.; Abbas, S.; Naureen, L.; Batool, M.; Imran, M.; Nadeem, M. A. Nickel Containing Polyoxometalates Incorporated in Two Different Metal-Organic Frameworks for Hydrogen Evolution Reaction. *J. Environ. Chem. Eng*. 2021, 9, 106004. DOI: 10.1016/j.jece.2021.106004.

[144] Li, H.; Yao, S.; Wu, H. L.; Qu, J. Y.; Zhang, Z. M.; Lu, T. B.; Lin, W.; Wang, E. B. Charge-Regulated Sequential Adsorption of Anionic Catalysts and Cationic Photosensitizers into Metal-Organic Frameworks Enhances Photocatalytic Proton Reduction. *Appl. Catal. B*. 2018, 224, 46–52. DOI: 10.1016/j.apcatb.2017.10.031.

[145] Bu, Y.; Li, F.; Zhang, Y.; Liu, R.; Luo, X.; Xu, L. Immobilizing CdS Nanoparticles and MoS2/RGO on Zr-Based Metal–Organic Framework 12-Tungstosilicate@uiO-67 Toward Enhanced Photocatalytic H_2 Evolution. *R.S.C. Adv*. 2016, 6, 40560–40566. DOI: 10.1039/C6RA05522B.

[146] Zhang, Z. M.; Zhang, T.; Wang, C.; Lin, Z.; Long, L. S.; Lin, W. Photosensitizing Metal–Organic Framework Enabling Visible-Light-Driven Proton Reduction by a Wells–Dawson-type Polyoxometalate. *J. Am. Chem. Soc*. 2015, 137, 3197–3200. DOI: 10.1021/jacs.5b00075.

[147] Kong, X. J.; Lin, Z.; Zhang, Z. M.; Zhang, T.; Lin, W. Hierarchical Integration of Photosensitizing Metal–Organic Frameworks and Nickel-Containing Polyoxometalates for Efficient Visible-Light-Driven Hydrogen Evolution. *Angew. Chem. Int. Ed*. 2016, 55, 6411–6416. DOI: 10.1002/ANIE.201600431.

[148] Wang, H.; Tian, J.; Xu, Z. Y.; Zhang, D. W.; Wang, H.; Xie, S. H.; Xu, D. W.; Ren, Y. H.; Liu, Y.; Li, Z. T. Supramolecular Metal-Organic Frameworks That Display High Homogeneous and Heterogeneous Photocatalytic Activity for H_2 Production. *Nat. Commun*. 2016, 7, 1–9. DOI: 10.1038/ncomms11580.

[149] Tian, P.; He, X.; Li, W.; Zhao, L.; Fang, W.; Chen, H.; Zhang, F.; Zhang, W.; Wang, W. Zr-MOFs Based on Keggin-Type Polyoxometalates for Photocatalytic Hydrogen Production. *J. Mater. Sci*. 2018, 53, 12016–12029. DOI: 10.1007/s10853-018-2476-0.

[150] Sun, W.; An, B.; Qi, B.; Liu, T.; Jin, M.; Duan, C. Dual-Excitation Polyoxometalate-Based Frameworks for One-Pot Light-Driven Hydrogen Evolution and Oxidative Dehydrogenation. *ACS Appl. Mater. Interfaces*. 2018, 10, 13462–13469. DOI: 10.1021/acsami.8b00350.

[151] Sun, W.; He, C.; Liu, T.; Duan, C. Synergistic Catalysis for Light-Driven Proton Reduction Using a Polyoxometalate-Based Cu–Ni Heterometallic–Organic Framework. *Chem. Commun*. 2019, 55, 3805–3808. DOI: 10.1039/c8cc09285k.

[152] Jiao, L.; Dong, Y.; Xin, X.; Qin, L.; Lv, H. Facile Integration of Ni-Substituted Polyoxometalate Catalysts into Mesoporous Light-Responsive Metal-Organic Framework for Effective Photogeneration of Hydrogen. *Appl. Catal. B*. 2021, 291, 120091. DOI: 10.1016/j.apcatb.2021.120091.

[153] Shi, D.; Zheng, R.; Sen Liu, C.; Chen, D. M.; Zhao, J.; Du, M. Dual-Functionalized Mixed Keggin- and Lindqvist-Type Cu 24 -Based POM@MOF for Visible-Light-Driven H 2 and O 2 Evolution. *Inorg. Chem*. 2019, 58(11), 7229–7235. DOI: https://doi.org/10.1021/acs.inorgchem.9b00206.

[154] Wang, S.; Cao, Y.; Jia, W.; Lu, Z.; Jia, D. A Cage-Confinement Strategy to Fabricate Pt-Mo_6Co_6C Heterojunction for Highly Efficient PH-Universal Hydrogen Evolution. *Appl. Catal. B*. 2021, 298, 120579. DOI: 10.1016/j.apcatb.2021.120579.

[155] Samanta, D.; Verma, P.; Roy, S.; Maji, T. K. Nanovesicular MOF with Omniphilic Porosity: Bimodal Functionality for White-Light Emission and Photocatalysis by Dye

Encapsulation. *ACS Appl. Mater. Interfaces*. 2018, 10, 23140–23146. DOI: 10.1021/acsami.8b06363.

[156] He, J.; Wang, J.; Chen, Y.; Zhang, J.; Duan, D.; Wanga, Y.; Yan, Z. A Dye-Sensitized Pt@uiO-66(zr) Metal–Organic Framework for Visible-Light Photocatalytic Hydrogen Production. *Chem. Commun*. 2014, 50, 7063–7066. DOI: 10.1039/c4cc01086h.

[157] Thompson, W. A.; Perier, C.; Maroto-Valer, M. M. Systematic Study of Sol-Gel Parameters on TiO_2 Coating for CO_2 Photoreduction. *Appl. Catal. B*. 2018, 238, 136–146. DOI: 10.1016/j.apcatb.2018.07.018.

[158] Ren, R.; Zhao, H.; Sui, X.; Guo, X.; Huang, X.; Wang, Y.; Dong, Q.; Chen, J. Exfoliated Molybdenum Disulfide Encapsulated in a Metal Organic Framework for Enhanced Photocatalytic Hydrogen Evolution. *Catalysts*. 2019, 9, 89. DOI: 10.3390/catal9010089.

[159] Li, S.; Mei, H. M.; Yao, S. L.; Chen, Z. Y.; Lu, Y. L.; Zhang, L.; Su, C. Y. Well-Distributed Pt-Nanoparticles within Confined Coordination Interspaces of Self-Sensitized Porphyrin Metal-Organic Frameworks: Synergistic Effect Boosting Highly Efficient Photocatalytic Hydrogen Evolution Reaction. *Chem. Sci*. 2019, 10, 10577–10585. DOI: 10.1039/c9sc01866b.

[160] Wang, Y. Y.; Tang, Z.; Ji, X. Y.; Wang, S.; Yao, Z. S.; Tao, J. Encapsulating Low-Coordinated Pt Clusters within a Metal-Organic Framework Induces Spatial Charge Separation Boosting Photocatalytic Hydrogen Evolution. *Catal. Sci. Technol*. 2020, 10, 5048–5059. DOI: 10.1039/d0cy00809e.

[161] He, Y.; Luo, S.; Hu, X.; Cheng, Y.; Huang, Y.; Chen, S.; Fu, M.; Jia, Y.; Liu, X. NH_2-MIL-125(Ti) Encapsulated with in Situ-Formed Carbon Nanodots with Up-Conversion Effect for Improving Photocatalytic NO Removal and H_2 Evolution. *Chem. Eng. J*. 2021, 420, 127643. DOI: 10.1016/j.cej.2020.127643.

[162] Xiao, J. D.; Han, L.; Luo, J.; Yu, S. H.; Jiang, H. L. Integration of Plasmonic Effects and Schottky Junctions into Metal–Organic Framework Composites: Steering Charge Flow for Enhanced Visible-Light Photocatalysis. *Angew. Chem. Int. Ed*. 2018, 57, 1103–1107. DOI: 10.1002/ANIE.201711725.

[163] Zhen, W.; Ma, J.; Lu, G. Small-Sized Ni(1 1 1) Particles in Metal-Organic Frameworks with Low Over-Potential for Visible Photocatalytic Hydrogen Generation. *Appl. Catal. B*. 2016, 190, 12–25. DOI: 10.1016/J.APCATB.2016.02.061.

[164] Zhen, W.; Gao, H.; Tian, B.; Ma, J.; Lu, G. Fabrication of Low Adsorption Energy Ni–Mo Cluster Cocatalyst in Metal–Organic Frameworks for Visible Photocatalytic Hydrogen Evolution. *ACS Appl. Mater. Interfaces*. 2016, 8, 10808–10819. DOI: 10.1021/acsami.5b12524.

[165] Su, Y.; Zhang, Z.; Liu, H.; Wang, Y. $Cd_{0.2}Zn_{0.8}S$@UiO-66-NH_2 Nanocomposites as Efficient and Stable Visible-Light-Driven Photocatalyst for H_2 Evolution and CO_2 Reduction. *Appl. Catal. B*. 2017, 200, 448–457. DOI: 10.1016/J.APCATB.2016.07.032.

[166] Liu, H.; Zhang, J.; Ao, D. Construction of Heterostructured $ZnIn_2S_4$@NH_2-MIL-125(Ti) Nanocomposites for Visible-Light-Driven H_2 Production. *Appl. Catal. B*. 2018, 221, 433–442. DOI: 10.1016/J.APCATB.2017.09.043.

[167] Liu, H.; Xu, C.; Li, D.; Jiang, H.-L. Photocatalytic Hydrogen Production Coupled with Selective Benzylamine Oxidation Over MOF Composites. *Angewandte Chemie*. 2018, 130, 5477–5481. DOI: 10.1002/ANGE.201800320.

[168] Xu, J.; Liu, J.; Li, Z.; Wang, X.; Wang, Z. Synthesis, Structure and Properties of Pd@MOF-808. *J. Mater. Sci*. 2019, 54. 19. 54, 12911–12924. 10.1007/S10853-019-03786-0.

[169] Li, X.; Gao, K.; Mo, B.; Tang, J.; Wu, J.; Hou, H. BiOi Particles Confined into Metal-Organic Framework NU-1000 for Valid Photocatalytic Hydrogen Evolution

Under Visible-Light Irradiation. *Inorg. Chem.* 2021, 60, 1352–1358. DOI: 10.1021/acs.inorgchem.0c02423.

[170] Huang, X.; Li, X.; Luan, Q.; Zhang, K.; Wu, Z.; Li, B.; Xi, Z.; Dong, W.; Wang, G. Highly Dispersed Pt Clusters Encapsulated in MIL-125-NH_2 via in situ Auto-Reduction Method for Photocatalytic H_2 Production Under Visible Light. *Nano Res.* 2021, 14, 4250–4257. DOI: 10.1007/S12274-021-3597-3.

[171] Han, J.; Wang, D.; Du, Y.; Xi, S.; Hong, J.; Yin, S.; Chen, Z.; Zhou, T.; Xu, R. Metal–Organic Framework Immobilized Cobalt Oxide Nanoparticles for Efficient Photocatalytic Water Oxidation. *J. Mater. Chem. A.* 2015, 3, 20607–20613. DOI: 10.1039/c5ta04675k.

[172] Tang, H. L.; Sun, X. J.; Zhang, F. M. Development of MOF-Based Heterostructures for Photocatalytic Hydrogen Evolution. *Dalton Trans.* 2020, 49, 12136–12144. DOI: 10.1039/d0dt02309d.

[173] Wen, M.; Mori, K.; Kuwahara, Y.; An, T.; Yamashita, H. Design and Architecture of Metal Organic Frameworks for Visible Light Enhanced Hydrogen Production. *Appl. Catal. B.* 2017, 218, 555–569. DOI: 10.1016/j.apcatb.2017.06.082.

[174] Balestri, D.; Roux, Y.; Mattarozzi, M.; Mucchino, C.; Heux, L.; Brazzolotto, D.; Artero, V.; Duboc, C.; Pelagatti, P.; Marchiò, L., et al. Heterogenization of a [NiFe] Hydrogenase Mimic Through Simple and Efficient Encapsulation into a Mesoporous MOF. *Inorg. Chem.* 2017, 56(24), 14801–14808. DOI: https://doi.org/10.1021/acs.inorgchem.7b01824.

[175] Belousov, A. S.; Suleimanov, E. V. Application of Metal–Organic Frameworks as an Alternative to Metal Oxide-Based Photocatalysts for the Production of Industrially Important Organic Chemicals. *Green Chem.* 2021, 23, 6172–6204. DOI: 10.1039/d1gc01690c.

[176] Dhakshinamoorthy, A.; Li, Z.; Garcia, H. Catalysis and Photocatalysis by Metal Organic Frameworks. *Chem. Soc. Rev.* 2018, 47, 8134–8172. DOI: 10.1039/C8CS00256H.

[177] Gascon, J.; Corma, A.; Kapteijn, F.; Xamena, F. X. L. I. Metal Organic Framework Catalysis: Quo Vadis? *ACS Catal.* 2014, 4, 361–378. DOI: 10.1021/cs400959k.

[178] Yu, X.; Cohen, S. M. Photocatalytic Metal-Organic Frameworks for Selective 2,2,2-Trifluoroethylation of Styrenes. *J. Am. Chem. Soc.* 2016, 138, 12320–12323. DOI: 10.1021/jacs.6b06859.

[179] Hawes, C. S.; Mille, G. M. O.; Byrne, K.; Schmitt, W.; Gunnlaugsson, T. Tetraarylpyrrolo [3,2- b]pyrroles as versatile and responsive fluorescent linkers in metal–organic frameworks. *Dalton Trans.* 2018, 47, 10080–10092. DOI: 10.1039/c8dt01784k.

[180] Huang, C. W.; Nguyen, V. H.; Zhou, S. R.; Hsu, S. Y.; Tan, J. X.; Wu, K. C. W. Metal-Organic Frameworks: Preparation and Applications in Highly Efficient Heterogeneous Photocatalysis. *Sustain. Energy Fuels.* 2020, 4, 504–521. DOI: 10.1039/c9se00972h.

[181] Choudhuri, I.; Truhlar, D. G. Photogenerated Charge Separation in a CdSe Nanocluster Encapsulated in a Metal–Organic Framework for Improved Photocatalysis. *J. Phys. Chem. C.* 2020, 124, 8504–8513. DOI: 10.1021/acs.jpcc.0c00007.

[182] Yin, W.; An Tao, C.; Wang, F.; Huang, J.; Qu, T.; Wang, J. Tuning Optical Properties of MOF-Based Thin Films by Changing the Ligands of MOFs. *Sci. China Mater.* 2017, 61, 391–400. DOI: 10.1007/S40843-017-9143-5.

[183] Flage-Larsen, E.; Røyset, A.; Cavka, J. H.; Thorshaug, K. Band Gap Modulations in UiO Metal–Organic Frameworks. *J. Phys. Chem. C.* 2013, 117, 20610–20616. DOI: 10.1021/jp405335q.

[184] Ali Akbar Razavi, S.; Morsali, A. Linker Functionalized Metal-Organic Frameworks. *Coord. Chem. Rev.* 2019, 399, 213023. DOI: 10.1016/J.CCR.2019.213023.

[185] Assen, A. H.; Adil, K.; Cordova, K. E.; Belmabkhout, Y. The Chemistry of Metal–Organic Frameworks with Face-Centered Cubic Topology. *Coord. Chem. Rev*. 2022, 468, 214644. DOI: 10.1016/j.ccr.2022.214644.

[186] Yuan, S.; Feng, L.; Wang, K.; Pang, J.; Bosch, M.; Lollar, C.; Sun, Y.; Qin, J.; Yang, X.; Zhang, P., et al. Stable Metal–Organic Frameworks: Design. *Synthesis, And Applications, Advanced Materials*. 2018, 30, 1704303. DOI: 10.1002/ADMA.201704303.

[187] Li, X.; Liu, S.; Fan, K.; Liu, Z.; Song, B.; Yu, J. MOF-Based Transparent Passivation Layer Modified ZnO Nanorod Arrays for Enhanced Photo-Electrochemical Water Splitting. *Adv. Energy Mater*. 2018, 8, 1800101. DOI: 10.1002/AENM.201800101.

[188] Dong, Y. J.; Liao, J. F.; Kong, Z. C.; Xu, Y. F.; Chen, Z. J.; Chen, H. Y.; Bin Kuang, D.; Fenske, D.; Su, C. Y. Conformal Coating of Ultrathin Metal-Organic Framework on Semiconductor Electrode for Boosted Photoelectrochemical Water Oxidation. *Appl. Catal. B*. 2018, 237, 9–17. DOI: 10.1016/J.APCATB.2018.05.059.

[189] Zhang, Q.; Wang, H.; Dong, Y.; Yan, J.; Ke, X.; Wu, Q.; Xue, S. In situ Growth of Ultrathin Co-MOF Nanosheets on α-Fe_2O_3 Hematite Nanorods for Efficient Photoelectrochemical Water Oxidation. *Solar Energy*. 2018, 171, 388–396. DOI: 10.1016/J.SOLENER.2018.06.086.

[190] Liu, Z. Q.; Qiu, K.; Bai, H.; Wang, F.; Ge, Y.; Cui, W.; Zheng, G.; Cui, J.; Fan, W. *Ni-MOF in-Situ Decorating ZnO Photoelectrode for Photoelectrochemical Water Splitting*; //Doi. Org/10.1142/S1793604718500856: Https, 2018, p. 11. DOI: 10.1142/S1793604718500856.

[191] Yoon, J. W.; Kim, D. H.; Kim, J. H.; Jang, H. W.; Lee, J. H. NH2-MIL-125(Ti)/TiO_2 Nanorod Heterojunction Photoanodes for Efficient Photoelectrochemical Water Splitting. *Appl. Catal. B*. 2019, 244, 511–518. DOI: 10.1016/J.APCATB.2018.11.057.

[192] Gao, C.; Lyu, F.; Yin, Y. Encapsulated Metal Nanoparticles for Catalysis. *Chem. Rev*. 2021, 121(2), 834–881. DOI: https://doi.org/10.1021/acs.chemrev.0c00237.

[193] Ahsan, M. A.; Deemer, E.; Fernandez-Delgado, O.; Wang, H.; Curry, M. L.; El-Gendy, A. A.; Noveron, J. C. Fe Nanoparticles Encapsulated in MOF-Derived Carbon for the Reduction of 4-Nitrophenol and Methyl Orange in Water. *Catal. Commun*. 2019, 130, 105753. DOI: 10.1016/J.CATCOM.2019.105753.

[194] Liu, Y.; Shi, W. J.; Lu, Y. K.; Liu, G.; Hou, L.; Wang, Y. Y. Nonenzymatic Glucose Sensing and Magnetic Property Based on the Composite Formed by Encapsulating Ag Nanoparticles in Cluster-Based Co-MOF. *Inorg. Chem*. 2019, 58(24), 16743–16751. DOI: https://doi.org/10.1021/acs.inorgchem.9b02889.

[195] Zhu, K.; Chen, C.; Lu, S.; Zhang, X.; Alsaedi, A. Hayat, MOFs-Induced Encapsulation of Ultrafine Ni Nanoparticles into 3D N-Doped Graphene-CNT Frameworks as a Recyclable Catalyst for Cr(vi) Reduction with Formic Acid. *Carbon*. 2019, 148, 52–63. DOI: 10.1016/J.CARBON.2019.03.044.

[196] Zhang, J.; Chu, R.; Chen, Y.; Jiang, H.; Zeng, Y.; Chen, X.; Zhang, Y.; Huang, N. M.; Guo, H. MOF-Derived Transition Metal Oxide Encapsulated in Carbon Layer as Stable Lithium Ion Battery Anodes. *J. Alloys Compd*. 2019, 797, 83–91. DOI: 10.1016/J.JALLCOM.2019.04.162.

[197] Guo, S.; Zhao, Y.; Yuan, H.; Wang, C.; Jiang, H.; Cheng, G. J. Ultrafast Laser Manufacture of Stable, Efficient Ultrafine Noble Metal Catalysts Mediated with MOF Derived High Density Defective Metal Oxides. *Small*. 2020, 16, 2000749. DOI: 10.1002/SMLL.202000749.

[198] Huang, X.; Yan, S.; Deng, D.; Zhang, L.; Liu, R.; Lv, Y. Novel Strategy for Engineering the Metal-Oxide@mof Core@shell Architecture and Its Applications in Cataluminescence Sensing. *ACS Appl. Mater. Interfaces*. 2021, 13(2), 3471–3480. DOI: https://doi.org/10.1021/acsami.0c20799.

[199] Subudhi, S.; Tripathy, S. P.; Parida, K. Metal Oxide Integrated Metal Organic Frameworks (MO@MOF): Rational Design, Fabrication Strategy, Characterization and Emerging Photocatalytic Applications. *Inorg. Chem. Front*. 2021, 8, 1619–1636. DOI: 10.1039/D0QI01117G.

[200] Li, B.; Ma, J.-G.; Cheng, P. Silica-Protection-Assisted Encapsulation of Cu_2O Nanocubes into a Metal–Organic Framework (ZIF-8) to Provide a Composite Catalyst. *Angewandte Chemie*. 2018, 130, 6950–6953. DOI: 10.1002/ANGE.201801588.

[201] Zhan, G.; Zeng, H. C. Integrated Nanocatalysts with Mesoporous Silica/Silicate and Microporous MOF Materials. *Coord. Chem. Rev*. 2016, 320-321, 181–192. 320–321. DOI: 10.1016/J.CCR.2016.03.003.

[202] Tülek, A.; Yıldırım, D.; Aydın, D.; Binay, B. Highly-Stable Madurella Mycetomatis Laccase Immobilized in Silica-Coated ZIF-8 Nanocomposites for Environmentally Friendly Cotton Bleaching Process. *Colloids Surf. B Biointerfaces*. 2021, 202, 111672. DOI: 10.1016/J.COLSURFB.2021.111672.

[203] Begum, S.; Hassan, Z.; Bräse, S.; Tsotsalas, M. Polymerization in MOF-Confined Nanospaces: Tailored Architectures, Functions, and Applications. *Langmuir*. 2020, 36 (36), 10657–10673. DOI: https://doi.org/10.1021/acs.langmuir.0c01832.

[204] Zheng, X.; Wang, L.; Pei, Q.; He, S.; Liu, S.; Xie, Z. Metal-Organic Framework@porous Organic Polymer Nanocomposite for Photodynamic Therapy. *Chemistry Of Materials*. 2017, 29, 2374–2381. DOI: 10.1021/acs.chemmater.7b00228.

[205] Xie, W.; Cui, D.; Zhang, S. R.; Xu, Y. H.; Jiang, D. L. Iodine capture in porous organic polymers and metal–organic frameworks materials. *Mater. Horiz*. 2019, 6, 1571–1595. DOI: 10.1039/C8MH01656A.

[206] Lu, Y.; Wang, S.; Yu, K.; Yu, J.; Zhao, D.; Li, C. Encapsulating Carbon Quantum Dot and Organic Dye in Multi-Shell Nanostructured MOFs for Use in White Light-Emitting Diode. *Microporous Mesoporous Mater*. 2021, 319, 111062. DOI: 10.1016/J.MICROMESO.2021.111062.

[207] Yan, X.; Zhao, Y.; Du, G.; Guo, Q.; Chen, H.; He, Q.; Zhao, Q.; Ye, H.; Wang, J.; Yuan, Y., et al. Magnetic Capture of Sulfur Quantum Dots Encapsulated in MOF-5-NH_2 via a Target-Driven Self-Cycling Catalyzed Hairpin Assembly for the Sensitive Detection of Patulin. *Chem. Eng. J*. 2022, 433, 133624. DOI: 10.1016/J.CEJ.2021.133624.

[208] Wang, M.; Nian, L.; Cheng, Y.; Yuan, B.; Cheng, S.; Cao, C. Encapsulation of Colloidal Semiconductor Quantum Dots into Metal-Organic Frameworks for Enhanced Antibacterial Activity Through Interfacial Electron Transfer. *Chem. Eng. J*. 2021, 426, 130832. DOI: 10.1016/J.CEJ.2021.130832.

[209] Du, D.; Shu, J.; Guo, M.; Haghighatbin, M. A.; Yang, D.; Bian, Z.; Cui, H. Potential-Resolved Differential Electrochemiluminescence Immunosensor for Cardiac Troponin I Based on MOF-5-Wrapped CdS Quantum Dot Nanoluminophores. *Anal. Chem*. 2020, 92(20), 14113–14121. DOI: https://doi.org/10.1021/acs.analchem.0c03131.

[210] Qiao, G. Y.; Guan, D.; Yuan, S.; Rao, H.; Chen, X.; Wang, J. A.; Qin, J. S.; Xu, J. J.; Yu, J. Perovskite Quantum Dots Encapsulated in a Mesoporous Metal–Organic Framework as Synergistic Photocathode Materials. *J. Am. Chem. Soc*. 2021, 143, 14253–14260. DOI: 10.1021/jacs.1c05907.

[211] Angamuthu, M.; Satishkumar, G.; Landau, M. V. Precisely Controlled Encapsulation of Fe_3O_4 Nanoparticles in Mesoporous Carbon Nanodisk Using Iron Based MOF Precursor for Effective Dye Removal. *Microporous Mesoporous Mater*. 2017, 251, 58–68. DOI: 10.1016/J.MICROMESO.2017.05.045.

[212] Wang, L.; Jiao, Y.; Yao, S.; Li, P.; Wang, R.; Chen, G. MOF-Derived NiO/Ni Architecture Encapsulated into N-Doped Carbon Nanotubes for Advanced Asymmetric Supercapacitors. *Inorg. Chem. Front*. 2019, 6, 1553–1560. DOI: 10.1039/C9QI00274J.

[213] Liu, G.; Feng, K.; Cui, H.; Li, J.; Liu, Y.; Wang, M. MOF derived in-situ carbon-encapsulated Fe_3O_4@C to mediate polysulfides redox for ultrastable Lithium-sulfur batteries. *Chem. Eng. J.* 2020, 381, 122652. DOI: 10.1016/J.CEJ.2019.122652.

[214] Li, B.; Suo, T.; Xie, S.; Xia, A.; Jie Ma, Y.; Huang, H.; Zhang, X.; Hu, Q. Rational Design, Synthesis, and Applications of Carbon Dots@metal–Organic Frameworks (CD@MOF) Based Sensors. *TrAc Trends Anal. Chem*. 2021, 135, 116163. DOI: 10.1016/J.TRAC.2020.116163.

[215] Chen, S. S.; Hu, C.; Liu, C. H.; Chen, Y. H.; Ahamad, T.; Alshehri, S. M.; Huang, P. H.; Wu, K. C. W. De Novo Synthesis of Platinum-Nanoparticle-Encapsulated UiO-66-NH_2 for Photocatalytic Thin Film Fabrication with Enhanced Performance of Phenol Degradation. *J. Hazard. Mater*. 2020, 397, 122431. DOI: 10.1016/J.JHAZMAT.2020.122431.

[216] Chen, Y.; Yu, B.; Cui, Y.; Xu, S.; Gong, J. Core-Shell Structured Cyclodextrin Metal-Organic Frameworks with Hierarchical Dye Encapsulation for Tunable Light Emission. *Chemistry Of Materials*. 2019, 31, 1289–1295. DOI: 10.1021/acs.chemmater.8b04126.

[217] Chen, X.; Zhang, Y.; Zhao, Y.; Wang, S.; Liu, L.; Xu, W.; Guo, Z.; Wang, S.; Liu, Y.; Zhang, J. Encapsulating Pt Nanoparticles Through Transforming Fe 3 O 4 into MIL-100(fe) for Well-Defined Fe 3 O 4 @pt@MIL-100(fe) Core–Shell Heterostructures with Promoting Catalytic Activity. *Inorg. Chem*. 2019, 58, 12433–12440. DOI: 10.1021/acs.inorgchem.9b02114.

[218] Zheng, Z.; Xu, H.; Xu, Z.; Ge, J. A Monodispersed Spherical Zr-Based Metal–Organic Framework Catalyst, Pt/Au@pd@UIO-66, Comprising an Au@pd Core–Shell Encapsulated in a UIO-66 Center and Its Highly Selective CO_2 Hydrogenation to Produce CO. *Small*. 2018, 14, 1702812. DOI: 10.1002/SMLL.201702812.

[219] Wang, C.; Liao, K. Recent Advances in Emerging Metal– and Covalent–Organic Frameworks for Enzyme Encapsulation. *ACS Appl. Mater. Interfaces*. 2021, 13, 56752–56776. DOI: 10.1021/acsami.1c13408.

[220] Hsu, P. H.; Chang, C. C.; Wang, T. H.; Lam, P. K.; Wei, M. Y.; Chen, C. T.; Chen, C. Y.; Chou, L. Y.; Shieh, F. K. Rapid Fabrication of Biocomposites by Encapsulating Enzymes into Zn-MOF-74 via a Mild Water-Based Approach. *ACS Appl. Mater. Interfaces*. 2021, 13(44), 52014–52022. DOI: https://doi.org/10.1021/acsami.1c09052.

[221] Ren, Z.; Zhou, W.; Weng, J.; Qin, Z.; Liu, L.; Ji, N.; Chen, C.; Shi, H.; Shi, W.; Zhang, X., et al. Phase Transition of Metal–Organic Frameworks for the Encapsulation of Enzymes. *J. Mater. Chem. A*. 2022, 10(37), 19881–19892. DOI: https://doi.org/10.1039/D2TA02070J.

[222] Sun, Y.; Shi, J.; Zhang, S.; Wu, Y.; Mei, S.; Qian, W.; Jiang, Z. Hierarchically Porous and Water-Tolerant Metal–Organic Frameworks for Enzyme Encapsulation. *Ind. Eng. Chem. Res*. 2019, 58, 12835–12844. DOI: 10.1021/acs.iecr.9b02164.

[223] Guo, J.; Yang, L.; Gao, Z.; Zhao, C.; Mei, Y.; Song, Y. Y. Insight of MOF Environment-Dependent Enzyme Activity via MOFs-In-Nanochannels Configuration. *ACS Catal*. 2020, 10(10), 5949–5958. DOI: https://doi.org/10.1021/acscatal.0c00591.

[224] Li, X.; Feng, Q.; Lu, K.; Huang, J.; Zhang, Y.; Hou, Y.; Qiao, H.; Li, D.; Wei, Q. Encapsulating Enzyme into Metal-Organic Framework During in-Situ Growth on Cellulose Acetate Nanofibers as Self-Powered Glucose Biosensor. *Biosens. Bioelectron*. 2021, 171, 112690. DOI: 10.1016/J.BIOS.2020.112690.

[225] Mukhopadhyay, S.; Basu, O.; Kar, A.; Das, S. K. Efficient Electrocatalytic Water Oxidation by Fe(salen)–MOF Composite: Effect of Modified Microenvironment. *Inorg. Chem*. 2020, 59, 472–483. DOI: 10.1021/acs.inorgchem.9b02745.

[226] Freire, C.; Nunes, M.; Pereira, C.; Fernandes, D. M.; Peixoto, A. F.; Rocha, M. Metallo(salen) Complexes as Versatile Building Blocks for the Fabrication of Molecular Materials and Devices with Tuned Properties. *Coord. Chem. Rev*. 2019, 394, 104–134. DOI: 10.1016/J.CCR.2019.05.014.

[227] Fan, Y.; Ren, Y.; Li, J.; Yue, C.; Jiang, H. Enhanced Activity and Enantioselectivity of Henry Reaction by the Postsynthetic Reduction Modification for a Chiral Cu(salen)-Based Metal–Organic Framework. *Inorg. Chem*. 2018, 57, 11986–11994. DOI: 10.1021/acs.inorgchem.8b01551.

[228] Zuo, L. Q.; Zhang, T. F.; Zhang, Z. K.; Hou, J. X.; Liu, G. J.; Du, J. L.; Li, L. J. A 3D Binuclear Salen-Based Multifunctional MOF: Degradation of MO Dye and Highly Selective Sensing of Fe^{3+}. *Inorg. Chem. Commun*. 2019, 99, 113–118. DOI: 10.1016/J.INOCHE.2018.11.006.

[229] Bhunia, A.; Dey, S.; Moreno, J. M.; Diaz, U.; Concepcion, P.; Van Hecke, K.; Janiak, C.; Van Der Voort, P. A Homochiral Vanadium–Salen Based Cadmium Bpdc MOF with Permanent Porosity as an Asymmetric Catalyst in Solvent-Free Cyanosilylation. *Chem. Commun*. 2016, 52(7), 1401–1404. DOI: https://doi.org/10.1039/C5CC09459C.

[230] Xia, Q.; Li, Z.; Tan, C.; Liu, Y.; Gong, W.; Cui, Y. Multivariate Metal–Organic Frameworks as Multifunctional Heterogeneous Asymmetric Catalysts for Sequential Reactions. *J. Am. Chem. Soc*. 2017, 139, 8259–8266. DOI: 10.1021/jacs.7b03113.

[231] Dhakshinamoorthy, A.; Asiri, A. M.; Alvaro, M.; Garcia, H. Metal Organic Frameworks as Catalysts in Solvent-Free or Ionic Liquid Assisted Conditions. *Green Chem*. 2018, 20, 86–107. DOI: 10.1039/C7GC02260C.

[232] Meyer, T. J.; Sheridan, M. V.; Sherman, B. D. Mechanisms of Molecular Water Oxidation in Solution and on Oxide Surfaces. *Chem. Soc. Rev*. 2017, 46, 6148–6169. DOI: 10.1039/C7CS00465F.

[233] Han, Z.; Eisenberg, R. Fuel from Water: The Photochemical Generation of Hydrogen from Water. *Acc. Chem. Res*. 2014, 47(8), 2537–2544. DOI: https://doi.org/10.1021/ar5001605.

[234] Shamsipur, M.; Pashabadi, A. Latest Advances in PSII Features and Mechanism of Water Oxidation. *Coord. Chem. Rev*. 2018, 374, 153–172. DOI: 10.1016/J.CCR.2018.07.006.

[235] Ishizuka, T.; Watanabe, A.; Kotani, H.; Hong, D.; Satonaka, K.; Wada, T.; Shiota, Y.; Yoshizawa, K.; Ohara, K.; Yamaguchi, K., et al. Homogeneous Photocatalytic Water Oxidation with a Dinuclear Co III –Pyridylmethylamine Complex. *Inorg. Chem*. 2016, 55, 1154–1164. DOI: 10.1021/acs.inorgchem.5b02336.

[236] Zhao, Y.; Zhang, S.; Wang, M.; Han, J.; Wang, H.; Li, Z.; Liu, X. Engineering Iridium-Based Metal Organic Frameworks Towards Electrocatalytic Water Oxidation. *Dalton Trans*. 2018, 47, 4646–4652. DOI: 10.1039/C8DT00485D.

[237] Garrido-Barros, P.; Gimbert-Suriñach, C.; Matheu, R.; Sala, X.; Llobet, A. How to Make an Efficient and Robust Molecular Catalyst for Water Oxidation. *Chem. Soc. Rev*. 2017, 46, 6088–6098. DOI: 10.1039/C7CS00248C.

[238] Kuttassery, F.; Mathew, S.; Remello, S. N.; Thomas, A.; Sano, K.; Ohsaki, Y.; Nabetani, Y.; Tachibana, H. Inoue, Alternative Route to Bypass the Bottle-Neck of Water Oxidation: Two-Electron Oxidation of Water Catalyzed by Earth-Abundant Metalloporphyrins. *Coord. Chem. Rev*. 2018, 377, 64–72. DOI: 10.1016/J.CCR.2018.08.027.

[239] Chen, K.; De Wu, C. Designed Fabrication of Biomimetic Metal–Organic Frameworks for Catalytic Applications. *Coord. Chem. Rev*. 2019, 378, 445–465. DOI: 10.1016/J.CCR.2018.01.016.

[240] Xiao, Y.; Qi, Y.; Wang, X.; Wang, X.; Zhang, F.; Li, C. Visible-Light-Responsive 2D Cadmium–Organic Framework Single Crystals with Dual Functions of Water Reduction and Oxidation. *Adv.Mate*. 2018, 30, 1803401. DOI: 10.1002/ADMA.201803401.

[241] Thoresen, E. M.; Øien-Ødegaard, S.; Kaur, G.; Tilset, M.; Lillerud, K. P.; Amedjkouh, M. Strongly Visible Light-Absorbing Metal–Organic Frameworks Functionalized by Cyclometalated Ruthenium(ii) Complexes. *R.S.C. Adv*. 2020, 10, 9052–9062. DOI: 10.1039/C9RA06984D.

[242] Maurin, G.; Serre, C.; Cooper, A.; F?rey, G. The New Age of MOFs and of Their Porous-Related Solids. *Chem. Soc. Rev*. 2017, 46, 3104–3107. DOI: 10.1039/C7CS90049J.

[243] Wang, D.; Li, Z. Iron-Based Metal–Organic Frameworks (MOFs) for Visible-Light-Induced Photocatalysis. *Res. Chem. Intermed*. 2017, 43, 5169–5186. DOI: 10.1007/s11164-017-3042-0.

[244] Liang, R.; Jing, F.; Shen, L.; Qin, N.; Wu, L. MIL-53(fe) as a Highly Efficient Bifunctional Photocatalyst for the Simultaneous Reduction of Cr(vi) and Oxidation of Dyes. *J. Hazard. Mater*. 2015, 287, 364–372. DOI: 10.1016/j.jhazmat.2015.01.048.

[245] Jing, F.; Liang, R.; Xiong, J.; Chen, R.; Zhang, S.; Li, Y.; Wu, L. MIL-68(fe) as an Efficient Visible-Light-Driven Photocatalyst for the Treatment of a Simulated Waste-Water Contain Cr(vi) and Malachite Green. *Appl. Catal. B*. 2017, 206, 9–15. DOI: 10.1016/j.apcatb.2016.12.070.

[246] Zhang, F.; Jin, Y.; Shi, J.; Zhong, Y.; Zhu, W.; El-Shall, M. S. Polyoxometalates Confined in the Mesoporous Cages of Metal-Organic Framework MIL-100(fe): Efficient Heterogeneous Catalysts for Esterification and Acetalization Reactions. *Chem. Eng. J*. 2015, 269, 236–244. DOI: 10.1016/j.cej.2015.01.092.

[247] Redfern, L. R.; Ducamp, M.; Wasson, M. C.; Robison, L.; Son, F. A.; Coudert, F. X.; Farha, O. K. Isolating the Role of the Node-Linker Bond in the Compression of UiO-66 Metal–Organic Frameworks. *Chem. Mater*. 2020, 32, 5864–5871. DOI: 10.1021/acs.chemmater.0c01922.

[248] Ghasempour, H.; Wang, K. Y.; Powell, J. A.; ZareKarizi, F.; Lv, X. L.; Morsali, A.; Zhou, H. C. Metal–Organic Frameworks Based on Multicarboxylate Linkers. *Coord. Chem. Rev*. 2021, 426, 213542. DOI: 10.1016/J.CCR.2020.213542.

[249] Lv, X. L.; Yuan, S.; Xie, L. H.; Darke, H. F.; Chen, Y.; He, T.; Dong, C.; Wang, B.; Zhang, Y. Z.; Li, J. R., et al. Ligand Rigidification for Enhancing the Stability of Metal–Organic Frameworks. *J. Am. Chem. Soc*. 2019, 141, 10283–10293. DOI: 10.1021/jacs.9b02947.

[250] Chen, L.; Zhang, X.; Cheng, X.; Xie, Z.; Kuang, Q.; Zheng, L. The Function of Metal–Organic Frameworks in the Application of MOF-Based Composites. *Nanoscale Adv*. 2020, 2, 2628–2647. DOI: 10.1039/D0NA00184H.

[251] Cui, Y.; Zhang, J.; He, H.; Qian, G. Photonic Functional Metal–Organic Frameworks. *Chem. Soc. Rev*. 2018, 47, 5740–5785. DOI: 10.1039/C7CS00879A.

[252] Foster, M. E.; Azoulay, J. D.; Wong, B. M.; Allendorf, M. D. Novel Metal–Organic Framework Linkers for Light Harvesting Applications. *Chem. Sci*. 2014, 5, 2081–2090. DOI: 10.1039/C4SC00333K.

[253] Deng, H.; Grunder, S.; Cordova, K. E.; Valente, C.; Furukawa, H.; Hmadeh, M.; Gándara, F.; Whalley, A. C.; Liu, Z.; Asahina, S., et al. Large-Pore Apertures in a Series of Metal-Organic Frameworks. *Science*. 1979, 336, 1018–1023. 2012. DOI: 10.1126/science.1220131.

[254] Lin, X.; Jia, J.; Zhao, X.; Thomas, K. M.; Blake, A. J.; Walker, G. S.; Champness, N. R.; Hubberstey, P.; Schröder, M. High H_2 Adsorption by Coordination-Framework Materials. *Angew. Chem. Int. Ed. Engl*. 2006, 45, 7358–7364. DOI: 10.1002/ANIE.200601991.

[255] Cavka, J. H.; Jakobsen, S.; Olsbye, U.; Guillou, N.; Lamberti, C.; Bordiga, S.; Lillerud, K. P. A New Zirconium Inorganic Building Brick Forming Metal Organic

Frameworks with Exceptional Stability. *J. Am. Chem. Soc.* 2008, 130(42), 13850–13851. DOI: https://doi.org/10.1021/ja8057953.

[256] Xue, D. X.; Cairns, A. J.; Belmabkhout, Y.; Wojtas, L.; Liu, Y.; Alkordi, M. H.; Eddaoudi, M. Tunable Rare-Earth Fcu-MOFs: A Platform for Systematic Enhancement of CO_2 Adsorption Energetics and Uptake. *J. Am. Chem. Soc.* 2013, 135 (20), 7660–7667. DOI: https://doi.org/10.1021/ja401429x.

[257] Kim, M.; Cahill, J. F.; Fei, H.; Prather, K. A.; Cohen, S. M. Postsynthetic Ligand and Cation Exchange in Robust Metal–Organic Frameworks. *J. Am. Chem. Soc.* 2012, 134, 18082–18088. DOI: 10.1021/ja3079219.

[258] Li, T.; Kozlowski, M. T.; Doud, E. A.; Blakely, M. N.; Rosi, N. L. Stepwise Ligand Exchange for the Preparation of a Family of Mesoporous MOFs. *J. Am. Chem. Soc.* 2013, 135, 11688–11691. DOI: 10.1021/ja403810k.

[259] Burnett, B. J.; Barron, P. M.; Hu, C.; Choe, W. Stepwise Synthesis of Metal - Organic Frameworks: Replacement of Structural Organic Linkers. *J. Am. Chem. Soc.* 2011, 133, 9984–9987. DOI: 10.1021/ja201911v.

[260] Marshall, R. J.; Kalinovskyy, Y.; Griffin, S. L.; Wilson, C.; Blight, B. A.; Forgan, R. S. Functional Versatility of a Series of Zr Metal–Organic Frameworks Probed by Solid-State Photoluminescence Spectroscopy. *J. Am. Chem. Soc.* 2017, 139, 6253–6260. DOI: 10.1021/jacs.7b02184.

[261] Hobday, C. L.; Bennett, T. D.; Fairen-Jimenez, D.; Graham, A. J.; Morrison, C. A.; Allan, D. R.; Düren, T.; Moggach, S. A. Tuning the Swing Effect by Chemical Functionalization of Zeolitic Imidazolate Frameworks. *J. Am. Chem. Soc.* 2018, 140, 382–387. DOI: 10.1021/jacs.7b10897.

[262] Wang, Y.; Huang, N. Y.; Shen, J. Q.; Liao, P. Q.; Chen, X. M.; Zhang, J. P. Hydroxide Ligands Cooperate with Catalytic Centers in Metal-Organic Frameworks for Efficient Photocatalytic CO_2 Reduction. *J. Am. Chem. Soc.* 2018, 140, 38–41. DOI: 10.1021/jacs.7b10107.

[263] Deria, P.; Bury, W.; Hupp, J. T.; Farha, O. K. Versatile Functionalization of the Nu-1000 Platform by Solvent-Assisted Ligand Incorporation. *Chem. Commun.* 2014, 50, 1965–1968. DOI: 10.1039/c3cc48562e.

[264] Deria, P.; Bury, W.; Hod, I.; Kung, C. W.; Karagiaridi, O.; Hupp, J. T.; Farha, O. K. MOF Functionalization via Solvent-Assisted Ligand Incorporation: Phosphonates Vs Carboxylates. *Inorg. Chem.* 2015, 54, 2185–2192. DOI: 10.1021/ic502639v.

[265] Deria, P.; Mondloch, J. E.; Tylianakis, E.; Ghosh, P.; Bury, W.; Snurr, R. Q.; Hupp, J. T.; Farha, O. K. Perfluoroalkane Functionalization of NU-1000 via Solvent-Assisted Ligand Incorporation: Synthesis and CO_2 Adsorption Studies. *J. Am. Chem. Soc.* 2013, 135, 16801–16804. DOI: 10.1021/ja408959g.

[266] Ichiro Noro, S.; Nakamura, T. Fluorine-Functionalized Metal–Organic Frameworks and Porous Coordination Polymers, NPG Asia Mater. *NPG Asia Mater.* 2017, 9, e433. DOI: 10.1038/am.2017.165.

[267] Yuan, S.; Qin, J. S.; Xu, H. Q.; Su, J.; Rossi, D.; Chen, Y.; Zhang, L.; Lollar, C.; Wang, Q.; Jiang, H. L., et al. [Ti 8 Zr 2 O 12 (COO) 16] Cluster: An Ideal Inorganic Building Unit for Photoactive Metal–Organic Frameworks. *ACS Cent. Sci.* 2018, 4, 105–111. DOI: 10.1021/acscentsci.7b00497.

[268] Yi, P.; Huang, H.; Peng, Y.; Liu, D.; Zhong, C. A Series of Europium-Based Metal Organic Frameworks with Tuned Intrinsic Luminescence Properties and Detection Capacities. *R.S.C. Adv.* 2016, 6, 111934–111941. DOI: 10.1039/C6RA23263A.

[269] Zhang, Q.; Yu, J.; Cai, J.; Zhang, L.; Cui, Y.; Yang, Y.; Chen, B.; Qian, G. A Porous Zr-Cluster-Based Cationic Metal–Organic Framework for Highly Efficient Cr 2 O 7 2–

Removal from Water. *Chem. Commun*. 2015, 51, 14732–14734. DOI: 10.1039/c5cc05927e.

[270] Zhang, X.; Zhang, J.; Hu, Q.; Cui, Y.; Yang, Y.; Qian, G. Postsynthetic Modification of Metal-Organic Framework for Hydrogen Sulfide Detection. *Appl. Surf. Sci*. 2015, 355, 814–819. DOI: 10.1016/j.apsusc.2015.07.166.

[271] Shi, D.; Zheng, R.; Sun, M.-J.; Cao, X.; Sun, C.-X.; Cui, C.-J.; Liu, C.-S.; Zhao, J.; Du, M. Semiconductive Copper(i)–Organic Frameworks for Efficient Light-Driven Hydrogen Generation without Additional Photosensitizers and Cocatalysts. *Angew. Chem. Int. Ed*. 2017, 56, 14637–14641. DOI: 10.1002/anie.201709869.

[272] Chen, Y. F.; Tan, L. L.; Liu, J. M.; Qin, S.; Xie, Z. Q.; Huang, J. F.; Xu, Y. W.; Xiao, L. M.; Su, C. Y. Calix[4]arene Based Dye-Sensitized Pt@UiO-66-NH_2 Metal-Organic Framework for Efficient Visible-Light Photocatalytic Hydrogen Production. *Appl. Catal. B*. 2017, 206, 426–433. DOI: 10.1016/j.apcatb.2017.01.040.

[273] Jiao, L.; Seow, J. Y. R.; Skinner, W. S.; Wang, Z. U.; Jiang, H. L. Metal–Organic Frameworks: Structures and Functional Applications. *Mater. Today*. 2019, 27, 43–68. DOI: 10.1016/j.mattod.2018.10.038.

[274] Yang, W.; Zhao, Y.; Chen, S.; Ren, W.; Chen, X.; Jia, C.; Su, Z.; Wang, Y.; Zhao, C. Defective Indium/Indium Oxide Heterostructures for Highly Selective Carbon Dioxide Electrocatalysis. *Inorg. Chem*. 2020, 59, 12437–12444. DOI: 10.1021/acs.inorgchem.0c01544.

[275] Wang, L.; Zhang, T.; Huang, L.; Xu, J.; Wang, G.; Zhang, H.; Wang, L. Synthesis, Crystal Structure and Photoluminescent Property of a Novel Indium (III) Supramolecular 3D Framework. *J. Mol. Struct*. 2010, 975, 215–219. DOI: 10.1016/j.molstruc.2010.04.026.

[276] Hu, L.; Yang, S.; Zhao, Y.; He, J.; Jiang, S.; Sun, C.; Song, S. Spontaneous Polarization Electric Field Briskly Boosting Charge Separation and Transfer for Sustainable Photocatalytic H_2 Bubble Evolution. *Appl. Catal. B*. 2021, 283, 119631. DOI: 10.1016/j.apcatb.2020.119631.

[277] Huang, D.; Yan, X.; Yan, M.; Zeng, G.; Zhou, C.; Wan, J.; Cheng, M.; Xue, W. Graphitic Carbon Nitride-Based Heterojunction Photoactive Nanocomposites: Applications and Mechanism Insight. *ACS Appl. Mater. Interfaces*. 2018, 10, 21035–21055. DOI: 10.1021/acsami.8b03620.

[278] Lan, G.; Zhu, Y. Y.; Veroneau, S. S.; Xu, Z.; Micheroni, D.; Lin, W. Electron Injection from Photoexcited Metal-Organic Framework Ligands to Ru_2 Secondary Building Units for Visible-Light-Driven Hydrogen Evolution. *J. Am. Chem. Soc*. 2018, 140, 5326–5329. DOI: 10.1021/jacs.8b01601.

[279] Zhang, W.; Bu, H.; Wang, J.; Zhao, L.; Qu, Y.; Zhao, M. Multi-functional photocatalytic activity of transition-metal tetraaza[14]annulene frameworks. *J. Mater. Chem. A Mater*. 2021, 9, 4221–4229. DOI: 10.1039/d0ta09879e.

[280] Xu, H.; Cheng, D.; Cao, D.; Zeng, X. C. A Universal Principle for a Rational Design of Single-Atom Electrocatalysts. *Nat. Catal*. 2018, 1, 339–348. DOI: 10.1038/s41929-018-0063-z.

[281] Horiuchi, Y.; Toyao, T.; Miyahara, K.; Zakary, L.; Do Van, D.; Kamata, Y.; Kim, T. H.; Lee, S. W.; Matsuoka, M. Visible-Light-Driven Photocatalytic Water Oxidation Catalysed by Iron-Based Metal–Organic Frameworks. *Chem. Commun*. 2016, 52, 5190–5193. DOI: 10.1039/c6cc00730a.

[282] Chi, L.; Xu, Q.; Liang, X.; Wang, J.; Su, X. Iron-Based Metal-Organic Frameworks as Catalysts for Visible Light-Driven Water Oxidation. *Small*. 2016, 12, 1351–1358. DOI: 10.1002/smll.201503526.

[283] Abid, H. R.; Ang, H. M.; Wang, S. Effects of Ammonium Hydroxide on the Structure and Gas Adsorption of Nanosized Zr-MOFs (UiO-66. *Nanoscale*. 2012, 4, 3089–3094. DOI: 10.1039/c2nr30244f.

[284] Lionet, Z.; Kim, T. H.; Horiuchi, Y.; Lee, S. W.; Matsuoka, M. Linker Engineering of Iron-Based MOFs for Efficient Visible-Light-Driven Water Oxidation Reaction. *J. Phys. Chem. C*. 2019, 123, 27501–27508. DOI: 10.1021/acs.jpcc.9b06838.

[285] Shen, L.; Liang, R.; Luo, M.; Jing, F.; Wu, L. Electronic Effects of Ligand Substitution on Metal–Organic Framework Photocatalysts: The Case Study of UiO-66. *Phys. Chem. Chem. Phys*. 2015, 17, 117–121. DOI: 10.1039/c4cp04162c.

[286] Zhang, J.; Yu, J.; Jaroniec, M.; Gong, J. R. Noble Metal-Free Reduced Graphene Oxide-Zn $_{x}$Cd $_{1-x}$S Nanocomposite with Enhanced Solar Photocatalytic H $_{2}$-production Performance. *Nano Lett*. 2012, 12, 4584–4589. DOI: 10.1021/nl301831h.

[287] Parra, S.; Olivero, J.; Pacheco, L.; Pulgarin, C. Structural Properties and Photoreactivity Relationships of Substituted Phenols in TiO_2 Suspensions. *Appl. Catal. B*. 2003, 43, 293–301. DOI: 10.1016/S0926-3373(02)00324-7.

[288] Wang, Q.; Gao, Q.; Al-Enizi, A. M.; Nafady, A.; Ma, S. Recent Advances in MOF-Based Photocatalysis: Environmental Remediation Under Visible Light. *Inorg. Chem. Front*. 2020, 7, 300–339. DOI: 10.1039/C9QI01120J.

[289] Horiuchi, Y.; Toyao, T.; Saito, M.; Mochizuki, K.; Iwata, M.; Higashimura, H.; Anpo, M.; Matsuoka, M. Visible-Light-Promoted Photocatalytic Hydrogen Production by Using an Amino-Functionalized Ti(iv) Metal–Organic Framework. *J. Phys. Chem. C*. 2012, 116, 20848–20853. DOI: 10.1021/jp3046005.

[290] Inagaki, A.; Akita, M. Visible-Light Promoted Bimetallic Catalysis. *Coord. Chem. Rev*. 2010, 254, 1220–1239. DOI: 10.1016/j.ccr.2009.11.003.

[291] Zhu, M.; Lu, Y.; Du, Y.; Li, J.; Wang, X.; Yang, P. Photocatalytic Hydrogen Evolution without an Electron Mediator Using a Porphyrin-Pyrene Conjugate Functionalized Pt Nanocomposite as a Photocatalyst. *Int. J. Hydrogen. Energy*. 2011, 36, 4298–4304. DOI: 10.1016/j.ijhydene.2011.01.007.

[292] Zhu, M.; Dong, Y.; Du, Y.; Mou, Z.; Liu, J.; Yang, P.; Wang, X. Photocatalytic Hydrogen Evolution Based on Efficient Energy and Electron Transfers in Donor-Bridge-Acceptor Multibranched-Porphyrin-Functionalized Platinum Nanocomposites, Chemistry. *A European Journal*. 2012, 18, 4367–4374. DOI: 10.1002/chem.201102595.

[293] Becerra, J.; Nguyen, D. T.; Gopalakrishnan, V. N.; Do, T. O. Plasmonic Au Nanoparticles Incorporated in the Zeolitic Imidazolate Framework (ZIF-67) for the Efficient Sunlight-Driven Photoreduction of CO_2. *ACS Appl. Energy Mater*. 2020, 3, 7659–7665. DOI: 10.1021/acsaem.0c01083.

[294] Chen, L.; Wang, Y.; Yu, F.; Shen, X.; Duan, C. A Simple Strategy for Engineering Heterostructures of Au Nanoparticle-Loaded Metal–Organic Framework Nanosheets to Achieve Plasmon-Enhanced Photocatalytic CO_2 Conversion Under Visible Light. *J. Mater. Chem. A*. 2019, 7, 11355–11361. DOI: 10.1039/C9TA01840A.

[295] Guo, F.; Yang, S.; Liu, Y.; Wang, P.; Huang, J.; Sun, W. Y. Size Engineering of Metal–Organic Framework MIL-101(cr)–Ag Hybrids for Photocatalytic CO $_{2}$ Reduction. *ACS Catal*. 2019, 9, 8464–8470. DOI: 10.1021/acscatal.9b02126.

[296] Deng, X.; Yang, L.; Huang, H.; Yang, Y.; Feng, S.; Zeng, M.; Li, Q.; Xu, D. Shape-Defined Hollow Structural Co-MOF-74 and Metal Nanoparticles@co-MOF-74 Composite Through a Transformation Strategy for Enhanced Photocatalysis Performance. *Small*. 2019, 15, 1902287. DOI: 10.1002/SMLL.201902287.

[297] Robatjazi, H.; Weinberg, D.; Swearer, D. F.; Jacobson, C.; Zhang, M.; Tian, S.; Zhou, L.; Nordlander, P.; Halas, N. J. Metal-Organic Frameworks Tailor the Properties of Aluminum Nanocrystals. *Sci. Adv*. 2019, 5. DOI: 10.1126/SCIADV.AAV5340.

[298] Guo, F.; Wei, Y. P.; Wang, S. Q.; Zhang, X. Y.; Wang, F. M.; Sun, W. Y. Pt Nanoparticles Embedded in Flowerlike NH_2-UiO-68 for Enhanced Photocatalytic Carbon Dioxide Reduction. *J. Mater. Chem. A*. 2019, 7, 26490–26495. DOI: 10.1039/C9TA10575A.

[299] Han, Y.; Xu, H.; Su, Y.; Liang Xu, Z.; Wang, K.; Wang, W. Noble Metal (Pt, Au@pd) Nanoparticles Supported on Metal Organic Framework (MOF-74) Nanoshuttles as High-Selectivity CO_2 Conversion Catalysts. *J. Catal*. 2019, 370, 70–78. DOI: 10.1016/J.JCAT.2018.12.005.

[300] Su, Y.; Xu, H.; Wang, J.; Luo, X.; Liang Xu, Z.; Wang, K.; Wang, W. Nanorattle Au@ptag Encapsulated in ZIF-8 for Enhancing CO_2 Photoreduction to CO. *Nano Res*. 2018, 12, 625–630. DOI: 10.1007/S12274-018-2269-4.

[301] Yang, X.; Huang, T.; Gao, S.; Cao, R. Boosting Photocatalytic Oxidative Coupling of Amines by a Ru-Complex-Sensitized Metal-Organic Framework. *J. Catal*. 2019, 378, 248–255. DOI: 10.1016/J.JCAT.2019.08.038.

[302] Lang, P.; Habermehl, J.; Troyanov, S. I.; Rau, S.; Schwalbe, M. Photocatalytic Generation of Hydrogen Using Dinuclear π-Extended Porphyrin-Platinum Compounds, Chemistry. *A European Journal*. 2018, 24, 3225–3233. DOI: 10.1002/chem.201704999.

[303] Ladomenou, K.; Natali, M.; Iengo, E.; Charalampidis, G.; Scandola, F.; Coutsolelos, A. G. Photochemical Hydrogen Generation with Porphyrin-Based Systems. *Coord. Chem. Rev*. 2015, 304-305, 38–54. 304–305. DOI: 10.1016/J.CCR.2014.10.001.

[304] Tinker, L. L.; McDaniel, N. D.; Curtin, P. N.; Smith, C. K.; Ireland, M. J.; Bernhard, S. Visible Light Induced Catalytic Water Reduction without an Electron Relay, Chemistry. *A European Journal*. 2007, 13, 8726–8732. DOI: 10.1002/chem.200700480.

[305] Mori, K.; Aoyama, J.; Kawashima, M.; Yamashita, H. Visible-light driven H_2 production utilizing iridium and rhodium complexes intercalated into a zirconium phosphate layered matrix. *Dalton Trans*. 2014, 43, 10541–10547. DOI: 10.1039/c3dt53110d.

[306] Hong, Y. H.; Lee, Y. M.; Nam, W.; Fukuzumi, S. Molecular Photocatalytic Water Splitting by Mimicking Photosystems I and II. *J. Am. Chem. Soc*. 2022, 144, 695–700. DOI: 10.1021/jacs.1c11707.

[307] Zhang, R.; Zhang, L.; Zheng, Q.; Gao, P.; Zhao, J.; Yang, J. Direct Z-Scheme Water Splitting Photocatalyst Based on Two-Dimensional Van der Waals Heterostructures. *J. Phys. Chem. Lett*. 2018, 9, 5419–5424. DOI: 10.1021/acs.jpclett.8b02369.

[308] Sasan, K.; Lin, Q.; Mao, C. Y.; Feng, P. Incorporation of Iron Hydrogenase Active Sites into a Highly Stable Metal–Organic Framework for Photocatalytic Hydrogen Generation. *Chem. Commun*. 2014, 50, 10390–10393. DOI: 10.1039/c4cc03946g.

[309] Lazarides, T.; Delor, M.; Sazanovich, I. V.; Mc Cormick, T. M.; Georgakaki, I.; Charalambidis, G.; Weinstein, J. A.; Coutsolelos, A. G. Photocatalytic Hydrogen Production from a Noble Metal Free System Based on a Water Soluble Porphyrin Derivative and a Cobaloxime Catalyst. *Chem. Commun*. 2014, 50, 521–523. DOI: 10.1039/c3cc45025b.

[310] Roy, S.; Pascanu, V.; Pullen, S.; González Miera, G.; Martín-Matute, B.; Ott, S. Catalyst Accessibility to Chemical Reductants in Metal–Organic Frameworks. *Chem. Commun*. 2017, 53, 3257–3260. DOI: 10.1039/c7cc00022g.

[311] Berardi, S.; Drouet, S.; Francàs, L.; Gimbert-Suriñach, C.; Guttentag, M.; Richmond, C.; Stoll, T.; Llobet, A. *Chem. Soc. Rev*. 2014, 43, 7501–7519. DOI: 10.1039/c3cs60405e.

[312] Juris, A.; Balzani, V.; Barigelletti, F.; Campagna, S.; Belser, P.; von Zelewsky, A. Ru(ii) Polypyridine Complexes: Photophysics, Photochemistry, Eletrochemistry, and Chemiluminescence. *Coord. Chem. Rev*. 1988, 84, 85–277. DOI: 10.1016/0010-8545(88)80032-8.

[313] De Sio, L.; Placido, T.; Comparelli, R.; Lucia Curri, M.; Striccoli, M.; Tabiryan, N.; Bunning, T. J. Next-Generation Thermo-Plasmonic Technologies and Plasmonic

Nanoparticles in Optoelectronics. *Prog Quantum Electron*. 2015, 41, 23–70. DOI: 10.1016/j.pquantelec.2015.03.001.

[314] Pfeffer, M. G.; Kowacs, T.; Wächtler, M.; Guthmuller, J.; Dietzek, B.; Vos, J. G.; Rau, S. Optimization of Hydrogen-Evolving Photochemical Molecular Devices. *Angew. Chem. Int. Ed*. 2015, 54, 6627–6631. DOI: 10.1002/anie.201409442.

[315] Granadeiro, C. M.; Barbosa, A. D. S.; Ribeiro, S.; Santos, I. C. M. S.; De Castro, B.; Cunha-Silva, L.; Balula, S. S. Oxidative Catalytic Versatility of a Trivacant Polyoxotungstate Incorporated into MIL-101(cr. *Catal. Sci. Technol*. 2014, 4, 1416–1425. DOI: 10.1039/c3cy00853c.

[316] Samaniyan, M.; Mirzaei, M.; Khajavian, R.; Eshtiagh-Hosseini, H.; Streb, C. Heterogeneous Catalysis by Polyoxometalates in Metal-Organic Frameworks. *ACS Catal*. 2019, 9, 10174–10191. DOI: 10.1021/acscatal.9b03439.

[317] Paille, G.; Gomez-Mingot, M.; Roch-Marchal, C.; Haouas, M.; Benseghir, Y.; Pino, T.; Ha-Thi, M. H.; Landrot, G.; Mialane, P.; Fontecave, M., et al. Thin Films of Fully Noble Metal-Free POM@MOF for Photocatalytic Water Oxidation. *ACS Appl. Mater. Interfaces*. 2019, 11, 47837–47845. DOI: 10.1021/acsami.9b13121.

[318] Stuckart, M.; Monakhov, K. Y. Polyoxometalate Encapsulation into Metal–Organic Frameworks: The Way Towards Functional Nanomaterials for Water Splitting. *J. Mater. Chem. A*. 2018, 6, 17849–17853. DOI: 10.1039/c8ta06213g.

[319] Suzuki, K.; Mizuno, N.; Yamaguchi, K. Polyoxometalate Photocatalysis for Liquid-Phase Selective Organic Functional Group Transformations. *ACS Catal*. 2018, 8, 10809–10825. DOI: 10.1021/acscatal.8b03498.

[320] Guo, Y.; Hu, C. Heterogeneous Photocatalysis by Solid Polyoxometalates. *J. Mol. Catal A Chem*. 2007, 262, 136–148. DOI: 10.1016/j.molcata.2006.08.039.

[321] Ye, J. J.; De Wu, C. Immobilization of Polyoxometalates in Crystalline Solids for Highly Efficient Heterogeneous Catalysis. *Dalton Trans*. 2016, 45, 10101–10112. DOI: 10.1039/c6dt01378c.

[322] Sun, J.; Abednatanzi, S.; Van Der Voort, P.; Liu, Y.-Y.; Leus, K. POM@MOF Hybrids: Synthesis and Applications. *Catalysts*. 2020, 10, 578. DOI: 10.3390/catal10050578.

[323] Zhang, S.; Ou, F.; Ning, S.; Cheng, P. Polyoxometalate-Based Metal-Organic Frameworks for Heterogeneous Catalysis. *Inorg. Chem. Front*. 2021, 8, 1865–1899. DOI: 10.1039/d0qi01407a.

[324] Mialane, P.; Mellot-Draznieks, C.; Gairola, P.; Duguet, M.; Benseghir, Y.; Oms, O.; Dolbecq, A. Heterogenisation of Polyoxometalates and Other Metal-Based Complexes in Metal-Organic Frameworks: From Synthesis to Characterisation and Applications in Catalysis. *Chem. Soc. Rev*. 2021, 50, 6152–6220. DOI: 10.1039/d0cs00323a.

[325] Jiao, L.; Dong, Y.; Xin, X.; Wang, R.; Lv, H. Three-In-One: Achieving a Robust and Effective Hydrogen-Evolving Hybrid Material by Integrating Polyoxometalate, a Photo-Responsive Metal–Organic Framework, and in situ Generated Pt Nanoparticles. *J. Mater. Chem. A*. 2021, 9, 19725–19733. DOI: 10.1039/d1ta02792a.

[326] Cui, T.; Qin, L.; Fu, F.; Xin, X.; Li, H.; Fang, X.; Lv, H. Pentadecanuclear Fe-Containing Polyoxometalate Catalyst for Visible-Light-Driven Generation of Hydrogen. *Inorg. Chem*. 2021, 60, 4124–4132. DOI: 10.1021/acs.inorgchem.1c00267.

[327] Zhang, Z. M.; Zhang, T.; Wang, C.; Lin, Z.; Long, L. S.; Lin, W. Photosensitizing Metal-Organic Framework Enabling Visible-Light-Driven Proton Reduction by a Wells-Dawson-Type Polyoxometalate. *J. Am. Chem. Soc*. 2015, 137, 3197–3200. DOI: 10.1021/jacs.5b00075.

[328] Shah, W. A.; Waseem, A.; Nadeem, M. A.; Kögerler, P. Leaching-Free Encapsulation of Cobalt-Polyoxotungstates in MIL-100 (Fe) for Highly Reproducible Photocatalytic Water Oxidation. *Appl. Catal. A*. 2018, 567, 132–138. DOI: 10.1016/j.apcata.2018.08.002.

[329] Buru, C. T.; Li, P.; Mehdi, B. L.; Dohnalkova, A.; Platero-Prats, A. E.; Browning, N. D.; Chapman, K. W.; Hupp, J. T.; Farha, O. K. Adsorption of a Catalytically Accessible Polyoxometalate in a Mesoporous Channel-Type Metal–Organic Framework. *Chem. Mater*. 2017, 29, 5174–5181. DOI: 10.1021/acs.chemmater.7b00750.

[330] Sun, D.; Li, Z. Double-Solvent Method to Pd Nanoclusters Encapsulated Inside the Cavity of NH_2 –Uio-66(Zr) for Efficient Visible-Light-Promoted Suzuki Coupling Reaction. *J. Phys. Chem. C*. 2016, 120, 19744–19750. DOI: 10.1021/acs.jpcc.6b06710.

[331] Liu, J.; Li, R.; Wang, Y.; Wang, Y.; Zhang, X.; Fan, C. The Active Roles of ZIF-8 on the Enhanced Visible Photocatalytic Activity of Ag/AgCl: Generation of Superoxide Radical and Adsorption. *J. Alloys Compd*. 2017, 693, 543–549. DOI: 10.1016/J.JALLCOM.2016.09.201.

[332] Qiu, J.; Zhang, X.; Feng, Y.; Zhang, X.; Wang, H.; Yao, J. Modified Metal-Organic Frameworks as Photocatalysts. *Appl. Catal. B*. 2018, 231, 317–342. DOI: 10.1016/J.APCATB.2018.03.039.

[333] Chughtai, A. H.; Ahmad, N.; Younus, H. A.; Laypkov, A.; Verpoort, F. Metal–Organic Frameworks: Versatile Heterogeneous Catalysts for Efficient Catalytic Organic Transformations. *Chem. Soc. Rev*. 2015, 44, 6804–6849. DOI: 10.1039/C4CS00395K.

[334] Song, J.; Gu, X.; Cheng, J.; Fan, N.; Zhang, H.; Su, H. Remarkably Boosting Catalytic H_2 Evolution from Ammonia Borane Through the Visible-Light-Driven Synergistic Electron Effect of Non-Plasmonic Noble-Metal-Free Nanoparticles and Photoactive Metal-Organic Frameworks. *Appl. Catal. B*. 2018, 225, 424–432. DOI: 10.1016/J.APCATB.2017.12.024.

[335] Sun, D.; Mazumder, V.; Metin, Ö.; Sun, S. Catalytic hydrolysis of ammonia borane via cobalt palladium nanoparticles. *ACS Nano*. 2011, 5(8), 6458–6464. DOI: https://doi.org/10.1021/nn2016666.

[336] Akbayrak, S.; Kaya, M.; Volkan, M.; Özkar, S. Palladium(0) Nanoparticles Supported on Silica-Coated Cobalt Ferrite: A Highly Active, Magnetically Isolable and Reusable Catalyst for Hydrolytic Dehydrogenation of Ammonia Borane. *Appl. Catal. B*. 2014, 147, 387–393. DOI: 10.1016/J.APCATB.2013.09.023.

[337] Védrine, J. C. Metal Oxides in Heterogeneous Oxidation Catalysis: State of the Art and Challenges for a More Sustainable World. *ChemSuschem*. 2019, 12, 577–588. DOI: 10.1002/CSSC.201802248.

[338] Huang, D.; Hu, Z.; Peng, Z.; Zeng, G.; Chen, G.; Zhang, C.; Cheng, M.; Wan, J.; Wang, X.; Qin, X. Cadmium Immobilization in River Sediment Using Stabilized Nanoscale Zero-Valent Iron with Enhanced Transport by Polysaccharide Coating. *J. Environ. Manage*. 2018, 210, 191–200. DOI: 10.1016/J.JENVMAN.2018.01.001.

[339] Shen, L.; Wu, W.; Liang, R.; Lin, R.; Wu, L. Highly Dispersed Palladium Nanoparticles Anchored on UiO-66(NH_2) Metal-Organic Framework as a Reusable and Dual Functional Visible-Light-Driven Photocatalyst. *Nanoscale*. 2013, 5, 9374–9382. DOI: 10.1039/C3NR03153E.

[340] Liang, R.; Luo, S.; Jing, F.; Shen, L.; Qin, N.; Wu, L. A Simple Strategy for Fabrication of Pd@MIL-100(fe) Nanocomposite as a Visible-Light-Driven Photocatalyst for the Treatment of Pharmaceuticals and Personal Care Products (PPCPs. *Appl. Catal. B*. 2015, 176-177, 240–248. 176–177. DOI: 10.1016/J.APCATB.2015.04.009.

[341] Liang, R.; Jing, F.; Shen, L.; Qin, N.; Wu, L. M@MIL-100(fe) (M = Au, Pd, Pt) Nanocomposites Fabricated by a Facile Photodeposition Process: Efficient Visible-Light Photocatalysts for Redox Reactions in Water. *Nano Res*. 2015, 8, 3237–3249. DOI: 10.1007/S12274-015-0824-9.

[342] Wang, B.; Deng, Z.; Fu, X.; Xu, C.; Li, Z. Photodeposition of Pd Nanoparticles on $ZnIn_2S_4$ for Efficient Alkylation of Amines and ketones' α-H with Alcohols Under Visible Light. *Appl. Catal. B*. 2018, 237, 970–975. DOI: 10.1016/J.APCATB.2018.06.067.

[343] Lin, L.; Liu, H.; Zhang, X. Flower-Like ZnO-Assisted One-Pot Encapsulation of Noble Metal Nanoparticles Supported Catalysts with ZIFs. *Appl. Surf. Sci*. 2018, 433, 602–609. DOI: 10.1016/J.APSUSC.2017.10.047.

[344] Yang, X.; Yuan, S.; Zou, L.; Drake, H.; Zhang, Y.; Qin, J.; Alsalme, A.; Zhou, H.-C. One-Step Synthesis of Hybrid Core–Shell Metal–Organic Frameworks. *Angewandte Chemie*. 2018, 130, 3991–3996. DOI: 10.1002/ANGE.201710019.

[345] Chang, L.; Li, Y. One-Step Encapsulation of Pt-Co Bimetallic Nanoparticles within MOFs for Advanced Room Temperature Nanocatalysis. *Mol. Catal*. 2017, 433, 77–83. DOI: 10.1016/J.MCAT.2017.01.009.

[346] Martindale, B. C. M.; Hutton, G. A. M.; Caputo, C. A.; Reisner, E. Solar Hydrogen Production Using Carbon Quantum Dots and a Molecular Nickel Catalyst. *J. Am. Chem. Soc*. 2015, 137, 6018–6025. DOI: 10.1021/jacs.5b01650.

[347] Yang, Q.; Xu, Q.; Yu, S. H.; Jiang, H. L. Pd Nanocubes@ZIF-8: Integration of Plasmon-Driven Photothermal Conversion with a Metal–Organic Framework for Efficient and Selective Catalysis. *Angew. Chem. Int. Ed*. 2016, 55, 3685–3689. DOI: 10.1002/ANIE.201510655.

[348] Hao, X.; Jin, Z.; Yang, H.; Lu, G.; Bi, Y. Peculiar Synergetic Effect of MoS_2 Quantum Dots and Graphene on Metal-Organic Frameworks for Photocatalytic Hydrogen Evolution. *Appl. Catal. B*. 2017, 210, 45–56. DOI: 10.1016/J.APCATB.2017.03.057.

[349] Guo, H.; Guo, D.; Zheng, Z.; Weng, W.; Chen, J. Visible-Light Photocatalytic Activity of Ag@MIL-125(ti) Microspheres. *Appl. Organomet. Chem*. 2015, 29, 618–623. DOI: 10.1002/AOC.3341.

[350] Gong, M.; Zhou, W.; Tsai, M. C.; Zhou, J.; Guan, M.; Lin, M. C.; Zhang, B.; Hu, Y.; Wang, D. Y.; Yang, J., et al. Nanoscale nickel oxide/nickel heterostructures for active hydrogen evolution electrocatalysis. *Nat. Commun*. 2014, 5(1), 1–6. DOI: https://doi.org/10.1038/ncomms5695.

[351] Wang, D. Y.; Gong, M.; Chou, H. L.; Pan, C. J.; Chen, H. A.; Wu, Y.; Lin, M. C.; Guan, M.; Yang, J.; Chen, C. W., et al. Highly Active and Stable Hybrid Catalyst of Cobalt-Doped FeS_2 Nanosheets–Carbon Nanotubes for Hydrogen Evolution Reaction. *J. Am. Chem. Soc*. 2015, 137, 1587–1592. DOI: 10.1021/ja511572q.

[352] Peters, A. W.; Li, Z.; Farha, O. K.; Hupp, J. T. Toward Inexpensive Photocatalytic Hydrogen Evolution: A Nickel Sulfide Catalyst Supported on a High-Stability Metal–Organic Framework. *ACS Appl. Mater. Interfaces*. 2016, 8, 20675–20681. DOI: 10.1021/acsami.6b04729.

[353] Noh, H.; Cui, Y.; Peters, A. W.; Pahls, D. R.; Ortuno, M. A.; Vermeulen, N. A.; Cramer, C. J.; Gagliardi, L.; Hupp, J. T.; Farha, O. K. An Exceptionally Stable Metal–Organic Framework Supported Molybdenum(VI) Oxide Catalyst for Cyclohexene Epoxidation. *J. Am. Chem. Soc*. 2016, 138, 14720–14726. DOI: 10.1021/jacs.6b08898.

[354] Ikuno, T.; Zheng, J.; Vjunov, A.; Sanchez-Sanchez, M.; Ortuño, M. A.; Pahls, D. R.; Fulton, J. L.; Camaioni, D. M.; Li, Z.; Ray, D., et al. Methane Oxidation to Methanol Catalyzed by Cu-Oxo Clusters Stabilized in NU-1000 Metal–Organic Framework. *J. Am. Chem. Soc*. 2017, 139, 10294–10301. DOI: 10.1021/jacs.7b02936.

[355] Huang, Y.; Zhang, Y.; Chen, X.; Wu, D.; Yi, Z.; Cao, R. Bimetallic Alloy Nanocrystals Encapsulated in ZIF-8 for Synergistic Catalysis of Ethylene Oxidative Degradation. *Chem. Commun*. 2014, 50, 10115–10117. DOI: 10.1039/C4CC04479G.

[356] Zhang, Y.; Park, S. J. Stabilization of Dispersed CuPd Bimetallic Alloy Nanoparticles on ZIF-8 for Photoreduction of Cr(vi) in Aqueous Solution. *Chem. Eng. J.* 2019, 369, 353–362. DOI: 10.1016/J.CEJ.2019.03.083.

[357] Kampouri, S.; Nguyen, T. N.; Ireland, C. P.; Valizadeh, B.; Ebrahim, F. M.; Capano, G.; Ongari, D.; Mace, A.; Guijarro, N.; Sivula, K., et al. Photocatalytic Hydrogen Generation from a Visible-Light Responsive Metal–Organic Framework System: The Impact of Nickel Phosphide Nanoparticles. *J. Mater. Chem. A*. 2018, 6, 2476–2481. DOI: 10.1039/c7ta10225a.

[358] Tong, Z.; Yang, D.; Li, Z.; Nan, Y.; Ding, F.; Shen, Y.; Jiang, Z. Thylakoid-Inspired Multishell G-C $_3$ N $_4$ Nanocapsules with Enhanced Visible-Light Harvesting and Electron Transfer Properties for High-Efficiency Photocatalysis. *ACS Nano*. 2017, 11, 1103–1112. DOI: 10.1021/ACSNANO.6B08251.

[359] Zada, A.; Humayun, M.; Raziq, F.; Zhang, X.; Qu, Y.; Bai, L.; Qin, C.; Jing, L.; Fu, H. Exceptional Visible-Light-Driven Cocatalyst-Free Photocatalytic Activity of g-C_3N_4 by Well Designed Nanocomposites with Plasmonic Au and SnO_2. *Adv. Energy Mater*. 2016, 6, 1601190. DOI: 10.1002/AENM.201601190.

[360] Bao, L.; Zhang, Z. L.; Tian, Z. Q.; Zhang, L.; Liu, C.; Lin, Y.; Qi, B.; Pang, D. W. Electrochemical Tuning of Luminescent Carbon Nanodots: From Preparation to Luminescence Mechanism. *Adv.Mate.* 2011, 23, 5801–5806. DOI: 10.1002/ADMA.201102866.

[361] Zhang, X.; Dong, H.; Sun, X. J.; Yang, D. D.; Sheng, J. L.; Tang, H. L.; Bin Meng, X.; Zhang, F. M. Step-By-Step Improving Photocatalytic Hydrogen Evolution Activity of NH $_2$ –UiO-66 by Constructing Heterojunction and Encapsulating Carbon Nanodots. *ACS Sustainable Chem. Eng.* 2018, 6(9), 11563–11569. DOI: https://doi.org/10.1021/acssuschemeng.8b01740.

[362] Mao, S.; Zou, Y.; Sun, G.; Zeng, L.; Wang, Z.; Ma, D.; Guo, Y.; Cheng, Y.; Wang, C.; Shi, J. W. Thio Linkage Between CdS Quantum Dots and UiO-66-type MOFs as an Effective Transfer Bridge of Charge Carriers Boosting Visible-Light-Driven Photocatalytic Hydrogen Production. *J. Colloid. Interface. Sci.* 2021, 581, 1–10. DOI: 10.1016/j.jcis.2020.07.121.

[363] Lalonde, M.; Bury, W.; Karagiaridi, O.; Brown, Z.; Hupp, J. T.; Farha, O. K. Transmetalation: Routes to Metal Exchange within Metal–Organic Frameworks. *J. Mater. Chem. A*. 2013, 1, 5453–5468. DOI: 10.1039/C3TA10784A.

[364] Sheybani, S.; Abbas, M.; Firouzi, H. R.; Xiao, Z.; Zhou, H. C.; Balkus, K. J. Synthesis of Fluoro-Bridged Ho^{3+} and Gd^{3+} 1,3,5-Tris(4-Carboxyphenyl)benzene Metal-Organic Frameworks from Perfluoroalkyl Substances. *Inorg. Chem*. 2022. DOI: 10.1021/acs.inorgchem.2c04470.

[365] Wasson, M. C.; Buru, C. T.; Chen, Z.; Islamoglu, T.; Farha, O. K. Metal–Organic Frameworks: A Tunable Platform to Access Single-Site Heterogeneous Catalysts. *Appl. Catal. A*. 2019, 586, 117214. DOI: 10.1016/J.APCATA.2019.117214.

[366] Liu, T. F.; Zou, L.; Feng, D.; Chen, Y. P.; Fordham, S.; Wang, X.; Liu, Y.; Zhou, H. C. Stepwise Synthesis of Robust Metal–Organic Frameworks via Postsynthetic Metathesis and Oxidation of Metal Nodes in a Single-Crystal to Single-Crystal Transformation. *J. Am. Chem. Soc*. 2014, 136, 7813–7816. DOI: 10.1021/ja5023283.

[367] Melillo, A.; Franconetti, A.; Alvaro, M.; Ferrer, B.; Garcia, H. Metal Nodes of Metal-Organic Frameworks can Activate Molecular Hydrogen, Chemistry. *A European Journal*. 2023, 29, e202202625. DOI: 10.1002/CHEM.202202625.

[368] Ye, G.; Gu, Y.; Zhou, W.; Xu, W.; Sun, Y. Synthesis of Defect-Rich Titanium Terephthalate with the Assistance of Acetic Acid for Room-Temperature Oxidative

Desulfurization of Fuel Oil. *ACS Catal.* 2020, 10, 2384–2394. DOI: 10.1021/acscatal.9b04937.

[369] Ye, G.; Wan, L.; Zhang, Q.; Liu, H.; Zhou, J.; Wu, L.; Zeng, X.; Wang, H.; Chen, X.; Wang, J. Boosting Catalytic Performance of MOF-808(zr) by Direct Generation of Rich Defective Zr Nodes via a Solvent-Free Approach. *Inorg. Chem.* 2022. DOI: 10.2139/ssrn.4289676.

[370] Jiao, Y.; Pei, J.; Chen, D.; Yan, C.; Hu, Y.; Zhang, Q.; Chen, G. Mixed-Metallic MOF Based Electrode Materials for High Performance Hybrid Supercapacitors. *J. Mater. Chem. A*. 2017, 5, 1094–1102. DOI: 10.1039/C6TA09805C.

[371] Duan, H.; Chen, X.; Yang, Y. N.; Zhao, J.; Lin, X. C.; Tang, W. J.; Gao, Q.; Ning, G. H.; Li, D. Tailoring Stability, Catalytic Activity and Selectivity of Covalent Metal–Organic Frameworks via Steric Modification of Metal Nodes. *J. Mater. Chem. A Mater.* 2023, 11, 12777–12783. DOI: 10.1039/D2TA08797A.

[372] Lin, Y.; Wu, S.; Yang, C.; Chen, M.; Li, X. Preparation of Size-Controlled Silver Phosphate Catalysts and Their Enhanced Photocatalysis Performance via Synergetic Effect with MWCNTs and PANI. *Appl. Catal. B.* 2019, 245, 71–86. DOI: 10.1016/J.APCATB.2018.12.048.

[373] Xiang, Q.; Lang, D.; Shen, T.; Liu, F. Graphene-Modified Nanosized Ag_3PO_4 Photocatalysts for Enhanced Visible-Light Photocatalytic Activity and Stability. *Appl. Catal. B.* 2015, 162, 196–203. DOI: 10.1016/J.APCATB.2014.06.051.

[374] Rehan, M.; Barhoum, A.; Khattab, T. A.; Gätjen, L.; Wilken, R. Colored, Photocatalytic, Antimicrobial and UV-Protected Viscose Fibers Decorated with Ag/Ag_2CO_3 and Ag/Ag_3PO_4 Nanoparticles. *Cellulose*. 2019, 26, 5437–5453. DOI: 10.1007/s10570-019-02497-8.

[375] Miao, X.; Yue, X.; Ji, Z.; Shen, X.; Zhou, H.; Liu, M.; Xu, K.; Zhu, J.; Zhu, G.; Kong, L., et al. Nitrogen-Doped Carbon Dots Decorated on $g\text{-}C_3N_4/Ag_3PO_4$ Photocatalyst with Improved Visible Light Photocatalytic Activity and Mechanism Insight. *Appl. Catal. B.* 2018, 227, 459–469. DOI: 10.1016/J.APCATB.2018.01.057.

[376] Cai, T.; Zeng, W.; Liu, Y.; Wang, L.; Dong, W.; Chen, H.; Xia, X. A Promising Inorganic-Organic Z-Scheme Photocatalyst Ag_3PO_4/PDI Supermolecule with Enhanced Photoactivity and Photostability for Environmental Remediation. *Appl. Catal. B.* 2020, 263, 118327. DOI: 10.1016/J.APCATB.2019.118327.

[377] Zhang, L.; Zhang, J.; Yu, H.; Yu, J. Emerging S-Scheme Photocatalyst. *Adv.Mate.* 2022, 34, 2107668. DOI: 10.1002/ADMA.202107668.

[378] Xu, Q.; Wageh, S.; Al-Ghamdi, A. A.; Li, X. Design Principle of S-Scheme Heterojunction Photocatalyst. *J. Mater. Sci. Technol.* 2022, 124, 171–173. DOI: 10.1016/J.JMST.2022.02.016.

[379] Li, T.; Tsubaki, N.; Jin, Z. S-Scheme Heterojunction in Photocatalytic Hydrogen Production. *J. Mater. Sci. Technol.* 2023. DOI: 10.1016/J.JMST.2023.04.049.

[380] Shao, Y.; Hao, X.; Jin, Z. Construction of Double S-Scheme ZIF-67@gdy/CuI Heterojunction by Graphdiyne (G-nH2n−2) Nanosheets-Coated ZIF-67 on Synergized Charge Transfer for Enhanced Photocatalytic Hydrogen Evolution. *Solar Rrl.* 2023, 7, 2201054. DOI: 10.1002/SOLR.202201054.